CalVal Jason

Jason-1 validation and cross calibration activities [Annual Report 2011]

Contract No 104685 - lot1.2A

Reference : CLS.DOS/NT/12-017

Nomenclature : SALP-RP-MA-EA-22056-CLS

Issue : 1rev 0

Date : June 13, 2012

CLS - 8-10 Rue Hermès - Parc Technologique du Canal - 31520 Ramonville St-Agne - FRANCE
Telephone 33 5 61 39 47 00 / Fax 33 5 61 75 10 14

Chronology Issues :		
Issue :	Date :	Reason for change :
1.0	26/01/2012	Created

People involved in this issue :		
Written by :	H. Roinard	CLS
	G. Valladeau	CLS
	J.F. Legeais	CLS
	S. Philipps	CLS
	M. Ablain	CLS
Checked by :	S. d'Alessio	CLS
Approved by :	J.P. Dumont	CLS
	M. Ablain	CLS
Application authorized by :		

Index sheet :	
Context	
Keywords	Jason-1, Calval, orbits, 59-day signal
hyperlink	

Distribution :		
Company	Means of distribution	Names
CLS/DOS	1 electonic copy	G. DIBARBOURE
	1 electonic copy	V. ROSMORDUC
	1 electonic copy	P. ESCUDIER
	1 electonic copy	J. DORANDEU
DT/AQM (DOC/CLS)	DOCUMENTATION	1 printed copy + 1 cd-rom
CNES	1 electronic copy	thierry.guinle@cnes.fr
CNES	1 electronic copy	emilie.bronner@cnes.fr
CNES	1 electronic copy	nicolas.picot@cnes.fr
CNES	1 electronic copy	aqgp_rs@cnes.fr
CNES	1 electronic copy	dominique.chermain@cnes.fr
CNES	1 electronic copy	delphine.vergnoux@cnes.fr

.

List of tables and figures :

List of Tables

List of Figures

List of items to be defined or to be confirmed :

Applicable documents / reference documents :

Contents

1. Introduction

This document presents the synthesis report concerning validation activities of Jason-1 GDRs under SALP contract (N° 104685 Lot1.2A) supported by CNES at the CLS Space Oceanography Division. It is divided into several parts concerning mainly CAL/VAL Jason-1 activities, but when useful, results from Topex/Poseidon and Jason-2 are also shown for comparison.

Since the beginning of the mission, Jason-1 data have been analyzed and monitored in order to assess the quality of Jason-1 GDR products (AVISO and PODAAC User handbook, [85]) for oceanographic applications. This report is basically concerned with long-term monitoring of the Jason-1 altimeter system, from all GDR data available to date, that is for almost 10 years of data (cycles 1 to 365, corresponding to period from January 2002 to December 2011). This includes careful monitoring of all altimeter and radiometer parameters, performance assessment, geophysical evaluation and cross-calibration with T/P measurements (as long as T/P data were available). For comparison and cross-calibration with Jason-2 data, see [84]. For comparison and cross-calibration with Envisat data, see [76].

Moreover specific studies are presented in this document :

- Analysis of the 59.74 days signal
- Comparison between preliminary GDR-D orbit standard and current GDR-C orbit standard
- Investigations on σ_0 / altimeter wind speed stability
- Impact of fuel depletion maneuvers

This work is routinely performed at CLS and in this frame, besides continuous analyzes in terms of altimeter data quality, Jason-1 GDR Quality Assessment Reports (e.g. Ablain et al. 2011 [12]) are produced and associated to data dissemination. Even if only low order statistics are mainly presented here, other analyzes including histograms, plots and maps are continuously produced and used in the quality assessment process.
The work performed in terms of data quality assessment also includes cross-calibration analyzes mainly with the T/P mission until November 2005 (end of the T/P mission). Even if T/P mission is finished, cross-calibration analyzes are useful for the reprocessing activities in order to study the sea state bias or the SSH bias for instance. Cross-calibration analyzes with Jason-2 are also performed, but shown in annual report of Jason-2 (see [84]).
Indeed, it is now well recognized that the usefulness of any altimeter data only makes sense in a multi-mission context, given the growing importance of scientific needs and applications, particularly for operational oceanography. One major objective of the Jason-1 mission is to continue the T/P high precision altimetry and to allow combination with other missions (ENVISAT, Jason-2). This kind of comparisons between different altimeter missions flying together provides a large number of estimations and consequently efficient long term monitoring of instrument measurements. Of course, other sources of comparisons are also needed, using independent datasets (e.g. Queffeulou et al. 2004 [88], Ray and Beckley 2003 [91], Arnault et al. 2004 [16], Provost et al. 2004[86], Durrant et al. 2009 [44], Abdalla et al. 2010 [1]). [113] and [64] show comparisons between altimeter data and in-situ data (respectively tide gauges measurements and T/S profiles).

2. Processing status

2.1. IGDR, GDR and CAL/VAL Processing

To date, the whole mission of Jason-1 (GDR products) is available in version "c" of CMA ground processing software. The purpose of this document is to report the major features of the data quality from the Jason-1 mission. Moreover, the document is associated with comparison results from T/P GDRs. All these cycle reports are available on AVISO website: http://www.aviso.oceanobs.com. In addition to these reports, several meeting (CAVE, OSTST) have been performed to inform the Jason-1 GDR's users about the main results and the studies in progress.

2.1.1. Models and Standards History

Three versions of the Jason-1 Interim Geophysical Data Records (IGDRs) and Geophysical Data Records (GDRs) have been generated to date. These three versions are identified by the version numbers "a", "b" and "c" in the name of the data products. For example, version "a" GDRs are named "JA1_GDR_2Pa", version "b" GDRs are named "JA1_GDR_2Pb", and version "c" GDRs are named "JA1_GDR_2Pc". All versions adopt an identical data record format as described in Jason-1 User Handbook and differ only in the models and standards that they adopt. Version "a" I/GDRs were the first version released soon after launch. Version "b" I/GDRs were first implemented operationally from the start of cycle 140 for the IGDRs and cycle 136 for the GDRs. Reprocessing to generate version "b" GDRs for cycles 1-135 were performed in 2006 and 2007 in order to generate a consistent data set. Version "c" I/GDRs were first operationally implemented from mid cycle 237 for the IGDRs and cycle 233 for the GDRs. Reprocessing to generate version "c" GDRs for cycles 1-232 were performed from June 2008 to January 2010 in order to generate a consistent data set. Table 1 below summarizes the models and standards that are adopted in these three versions of the Jason-1 I/GDRs. More details on some of these models are provided in Jason-1 User Handbook document ([85]).

Model	Product Version "a"	Product Version "b"	Product Version "c"
Orbit	JGM3 Gravity Field	EIGEN-CG03C Gravity Field	EIGEN-GL04S with time-varying gravity
	DORIS tracking data for IGDRs	DORIS tracking data for IGDRs	DORIS tracking data for IGDRs
	DORIS+SLR tracking data for GDRs	DORIS+SLR+GPS tracking data for GDRs	DORIS+SLR+GPS tracking data for GDRs with increased weight of D/L
.../...			

Model	Product Version "a"	Product Version "b"	Product Version "c"
Altimeter Retracking	MLE3 + 1st order Brown model (mispointing estimated separately)	MLE4 + 2nd order Brown model : MLE4 simultaneously retrieves the 4 parameters that can be inverted from the altimeter waveforms: epoch, SWH, Sigma0 and mispointing angle. This algorithm is more robust for large off-nadir angles (up to 0.8°).	Identical to version "b"
Altimeter Instrument Corrections	Consistent with MLE3 retracking algorithm.	Consistent with MLE4 retracking algorithm.	Identical to version "b". A new correction is available in the product to account for the apparent datation bias (field 28). Users are advised to add this correction to the Ku-band altimeter range, as it is not a component of the net instrument correction that has already been applied to the provided Ku-band range
Jason Microwave Radiometer Parameters	Using calibration parameters derived from cycles 1-30.	Using calibration parameters derived from cycles 1-115.	Using calibration parameters derived from cycles 1-227
Dry Troposphere Range Correction	From ECMWF atmospheric pressures.	From ECMWF atmospheric pressures and model for S1 and S2 atmospheric tides.	From ECMWF atmospheric pressures and model for S1 and S2 atmospheric tides. Uses new ECMWF delivery to correct for spurious oscillation effects.
Wet Troposphere Range Correction from Model	From ECMWF model	From ECMWF model.	Identical to version "b"
			.../...

Model	Product Version "a"	Product Version "b"	Product Version "c"
Back up model for Ku-band ionospheric range correction.	Derived from DORIS measurements.	Derived from DORIS measurements.	Derived from JPL's Global Ionosphere Model (GIM) maps
Sea State Bias Model	Empirical model derived from cycles 19-30 of version "a" data.	Empirical model derived from cycles 11-100 of MLE3 altimeter data with version "b" geophysical models.	Empirical model derived from cycles 11-100 of MLE4 altimeter data with version "c" geophysical models"
Mean Sea Surface Model	GSFC00.1	CLS01	Identical to version "b"
Along Track Mean Sea Surface Model	None (set to default)	None (set to default)	None (set to default)
Geoid	EGM96	EGM96	Identical to version "b"
Bathymetry Model	DTM2000.1	DTM2000.1	Identical to version "b"
Mean Dynamic Topography	None (was a spare)	None (was a spare)	Rio 2005 solution
Inverse Barometer Correction	Computed from ECMWF atmospheric pressures	Computed from ECMWF atmospheric pressures after removing model for S1 and S2 atmospheric tides.	Identical to Version "b" but using new ECMWF delivery to correct for spurious oscillation effects
Non-tidal High-frequency De-aliasing Correction	None (set to default)	Mog2D ocean model on GDRs, none (set to default) on IGDRs. Ocean model forced by ECMWF atmospheric pressures after removing model for S1 and S2 atmospheric tides.	High resolution Mog2D model for both IGDR and GDR products
Tide Solution 1	GOT99	GOT00.2 + S1 ocean tide . S1 load tide ignored.	Identical to version "b"
Tide Solution 2	FES99	FES2004 + S1 and M4 ocean tides. S1 and M4 load tides ignored.	FES2004 + S1 and M4 ocean tides. S1, K2 and loading tides have been updated

.../...

Model	Product Version "a"	Product Version "b"	Product Version "c"
Equilibrium long-period ocean tide model.	From Cartwright and Taylor tidal potential.	From Cartwright and Taylor tidal potential.	Identical to version "b"
Non-equilibrium long-period ocean tide model.	None (set to default)	Mm, Mf, Mtm, and Msqm from FES2004.	Identical to version "b"
Solid Earth Tide Model	From Cartwright and Taylor tidal potential.	From Cartwright and Taylor tidal potential.	Identical to version "b"
Pole Tide Model	Equilibrium model	Equilibrium model.	Identical to version "b"
Wind Speed from Model	ECMWF model	ECMWF model	Identical to version "b"
Altimeter Wind Speed	Table derived from TOPEX/POSEIDON data.	Table derived from version "a" Jason-1 GDR data.	Identical to version "b"
Rain Flag	Derived from TOPEX/POSEIDON data.	Derived from version "a" Jason-1 GDRs.	Derived from version "b" Jason-1 GDRs using the AGC instead of sigma naught values
Ice Flag	Climatology table	Climatology table	New flag based on the comparison of the model wet tropospheric correction and of a radiometer bi frequency wet tropospheric correction (derived from 23.8 GHz and 34.0 GHz), accounting for a backup solution based on climatologic estimates of the latitudinal boundary of the ice shelf, and from altimeter wind speed.

Table 1: *M*odels and standards adopted for the Jason-1 product version "a", "b", and "c"

2.1.2. Differences in editing procedure for the different GDR product versions

For GDR version "c" the same editing criteria and thresholds like in GDR version "b" should be used. Since GDR version "b" the MLE4 retracking algorithm is used. It is based on a second-order altimeter echo model and is more robust for large off-nadir angles (up to 0.8 degrees). For product version "a" (CMA version 6.3), the maximum threshold on square off-nadir angle proposed in Jason-1 User Handbook document was set to 0.16 deg^2. Since GDR version "b", this threshold is too restrictive and has to be set to 0.64 deg^2.

However, this editing criteria had the side effect of removing some bad measurements impacted by rain cells, sigma0 blooms or ice. With the new threshold (0.64 deg^2), these measurements are not rejected anymore.

2.1.3. Impact of product versions

The main changes between GDRs version "a" and "b" were the new orbit, the retracking of the wave forms with MLE4 algorithm, and new geophysical corrections. This had not only an impact on editing procedure, but also on crossover performances. For version "c", the main changes are the new orbit, new JMR calibration and new sea state bias. For information concerning reprocessing in version "b", please refer to [81] or [8]. Concerning reprocessing in version "c", please refer to [30] or [109].

2.2. CAL/VAL status

2.2.1. Missing measurements

This section presents a summary of major satellite events that occurred from cycle 1 to 365. Table 2 gives a status about the number of missing passes (or partly missing) for GDRs version "c" and the associated events for each cycle.
Gyro calibration, Star Tracker unavailability and ground processing issues were the main events which produced missing data from cycle 1 to 64 (2002 and 2003).
During year 2004 (cycle 65 to 109), 2 safe hold mode incidents have produced 15 days of missing data due to a wheel anomaly. As result of this incident, only 3 wheels have been available but this has had no impact on scientific applications.
During year 2005 (110-146), most of incidents are due to SEU. The altimeter was reinitialized automatically without C-band. Few passes have only been impacted each time, and they are rejected because of the lack of C-band data, and therefore lack of dual-frequency ionospheric correction.
During year 2006 (cycles 147 - 183) Jason-1 experienced a safe hold mode (cycle 177 to 179) producing 17 days of missing data due to mass memory error. In addition 2 altimeter SEU occurred. It also happened that small data gaps occur (less than one minute duration).
During 2007 (cycles 183 to 220) Jason-1 had experienced several altimeter SEU. In 2008 (cycles 221 to 256), there were two major events : the altimeter switch-off in May, due to the close encounter with drifting TOPEX/Poseidon, and a safehold mode in August.
During 2009 (cycles 257 to 293), Jason-1 was moved from its original groundtrack to its new interleaved groundtrack from 26th January to 14th February 2009. During most of this time, no altimeter or radiometer data is available. Furthermore, the satellite experienced a safehold mode in September 2009 producing 10 days of missing data.
During 2010 (cycles 294 to 324) Jason-1 was particularly impacted by degraded performances of its Star Trackers and Gyro wheels, especially when the satellite is in yaw fix mode. This lead to high mispointing, which caused sometimes altimeter lost of track and altimeter incidences. To avoid the possibility of a spacecraft safe hold, Jason-1 swaped on 14th of April 2010 from Gyro wheel 1 to redundant Gyro wheel 3. Furthermore, during cycle 315 (July 2010), Jason-1 performed several out of plane maneuvers in order to deplete fuel (to reduce risk of explosion in case of loss of control). Groundtrack departed up to 7 km from nominal groundtrack.

During 2011 (cycles 325 to 365) Jason-1 continued the out of plane maneuvers in order to deplete fuel. The cycles impacted by these maneuvers are 356, and 358-360. Mispointing behavior was good in 2011. For further information of events occurred during 2011 see also section 8.5.. The following table gives an overview over missing data and why it is missing.

Jason-1 Cycles	Number of completely missing passes	Number of partly missing passes	Events
001	2	7	Science telemetry unavailability
002	14	3	On board Doris anomaly
.../...			

Jason-1 Cycles	Number of completely missing passes	Number of partly missing passes	Events
003	0	2	Gyro-calibration
004	2	5	Gyro-calibration and Science telemetry unavailability
006	1	4	Altimeter echo data unavailability
007	0	2	Science telemetry unavailability
008	2	5	Ground processing issue
009	3	4	Poseidon-2 altimeter SEU and Gyro-calibration
010	0	2	Gyro-calibration
015	0	1	Ground processing issue
019	0	1	Ground processing issue
021	0	1	Star tracker unavailability
023	0	1	Ground processing issue
026	0	2	Gyro-calibration
027	0	2	Gyro-calibration
031	0	1	Star tracker unavailability
038	0	4	Ground processing issue
039	0	1	Gyro-calibration
042	5	2	Poseidon-2 altimeter SEU
045	0	3	Gyro-calibration
046	0	1	Poseidon-2 altimeter SEU
048	0	1	Gyro-calibration
062	0	1	Ground processing issue
064	0	2	Exceptional calibrations
075	4	0	Poseidon-2 altimeter SEU
077	69	0	Safe hold mode (15/02/04 to 21/02/04)
078	82	0	Safe hold mode (15/02/04 to 21/02/04)
080	0	1	Calibration over ocean

.../...

Jason-1 Cycles	Number of completely missing passes	Number of partly missing passes	Events
082	54	1	Failure in module 3 of PLTM2
087	0	1	Calibration over ocean
091	2	4	DORIS instrument switch to redundancy and altimeter incident (no C band information)
094	0	1	Altimeter incident or star tracker unavailability
099	0	1	Altimeter incident or star tracker unavailability
101	0	1	Altimeter incident or star tracker unavailability
102	1	0	Altimeter SEU (no C band information)
103	0	2	Altimeter SEU (no C band information)
104	0	1	No data between 21:29:18 and 21:30:07 on November 8th pass 189
106	3	2	Altimeter SEU (no C band information)
108	0	2	Altimeter SEU (no C band information)
114	3	1	Altimeter SEU (no C band information)
115	0	4	2 altimeter SEU incidents (C band) and altimeter initialization procedure.
118	6	2	Altimeter SEU (no C band information)
131	0	7	TRSR2 "elephant packets" anomaly
132	0	1	Altimeter SEU (no C band information)
133	0	2	Altimeter SEU (no C band information)

.../...

Jason-1 Cycles	Number of completely missing passes	Number of partly missing passes	Events
136	104	2	Altimeter SEU (no C band information), Platform incident (20/09/05 to 28/09/05)
137	91	2	Platform incident (20/09/05 to 28/09/05)
161	0	5	TRSR elephant packets
165	0	1	(planned) Poseidon calibration (board filter)
173	0	3	Altimeter SEU (no C band information)
177	141	1	Safehold mode (30/10/2006 to 16/11/2006)
178	254	0	Safehold mode (30/10/2006 to 16/11/2006)
179	45	1	Safehold mode (30/10/2006 to 16/11/2006)
181	5	2	Altimeter SEU
185	0	3	calibration over ocean
191	0	2	Altimeter SEU
192	0	1	calibration over ocean
198	1	1	Altimeter SEU
200	0	3	calibration over ocean
206	0	2	Altimeter SEU
219	2	0	Missing telemetry
222	0	2	calibrations over ocean
231	0	1	erroneous command sent by JTCCS
233	142	2	altimeter switch off (TP/J1 close encounter)
234	0	1	calibration
242	84	1	safehold mode
243	254	0	safehold mode

.../...

Jason-1 Cycles	Number of completely missing passes	Number of partly missing passes	Events
254	1	1	Altimeter SEU
260	254	0	Jason-1 moves to its new interleaved ground-track
261	254	0	Jason-1 moves to its new interleaved ground-track
262	12	4	Jason-1 moves to its new interleaved ground-track + calibrations over ocean
263	0	4	calibrations over ocean
276	0	2	calibrations over ocean
283	26	1	safehold mode (2009-09-15 to 2009-09-24)
284	233	0	safehold mode (2009-09-15 to 2009-09-24)
290	0	2	Altimeter SEU
301	0	3	Altimeter SEU + restart
304	0	42	Due to on-orbit degradation of star trackers and gyro wheel performances, altimeter lost track
305	0	5 2	Due to on-orbit degradation of star trackers and gyro wheel performances, altimeter lost track calibrations over ocean
306	0	3	Altimeter SEU + restart
310	39	53	Due to on-orbit degradation of star trackers performances, altimeter lost track + altimeter incidents + reinits
312	0	3	Altimeter SEU + restart
315	12	28	Due to on-orbit degradation of star trackers performances, altimeter lost track + altimeter incidents
316	0	5	calibrations + missing PLTM (probably linked to high mispointing)

.../...

Jason-1 Cycles	Number of completely missing passes	Number of partly missing passes	Events
318	0	2	calibrations over ocean
319	1	2	gyroscope calibration
324	0	2	calibrations over ocean
343	0	2	Due to calibrations, passes 106 and 107 are partially missing with respectively 62% and 23% of missing measurements over ocean
356	0	1	Due to missing PLTM there are 2 small (less than 2 minutes) data gaps on 2011-09-06 between 06 :20 :56 and 06 :22 :15 and between 06 :32 :46 and 06 :34 :38 (pass 153).
359	4	1	Passes 181 to 184 are completely missing and pass 180 is partly missing (24% of ocean measurements). These passes are missing related to DORIS DIODE autoinit mode, where precise datation is not possible
363	0	2	Due to calibrations, passes 106 and 107 are partly missing with respectively 68% and 15% of missing ocean measurements

Table 2: *M*issing pass status

2.2.2. Edited measurements

Table 3 indicates the cycles which have a larger amount of removed data due to editing criteria (see section 3.2.1.). Most of the occurrences correspond to dual-frequency ionospheric correction at default value (altimeter SEU) or missing radiometer wet troposphere correction (following safehold modes).
Notice that since cycle 78, the satellite operates with only 3 wheels: the maneuver impact (burn maneuver, yaw transition) is greater than before on the attitude control. Consequently for GDR "a" (which used MLE3 ground retracking algorithm), some measurements could be edited due to higher mispointing values when a maneuver occurs. Since the GDR "b" release, improvements in ground retracking algorithm have been set up and improvements on Star Tracker behavior have been performed in 2006. Therefore for the current GDR version ("c" release), generally only few measurements are edited by mispointing criterion.

Jason-1 Cycles	Comments
001	Passes 252 to 254 are edited due to radiometer wet troposphere correction at default value.
006	Pass 56 (in the Pacific ocean) is partly edited due to the bad quality of data. Indeed, the altimetric parameters values are out of the thresholds.
008	All the altimetric parameters are edited for 10% of pass 252 due to the bad quality of all the altimetric parameters as a result of a Star Tracker incident leading to a quite high off nadir angle.
009	Passes 004 and 005 partly edited by dual-ionospheric correction at default value (no c-band information).
021	Small part of pass 210 is edited after checking the square of the mispointing angle criterion.
069	Passes 209 to 211 are edited due to the radiometer wet troposphere correction at default value. This is linked to the safe hold mode on cycle 69 : the JMR has been set on 2 hours after the altimeter.
078	Passes 83 to 85 are edited due to the radiometer wet troposphere correction at default value. This is linked to the safe hold mode on cycle 88 : the JMR has been set on 2 hours after the altimeter.
091	Passes 126, 127 and partly 130 are edited by dual-ionospheric correction at default value (no c-band information).
102	Passes 187, 188 and partly 189 are edited by dual-ionospheric correction at default value (no c-band information).
103	Passes 29 to 31 are edited by dual-ionospheric correction at default value (no c-band information).
108	Passes 16 and 17, as well as part of passes 15 and 18 are edited by dual-ionospheric correction at default value (no c-band information).
115	Passes 19 to 21 and 29 to 31 are edited by dual-ionospheric correction at default value (no c-band information).
133	Pass 13 is partly edited due to dual-ionospheric correction at default value (no c-band information).
137	Passes 92, 93 and partly 94 are edited by radiometer wet tropospheric correction, since the radiometer was later switched on than the other instruments.
173	Due to an altimeter upset (no c-band information), the dual-frequency ionospheric correction is partially missing for passes 65 and 68 and fully for passes 66 and 67.
175	Pass 9 is partly edited by mispointing criterion out of threshold (probably aberrant quaternion).

.../...

Jason-1 Cycles	Comments
179	As radiometer was only switch on later, passes 046 to 058, as well as part of pass 059 are edited by radiometer wet troposphere correction at default values.
181	Pass 247 is partly edited by dual-frequency ionosphere at default value (no C-band information).
198	Pass 073 is partly edited by dual-frequency ionosphere at default value (no C-band information).
212	Pass 187 is entirely edited: one half by altimetric parameters at default value, other half by apparent squared mispointing values out of thresholds. Pass 186 is partly edited by apparent squared mispointing values out of thresholds.
220	Pass 189 is partly edited by altimetric parameters at default value.
224	Passes 30 and 163 are partly edited by altimetric parameters at default value. Just before and after these parts, they are edited by outbounded apparent squared mispointing values.
256	On passes 003 and 111 a portion is edited by several altimetric parameters at default value due to high mispointing (probably related to maneuver burn and yaw flip).
262	Passes 116 to 120 are completely edited by SLA out of thresholds (related to the last orbit change maneuvers).
279	On passes 241 and 242 a portion is edited by several altimetric parameters at default value due to high mispointing (probably related to yaw flip maneuver).
284	As radiometer was only switch on later after safehold, passes 234 to 236, as well as part of pass 237 are edited by radiometer wet troposphere correction at default values.
292	Pass 137 is partially edited by apparent squared mispointing out of threshold (related to Yaw flip maneuver).
301	Following altimeter reinit on 2010-03-04 at 04:40, though measurements are available since 04:53:11, they are edited till 07:03:27 as due to high off-nadir angles all altimeter parameters are at default values (passes 007, 008 and most of pass 009).
304	Due to high off-nadir angles, several passes are partly edited as altimeter parameters are at default values or mispointing are out of thresholds.
305	Due to high off-nadir angles, several passes are partly edited as altimeter parameters are at default values or mispointing are out of thresholds.
	.../...

Jason-1 Cycles	Comments
306	Following both altimeter reinit on 2010-04-26 at 09:57:03 and 11:22:13, though measurements are available since 10:00:49, they are edited till 11:43:09 as all altimeter parameters are at default values (passes 100, 101 and part of pass 102 over North America).
310	Apparent squared mispointing is very high for passes 62 to 216 (period between yaw flip and yaw ramp), leading to edited (altimeter parameters at default values) or missing measurements on many passes during this period .
312	Following altimeter reinit on 2010-06-28 at 17:03:26, though measurements are available since 17:07:00, they are edited till 17:27:42 as all altimeter parameters are at default values (pass 198 over North Atlantic).
315	Several passes are completely edited by SLA out of thresholds (2,27,29,54,57,182,183) or SLA pass statistics out of thresholds (3,4,28,53,55,136,160). Furthermore several passes are partly edited by SLA out of threshold. This is caused by the maneuvers. Several passes are completely (123,151,178,191,198,204,221,230,233) and several partly edited by altimeter parameters at default values. This is causes by high mispointing (too high for MLE4 algorithm). Passes 177 and 178 are partly edited by radiometer wet troposphere correction at default value.
316	Part of pass 1 is edited by the square of the off-nadir angle. Several part of passes (2, 3, 8, 10, 12, and 217) are edited as altimetric parameters are at default value (degraded star tracker performances).
327	Due to mispointing out of threshold, passes 115 and 239 are partly edited, respectively on 2010-11-21 and 2010-11-26.
328	Pass 011 is partially edited due to the Yaw Flip maneuver on 2010-11-27 from 01:53:34 to 02:12:37.
338	The star tracker performance seems to be degraded on pass 202, with very low tracking performance. This loss of STR tracking generated large off-nadir pointing. Apparent squared mispointing is thus high, but still within threshold . On pass 228 apparent squared mispointing is very high, leading to edited measurements (altimeter parameters at default values).
339	Due to mispointing out of thresholds, part of pass 088 is edited south of Australia and New-Zealand).
350	Apparent squared mispointing is very high on several passes, it is out of threshold or at default value in northern Pacific for passes 004, 006, and 032. For passes 004 and 006, altimeter parameters are partly at default value. This is probably due to low star tracker availability.
	.../...

Jason-1 Cycles	Comments
356	Due to inclination maneuvers the following passes were therefore partially or entirely invalidated: passes 120 to 123, 145 to 148, 196 to 199.
358	Due to inclination maneuvers, the following passes were partially or entirely invalidated: passes 226 to 229 and 252 to 254.
359	A portion of pass 101 has about 10 minutes of radiometer wet troposphere correction at default values. Due to inclination maneuvers 24 passes were partially or entirely invalidated: passes 001, 074 to 077, 101 to 104, 124 to 127, 150 to 153, 176 to 179, 252 to 254.
360	Due to inclination maneuvers 27 passes were partially or entirely invalidated: passes 001, 025 to 028, 051 to 054, 077 to 080, 101 to 104, 178 to 183, 204 to 206, and 231.

Table 3: *E*dited measurement status

3. Data coverage and edited measurements

3.1. Missing measurements

3.1.1. Over ocean

Determination of missing measurements relative to the theoretically expected orbit ground pattern is used to detect missing telemetry in Jason-1 datasets due to altimetry events for instance. This procedure is applied cycle per cycle and leads to results plotted on the left figure 1. It represents the percentage of missing measurements relative to the theory, when limited to ocean surfaces. The mean value is about 3.6% but this figure is not significant due to several events where the measurements are missing. All these events are described on table 2. Moreover, events which occurred during 2011 are also indicated by colored lines and stripes on bottom part of figure 1.
On figure 1 on the right, the percentage of missing measurements is plotted without taking into account the cycles where instrumental events or other anomalies occurred. Moreover shallow waters and high latitudes have been removed. This allows us to detect small data gaps in open ocean. The mean value is about 0.03%. This weak percentage of missing measurements is mainly explained by the rain cells, sea ice or sigma0 blooms. These sea states can disturb significantly the Ku band waveform shape leading to a non significant measure.
Another reason for these small data gaps in open ocean are datation gaps, which occur occasionally.

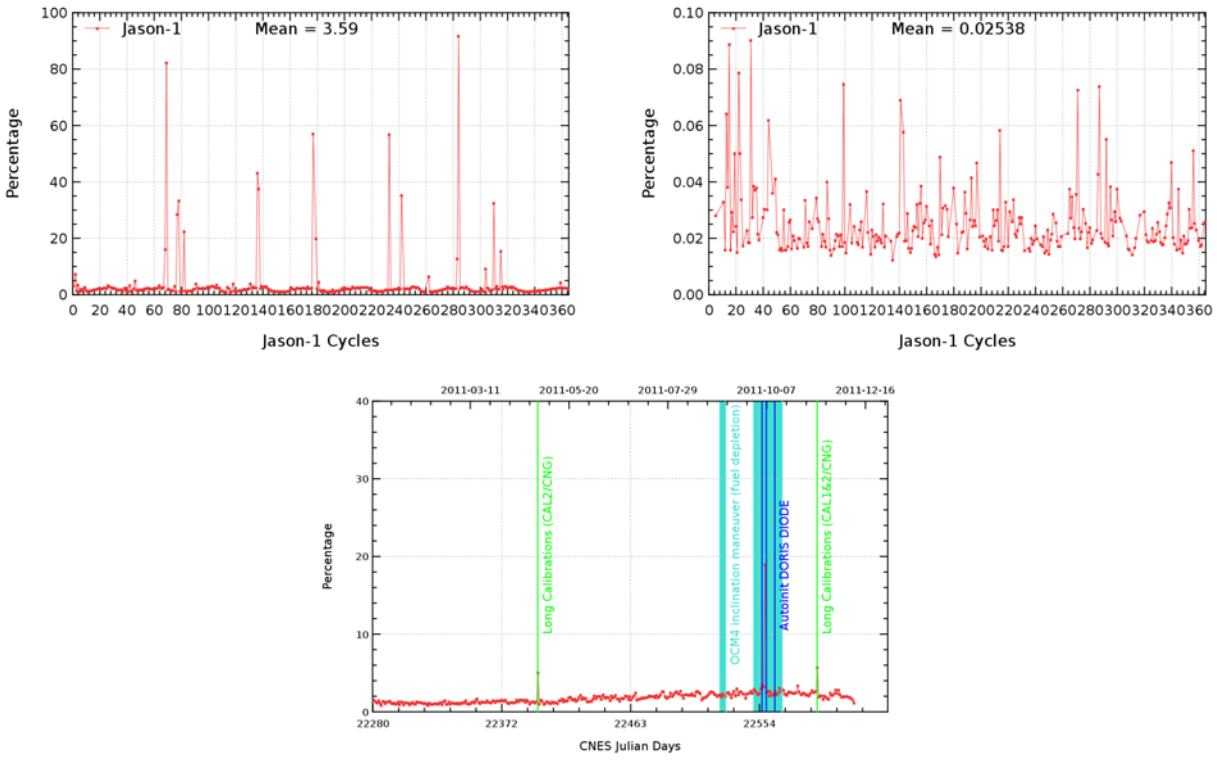

Figure 1: *Percentage of missing measurements over ocean on cyclic basis over the whole mission period (top) and on a daily basis for 2011 (bottom).*

3.1.2. Over land and ocean

Figure 2 shows the percentage of missing measurements for Jason-1 and T/P (all surfaces) computed with respect to a theoretical possible number of measurements. Due to differences between tracker algorithms, the number of data is greater for T/P (excepted when T/P experienced problems, especially since the tape recorders were no longer in service (T/P cycle 444, Jason-1 cycle 101)) than for Jason-1. Differences appear on land surfaces as shown in figure 3.

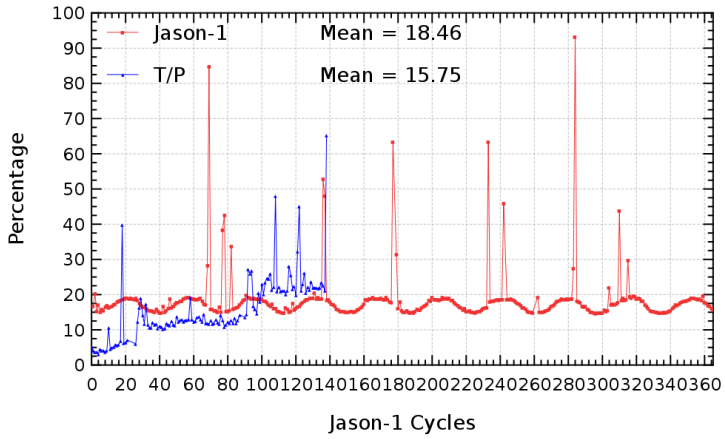

Figure 2: *Percentage of missing measurements over ocean and land for J1 and T/P*

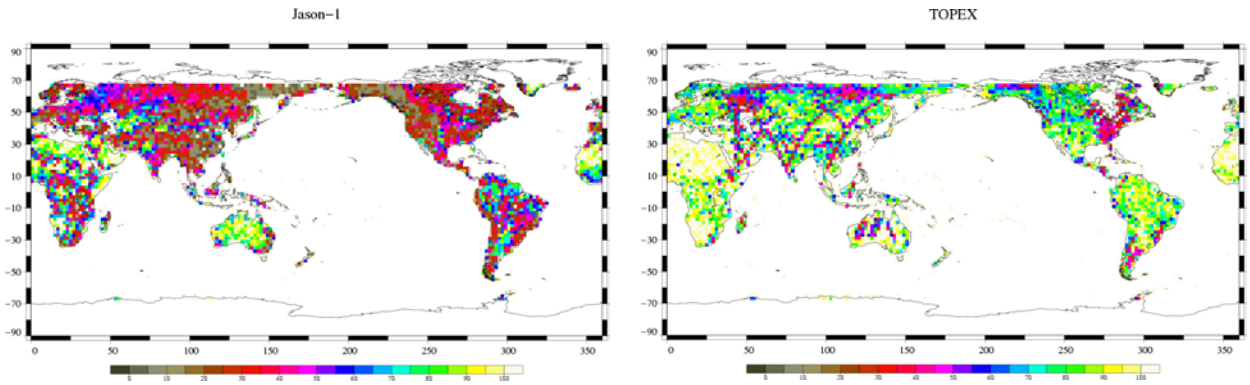

Figure 3: *Map of percentage of available measurements over land for Jason-1 on cycle 61 (left) and for TOPEX on cycle 404 (right)*

3.2. Edited measurements

3.2.1. Editing criteria definition

Editing criteria are used to select valid measurements over ocean. The editing process is divided into 4 parts. First, only measurements over ocean and lakes are kept (see section 3.2.2.). Second, the quality criteria concern the flags which are described in section 3.2.3. and 3.2.4. Then, threshold criteria are applied on altimeter, radiometer and geophysical parameters and are described in table 4. Moreover, a spline criterion is applied to remove the remaining spurious data. These criteria are also defined in AVISO and PODAAC User handbook. For each criterion, the cycle per cycle percentage of edited measurements has been monitored. This allows detection of anomalies in the number of removed data, which could come from instrumental, geophysical or algorithmic changes.

Parameter	Min thresholds	Max thresholds	mean edited
Sea surface height	$-130\,m$	$100\,m$	0.94%
Sea level anomaly	$-10\,m$	$10.0\,m$	1.18%
Number measurements of range	10	*Not applicable*	1.30%
Standard deviation of range	$0\,m$	$0.2\,m$	1.48%
Square off-nadir angle	$-0.2\,deg2$	$0.64\,deg2$	0.68%
Dry troposphere correction	$-2.5\,m$	$-1.9\,m$	0.00%
Inverted barometer correction	$-2.0\,m$	$2.0\,m$	0.00%
JMR wet troposphere correction	$-0.5m$	$-0.001\,m$	0.14%
Ionosphere correction	$-0.4\,m$	$0.04\,m$	1.26%
Significant waveheight	$0.0\,m$	$11.0\,m$	0.71%
Sea State Bias	$-0.5\,m$	$0.0\,m$	0.63%
Number measurements of Ku-band Sigma0	10	*Not applicable*	1.28%
Standard deviation of Ku-band Sigma0	$0\,dB$	$1.0\,dB$	1.81%
Ku-band Sigma0 [1]	$7.0\,dB$	$30.0\,dB$	0.67%
Ocean tide	$-5.0\,m$	$5.0\,m$	0.06%
Equilibrium tide	$-0.5\,m$	$0.5\,m$	0.00%
Earth tide	$-1.0\,m$	$1.0\,m$	0.00%
Pole tide	$-15.0\,m$	$15.0\,m$	0.00%

.../...

Parameter	Min thresholds	Max thresholds	mean edited
Altimeter wind speed	$0\,m.s^{-1}$	$30.0\,m.s^{-1}$	1.08%
All together	-	-	3.19%

Table 4: *E*diting criteria

3.2.2. Selection of measurements over ocean and lakes

In order to remove data over land, a land-water mask is used. Only measurements over ocean or lakes are kept. Indeed, this allows us to keep more data near the coasts and then detecting potential anomalies in these areas. Furthermore, there is no impact on global performance estimates since the most significant results are derived from analyzes in deep ocean areas. Figure 4 (left) displays the cycle per cycle percentage of measurements eliminated by this selection. It shows a seasonal signal which is due to the varying number of measurements available in the GDRs and varies not only over ocean but also over land. After removing the annual signal, there is no trend noticeable (see figure 4 (right)).

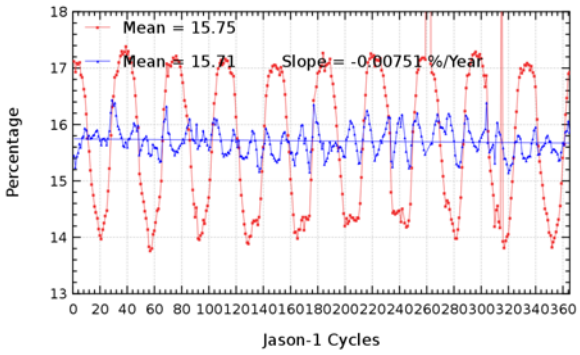

Figure 4: *Cycle per cycle percentage of eliminated measurements during selection of ocean/lake measurements with annual signal (in red) and trend of eliminated measurements after removing annual signal (in blue).*

[1]The thresholds used for the Ku-band Sigma0 are the same than for T/P, but the sigma0 bias between Jason-1 and T/P (about 2.4 dB) is applied.

3.2.3. Flagging quality criteria: Ice flag

The ice flag is used to remove the sea ice data. Figure 5 shows the cycle per cycle percentage of measurements edited by this criterion. No anomalous trend is detected (figure 5) but an annual cycle is visible. Indeed, the maximum number of points over ice is reached during the northern fall. As Jason-1 takes measurements between 66° north and south, it does not detect thawing of sea ice (due to global warming), which takes place especially in northern hemisphere beyond 66°N.
For some cycles (304, 310 and 315), the percentage of edited measurements by ice flag is increased. This is not related to real sea ice. It is related to high mispointing (number of elementary range measurements used in computation of ice flag is zero due to high mispointing). The ice flag edited measurements are plotted in Figure 5 for one cycle.

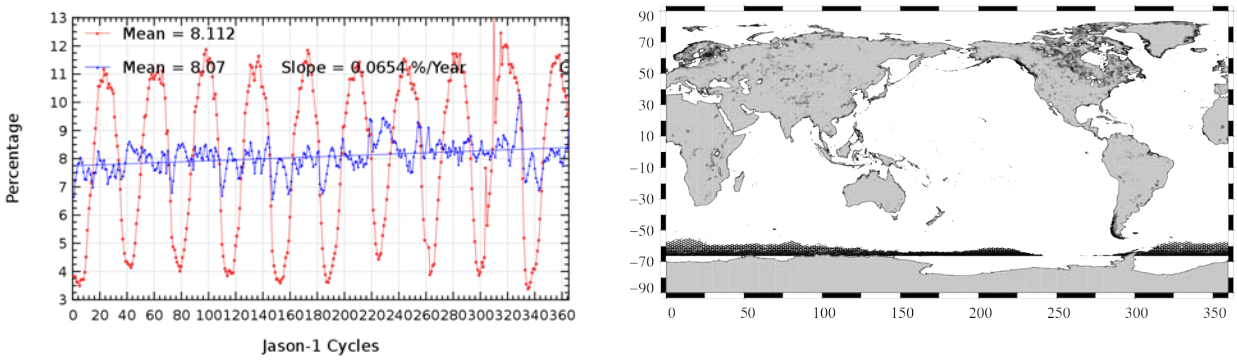

Figure 5: *Cycle per cycle percentage of edited measurements by ice flag criterion with and without annual and semi-annual signal (left), Map of edited measurements by ice flag criterion on cycle 361 (right).*

3.2.4. Flagging quality criteria: Rain flag

The rain flag is not used for data selection since it is quite restrictive. It is thus recommended not to be used by users. The rain flag has changed in version "c", making it even more restrictive. The percentage of rain edited measurements is plotted in figure 6 over cycles 329 to 365 (covering 12 month). It shows that measurements are especially edited near coasts, but also in the equatorial zone and open ocean. The rain flag seems to be too strict, using it would lead to editing 10.4% of additional measurements.

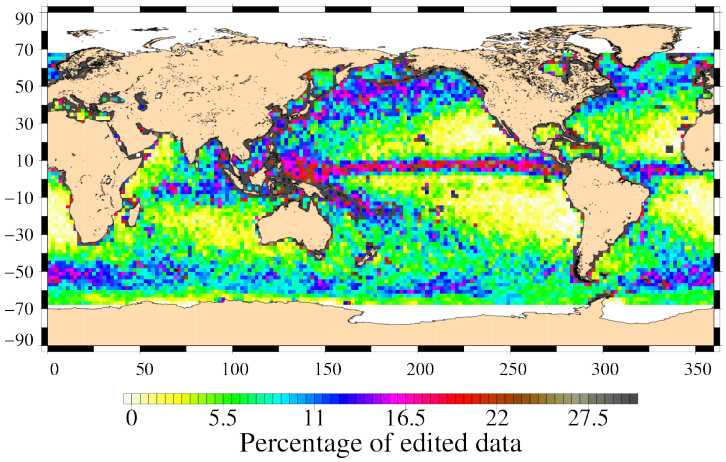

Figure 6: *Map of percentage of edited measurements by rain flag criterion over a 12-month period (cycles 329 to 365).*

3.2.5. Threshold criteria: Global

Instrumental and geophysical parameters have also been analyzed from comparison with thresholds, after selecting only ocean/lake measurements and applying flagging quality criteria (ice flag). Note that no measurements are edited by threshold criteria on the following corrections : dry troposphere correction, inverted barometer correction, equilibrium tide, earth and pole tide, which are all model corrections. Indeed these parameters are only verified in order to detect data at default values, which might happen during a processing anomaly.

The percentage of measurements edited by each criterion has been monitored on a cycle per cycle basis (figure 7). The mean percentage of edited measurements is about 3.2%. An annual cycle is visible due to the seasonal sea ice coverage in the northern hemisphere. Indeed most of northern hemisphere coasts are without ice during its summer. Consequently some of these coastal measurements are edited by the thresholds criteria in summer instead of the ice flag in winter. This seasonal effect visible in the statistics is not balanced by the southern hemisphere coasts due to the shore distribution between both hemispheres.
Note that for some cycles, the percentage of edited measurements is higher than usual. Concerning cycles 69, 179 and 284, this is mostly due to the lack of radiometer wet troposphere correction, as after safehold modes radiometer is usually switched on some time after the altimeter, see also section 3.2.10.. For cycles 304, 310 and 315, edited measurements are partly due to mispointing out of thresholds. As during 2010 squared off-nadir angle got for several cycles very high, MLE4 retracking could sometimes no longer retrieve altimeter parameters, they are therefore at default value and edited. In the following sections, all altimeter parameters show an increased percentage of edited measurements for the period of cycles 304 to 316, and especially for cycles 304, 310 and 315.

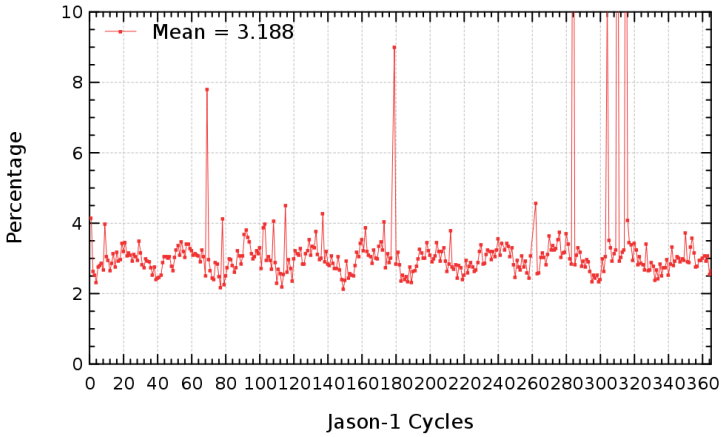

Figure 7: *Cycle per cycle percentage of edited measurements by threshold criteria*

3.2.6. Threshold criteria: 20-Hz measurements number

The percentage of edited measurements because of a too low number of 20-Hz measurements is represented on left side of figure 8. Neither a trend nor any anomaly has been detected, except for cycle 212 and period between cycles 304 and 315.
Indeed during cycle 212, about half of a pass had all altimetric parameters set at default values, due to satellite off-pointing, avoiding the retrieval of altimetric parameters. During 304 to 316, several portions of passes were concerned.

The map of measurements edited by the 20-Hz measurements number criterion is plotted on the right panel of figure 8 and shows correlation with heavy rain, wet areas, sigma0 bloom as well as coastal regions. Indeed the waveforms are distorted by rain cells, which makes them often unexploitable for SSH calculation. In consequence edited measurements due to several altimetric criteria are often correlated with wet areas. Furthermore the sections of passes with altimeter parameters at default values due to very high mispointing are slightly noticeable.

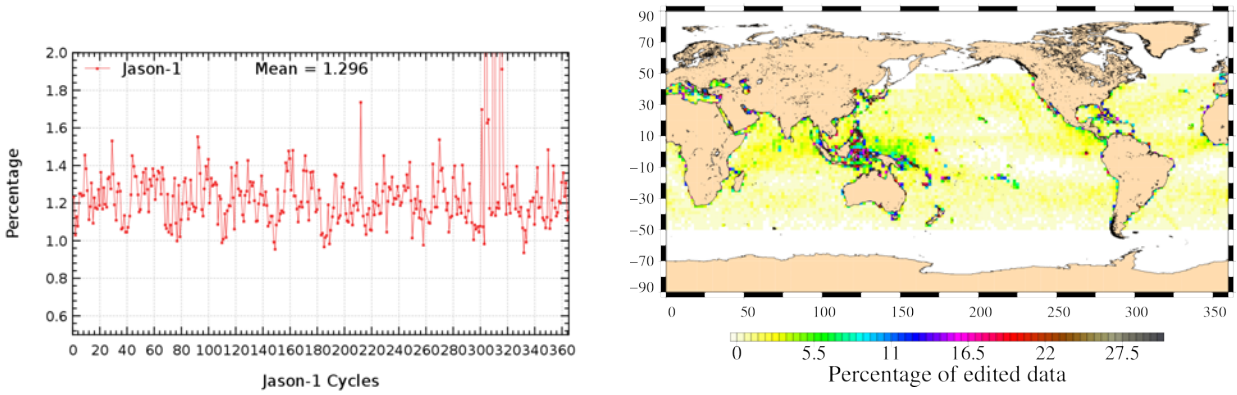

Figure 8: *Cycle per cycle percentage of edited measurements by 20-Hz measurements number criterion (left). Right: Map of percentage of edited measurements by 20-Hz measurements number criterion over an one-year period (cycles 329 to 365).*

3.2.7. Threshold criteria: 20-Hz measurements standard deviation

The percentage of edited measurements due to 20-Hz measurements standard deviation criterion is shown in left of figure 9. The observed annual signal is linked to the seasonal variability associated with ice coverage. After removing the annual signal and not taking into account cycles which were impacted by very high mispointing (figure 9 right), no trend is visible.

Figure 9 (right part) shows a map of measurements edited by the 20-Hz measurements standard deviation criterion. Besides editing due to measurements at default value, edited measurements are mainly correlated with wet areas.

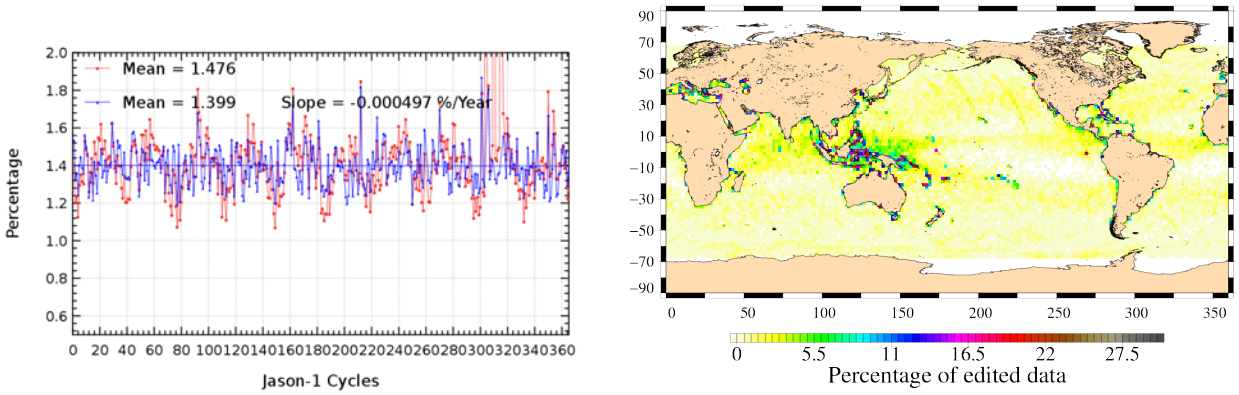

Figure 9: *Cycle per cycle percentage of edited measurements by 20-Hz measurements standard deviation criterion with and without annual signal (left) , Map of percentage of edited measurements by 20-Hz measurements standard deviation criterion over an one-year period (cycles 329 to 365) (right).*

3.2.8. Threshold criteria: Significant wave height

The percentage of edited measurements due to significant wave height criterion is represented in figure 10. It is about 0.71%. No drift has been detected over the Jason-1 period. Peaks visible for cyles 304 to 316 are due to altimeter parameters at default values caused by very high mispointing. Smaller peaks visible for cycles 212 and 224 are also due to a portion of a pass at default values. The effect is barely visible on the global rejected measurements figure 7 for cycle 212, and unseen for cycle 224, because of the weak impact of the SWH criterion with regard to the global rejection criteria. Figure 10 (right part) shows that measurements edited by SWH criterion are especially found near coasts in the equatorial regions. Three portions of edited passes are visible in North Pacific. They belong to cycle 350. One of the few cycles during 2011, when star tracker had low availability and caused default values for altimeter parameters.

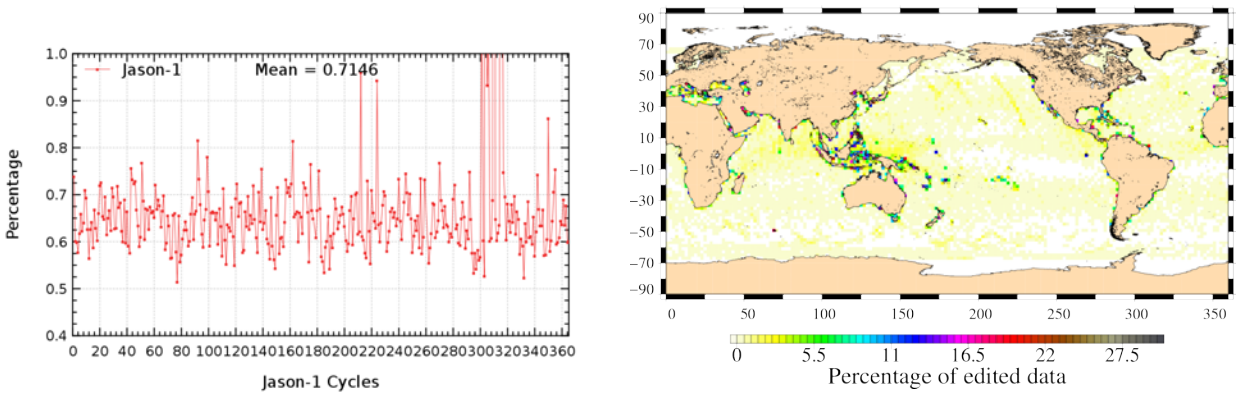

Figure 10: *Left: Cycle per cycle percentage of edited measurements by SWH criterion. Right: Map of percentage of edited measurements by SWH criterion over an one-year period (cycles 329 to 365).*

3.2.9. Backscatter coefficient

The percentage of edited measurements due to backscatter coefficient criterion is represented in figure 11. It is about 0.67% and shows no drift. The peaks visible for cycles 212 and 224 are due to a portion of a pass at default values. This is also the case for the peaks of cycles 304 to 316. The right part of figure 11 shows that measurements edited by backscatter coefficient criterion are especially found near coasts in the equatorial regions, besides of passes with altimeter parameters at default values.

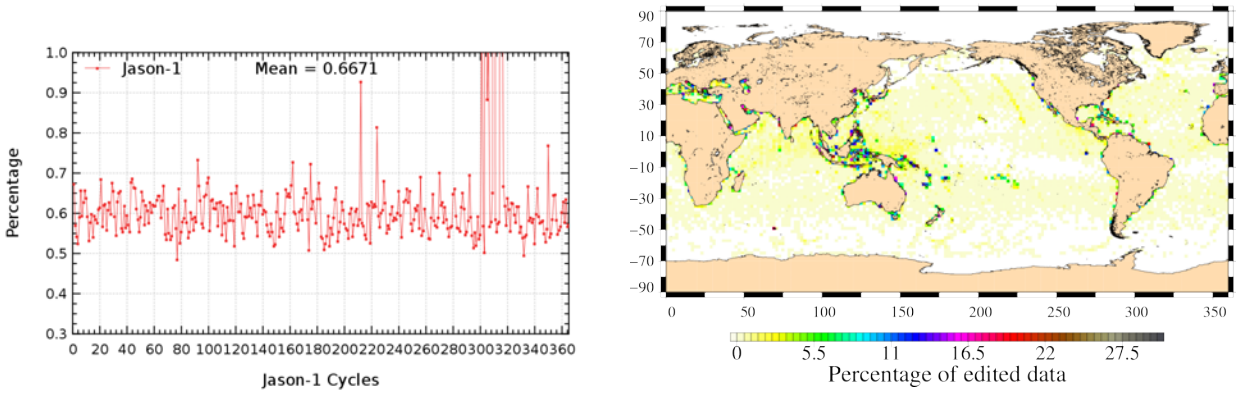

Figure 11: *Cycle per cycle percentage of edited measurements by Sigma0 criterion (left). Right: Map of percentage of edited measurements by Sigma0 criterion over an one-year period (cycles 329 to 365).*

3.2.10. Radiometer wet troposphere correction

The percentage of edited measurements due to radiometer wet troposphere correction criterion is represented in figure 12. It is about 0.15%. When removing cycles which experienced problems, percentage of edited measurements drops to 0.05%. The figure shows irregular oscillations which are not correlated to annual cycle. The map 12 shows that only few measurements are edited by radiometer wet troposphere correction criterion.

Notice that for some cycles the percentage of edited measurements is higher than usual. This is often linked to the Jason safe hold mode on some of these cycles (69, 78, 137, 179, 284 and 316): the radiometer has been set on 2 hours later than the altimeter. As a result, the radiometer wet troposphere correction has been set to default value during this period and these measurements have been edited.
Since cycle 280, there seems to be a slight increase of edited measurements. This is under investigation.

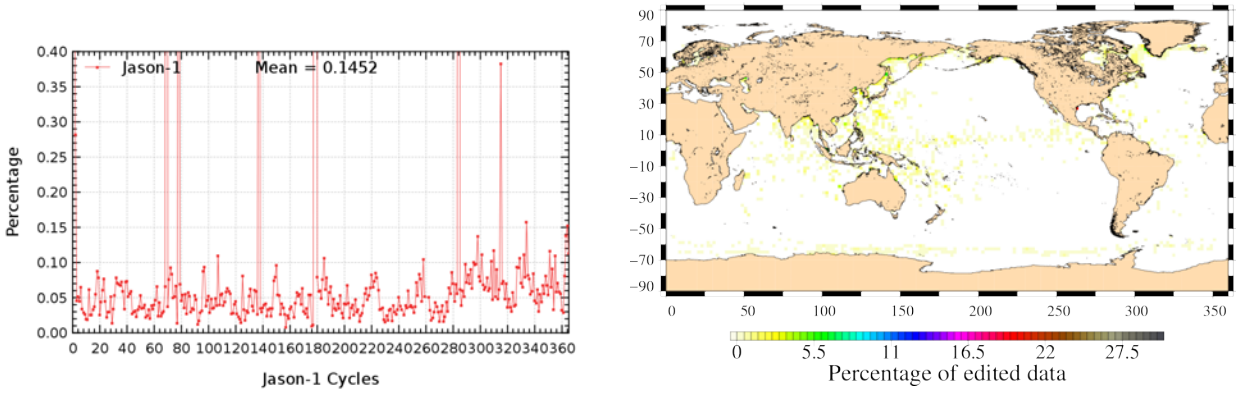

Figure 12: *Cycle per cycle percentage of edited measurements by radiometer wet troposphere criterion (left). Map of percentage of edited measurements by radiometer wet troposphere criterion over an one-year period (cycles 329 to 365).*

3.2.11. Dual frequency ionosphere correction

The editing procedure is applied to the dual frequency ionosphere correction as it is available in the GDR products (before filtering). The percentage of edited measurements due to dual frequency ionosphere correction criterion is represented in figure 13. It is about 1.26% and shows no drift. The map 13 shows that measurements edited by dual frequency ionosphere correction are mostly found in equatorial regions.
Notice that for cycles 9, 91, 102, 103, 108, 115, 133, 173, 198, 212, 301, 304-306, 310, 315 and 316 the percentage of edited measurements is higher than usual. Till cycle 198, this is linked to an altimeter SEU occurred on these cycles. The dual frequency ionospheric correction is not available during a few hours following the altimeter incidents (lack of C-band parameters requirering ground TC to resume nominal configurations). Peaks from cycle 212 onwards are mostly due to altimeter parameters at default value related to very high mispointing (see section 3.2.6.).

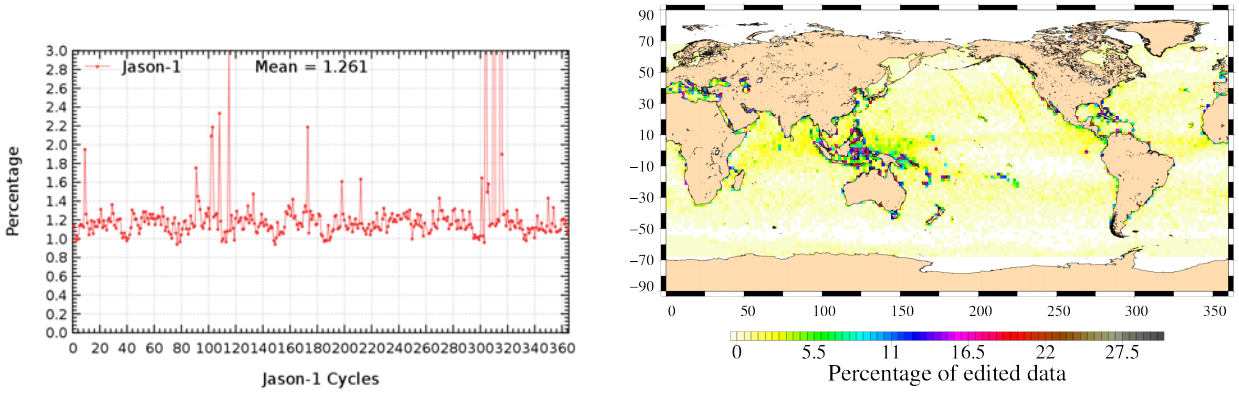

Figure 13: *Cycle per cycle percentage of edited measurements by (non-smoothed) dual frequency ionosphere criterion (left). Map of percentage of edited measurements by dual frequency ionosphere criterion over an one-year period (cycles 329 to 365).*

3.2.12. Square off-nadir angle

The percentage of edited measurements due to square off-nadir angle criterion is represented in figure 14. It is about 0.68%. During 2010, Jason-1 experienced very high off-nadir angles due to low star tracker and gyro performances, especially for period between cycles 304 and 316. Mispointing was greatly improved end of 2010. During 2011, there were only a couple of cycles impacted by increased mispointing values. The map 14 shows that besides periods of low star tracker performances (cycle 338/pass 228 (South Atlantic), cycle 339/pass 088 (south of Australia), cycle 350/passes 004,006,032 (North Pacific)), edited measurements are mostly found in coastal regions.

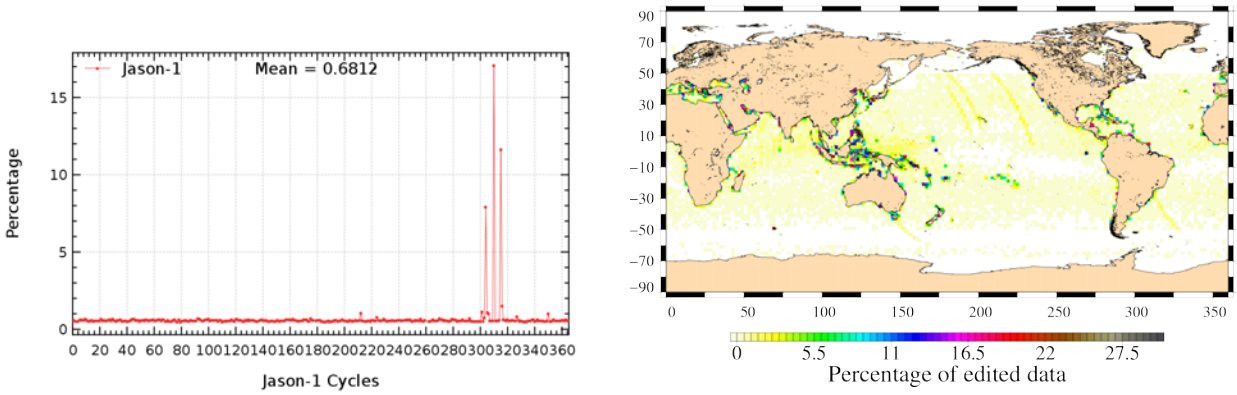

Figure 14: *Cycle per cycle percentage of edited measurements by square off-nadir angle criterion (left). Right: Map of percentage of edited measurements by square off-nadir angle criterion over an one-year period (cycles 329 to 365).*

3.2.13. Altimeter wind speed

The percentage of edited measurements due to altimeter wind speed criterion is represented in figure 15. It is about 1.08% and shows no drift. Measurements are generally edited, because they have default values, as happened due to very high mispointing for period between cycles 304 to 316. Otherwise, this is the case when sigma0 itself is at default value, or when it shows very high values (higher than 25 dB), which occur during sigma bloom and also over sea ice. The annual cycle is probably due to sea ice, which was not detected by the ice flag.

Note that percentage of edited altimeter wind speed is higher than that of edited sea state bias. This is very likely related to the fact, that in ground processing software, slightly negative altimeter wind speed values may occur, for which a sea state bias value is computed. Nevertheless in binary Jason-1 GDR product, the slightly negative wind speed values are replaced by the default value.

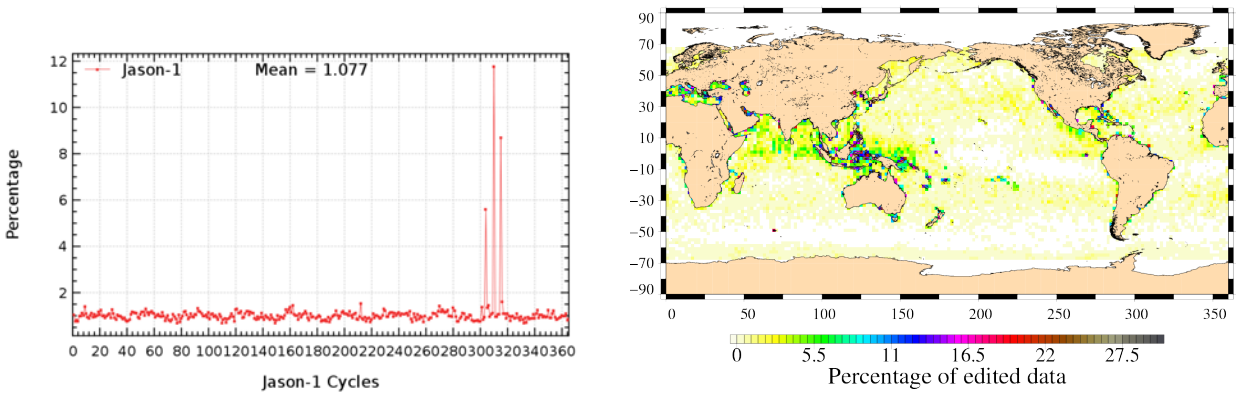

Figure 15: *Cycle per cycle percentage of edited measurements by altimeter wind speed criterion (left). Right: Map of percentage of edited measurements by altimeter wind speed criterion over an one-year period (cycles 329 to 365).*

3.2.14. Sea state bias correction

The percentage of edited measurements due to sea state bias correction criterion is represented in figure 16. The percentage of edited measurements is about 0.63% and shows no drift. But as other parameters, it was impacted by altimeter parameters at default values during period between cycles 304 and 316. The map 16 (right side) shows that edited measurements are mostly found in equatorial regions near coasts.
The map 16 showing percentage of measurements edited by sea state bias criterion is highly correlated with the map 15.

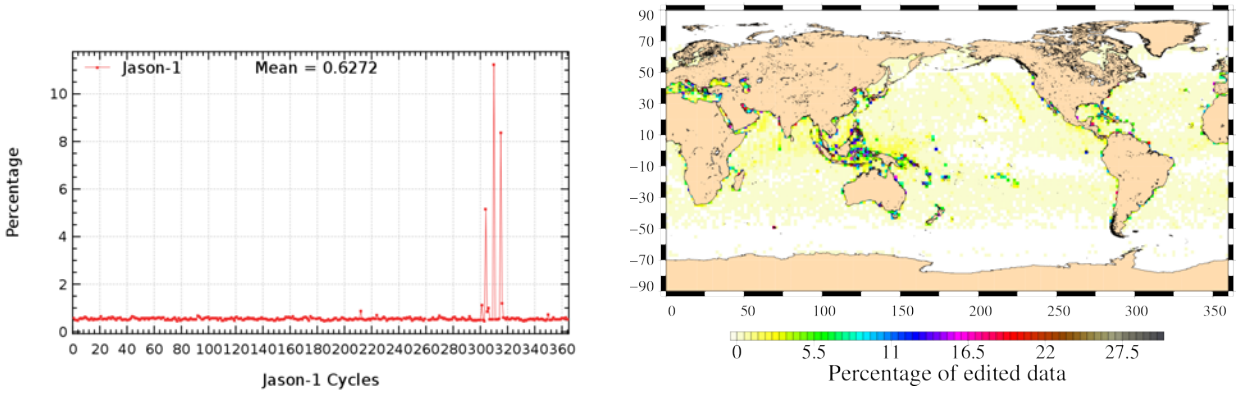

Figure 16: *Cycle per cycle percentage of edited measurements by sea state bias criterion (left). Right: Map of percentage of edited measurements by sea state bias criterion over an one-year period (cycles 329 to 365).*

3.2.15. Ocean tide correction

The percentage of edited measurements due to ocean tide correction criterion is represented in figure 17. It is about 0.06% and shows no drift. The ocean tide correction is a model output, there should therefore be no edited measurements. Indeed there are no measurements edited in open ocean areas, but only very few near coasts or in lakes or rivers (see map 17). These measurements are mostly at default values.
Generally approximatively the same amount of measurements is edited by ocean tide correction for each cycle. The small annual signal visible in figure 17 comes from the seasonal fluctuation of available ocean data (due to seasonal fluctuation of sea ice coverage).

A slight decrease in edited measurements is visible since cycle 262 (change of Jason-1 ground-track). This is related to the new ground track, which no longer overflows the same areas.

3.2.16. Sea surface height

The percentage of edited measurements due to sea surface height criterion is represented in figure 18. It is about 0.94% and shows no drift. There is however an annual signal visible. For the peaks see section 3.2.12.
Besides anomalies due to poor star tracker and gyro performances, the measurements edited by sea surface height criterion are mostly found near coasts in equatorial regions (see map 18).

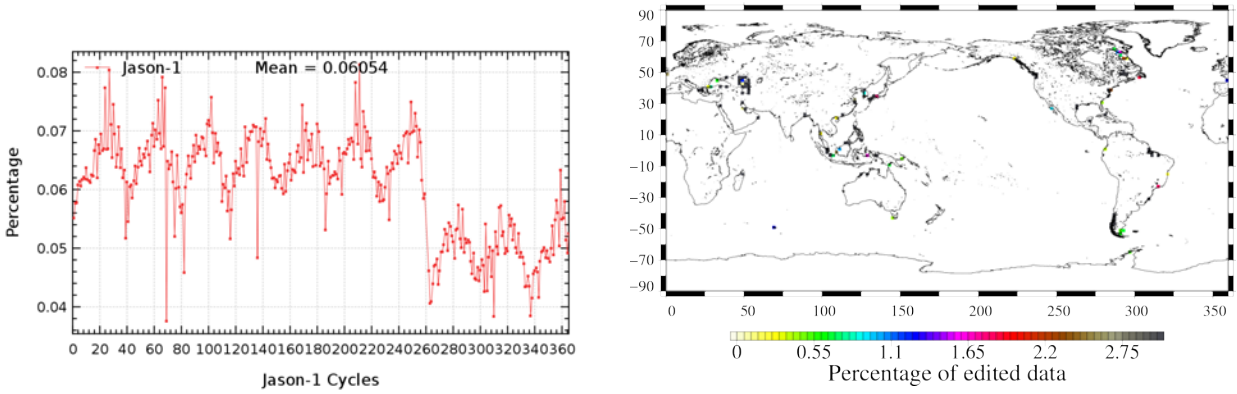

Figure 17: *Cycle per cycle percentage of edited measurements by ocean tide criterion (left). Right: Map of percentage of edited measurements by ocean tide criterion over an one-year period (cycles 329 to 365).*

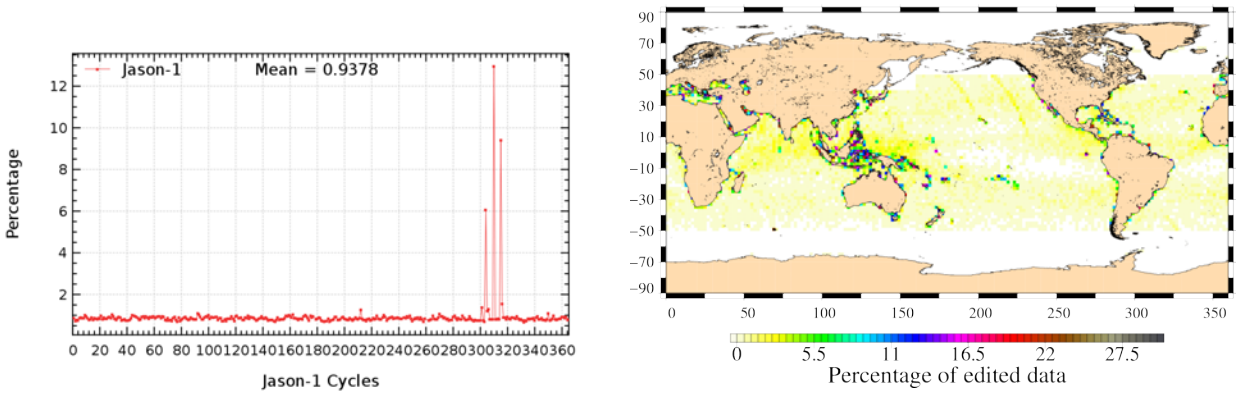

Figure 18: *Cycle per cycle percentage of edited measurements by sea surface height criterion (left). Right: Map of percentage of edited measurements by sea surface height criterion over an one-year period (cycles 329 to 365).*

3.2.17. Sea level anomaly

The percentage of edited measurements due to sea level anomaly criterion is represented in figure 19. It is about 1.18% and shows no drift. The graph is quite similar to the one in figure 7 (showing the percentage of measurements edited by all the threshold criteria), as the SLA clip contains many of the parameters used for editing.
Whereas the map in figure 19 allows us to plot the measurements edited due to sea level anomaly out of thresholds (after applying all other threshold criteria). These are generally only very few measurements.

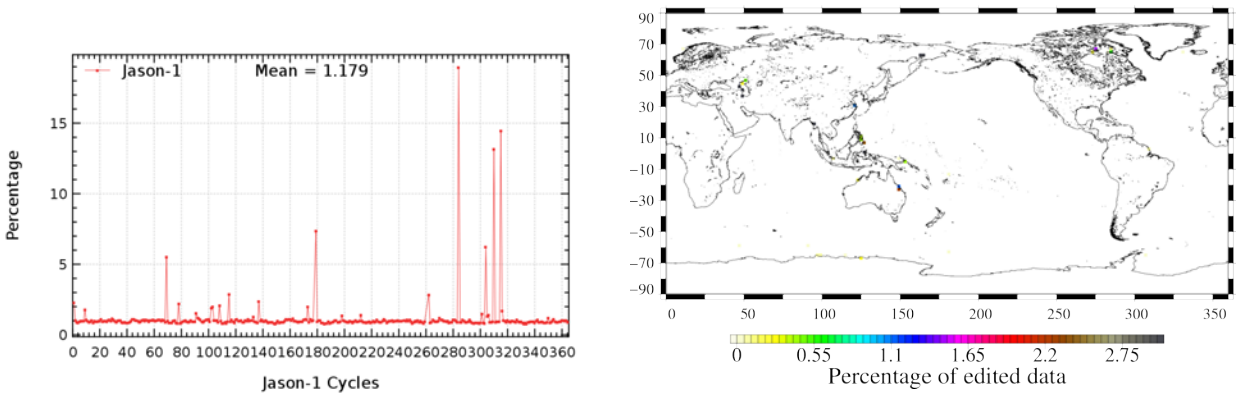

Figure 19: *Cycle per cycle percentage of edited measurements by sea level anomaly criterion (left). Right: Map of percentage of edited measurements by sea level anomaly criterion (after applying all other threshold criteria) over an one-year period (cycles 329 to 365).*

4. Monitoring of altimeter and radiometer parameters

4.1. Methodology

Both mean and standard deviation of the main parameters of Jason-1 have been monitored since the beginning of the mission. Moreover, a comparison with T/P parameters has been performed: it allows us to monitor the bias between the parameters of the 2 missions. The comparison is done till the end of scientific mission of T/P, which occurred during Jason-1 cycle 138. Two different methods have been used to compute the bias:

- During the verification phase, Jason-1 and T/P are on the same ground track and are spaced out about 1 minute apart. The mean of the T/P − Jason-1 differences can be computed using a point by point repeat track analysis.
- From cycle Jason-1 22 (Cycle T/P 365), the 15th of August 2002, a maneuver sequence was conducted over 30 days to move T/P to the new Tandem Mission orbit : further on T/P was located one half of the TP/Jason-1 track spacing to the West of Jason-1. Geographical variations are then too strong to directly compare Jason-1 and T/P parameters on a point by point basis. Therefore cycle per cycle differences have been carried out to monitor Jason-1 and T/P differences, but data gaps on both satellites have been taken into account.

For comparison between Jason-1 and Jason-2 please see annual Jason-2 report ([84]).

4.2. 20 Hz Measurements

The monitoring of the number and the standard deviation of 20 Hz elementary range measurements used to derive 1 Hz data is presented here. These two parameters are computed during the altimeter ground processing. Before a regression is performed to derive the 1 Hz range from 20 Hz data, a MQE criterion is used to select valid 20 Hz measurements. This first step of selection thus consists in verifying that the 20 Hz waveforms can be effectively approximated by a Brown echo model (Brown, 1977 [19]) (Thibaut et al. 2002 [100]). Through an iterative regression process, elementary ranges too far from the regression line are discarded until convergence is reached. Thus, monitoring the number of 20 Hz range measurements and the standard deviation computed among them is likely to reveal changes at instrumental level.

4.2.1. 20 Hz measurements number in Ku-Band and C-Band

Figure 20 shows the cycle per cycle mean of 20-Hz measurements number in Ku-Band (on the left) and C-Band (on the right). A very weak seasonal signal is visible, furthermore a weak negative trend is visible for C-Band.

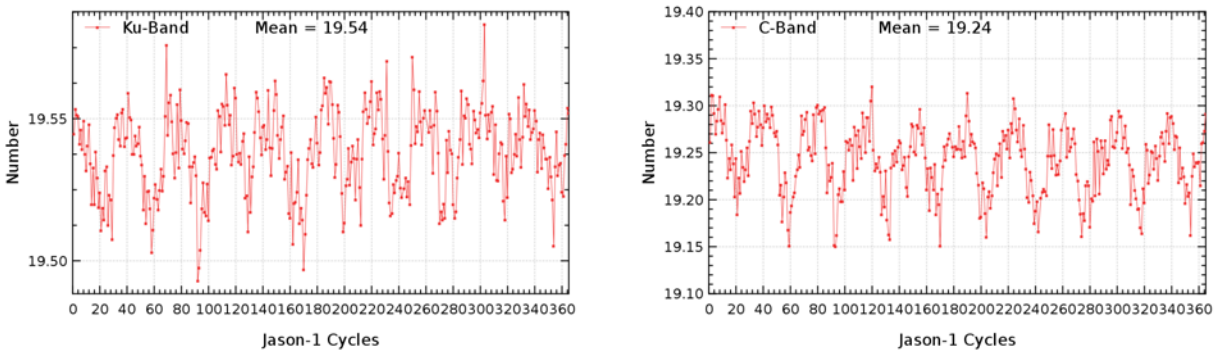

Figure 20: *Cycle per cycle mean of 20-Hz measurements number in Ku-Band (left) and C-Band (right)*

4.2.2. 20 Hz measurements standard deviation in Ku-Band and C-Band

Figure 21 shows the cycle per cycle standard deviation of the 20 Hz measurements in Ku-Band (on the left) and C-Band (on the right). Apart from a weak seasonal signal, neither trend nor any anomaly has been detected. Moreover, since integration is done over less waveforms, values of C-Band standard deviation of the 20 Hz measurements are higher than those of Ku-Band, which leads to an increased noise.

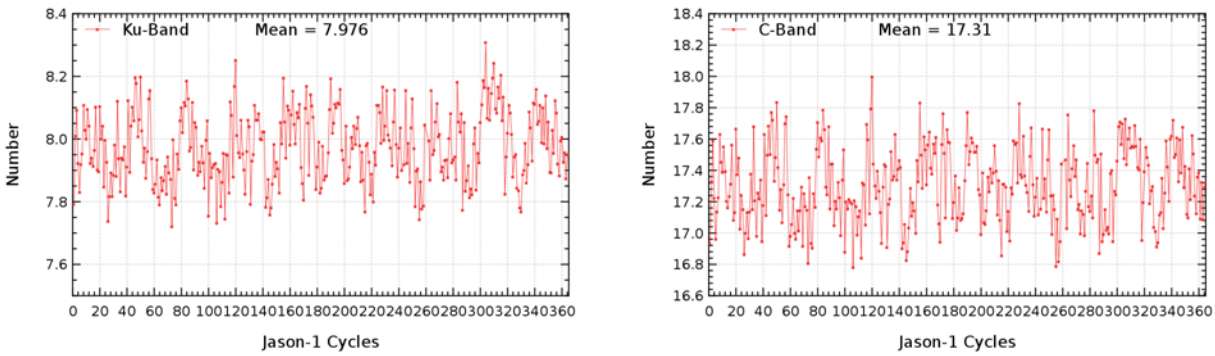

Figure 21: *Cycle per cycle mean of 20-Hz measurements standard deviation in Ku-Band (left) and C-Band (right)*

4.3. Off-Nadir Angle from waveforms

The off-nadir angle is estimated from the waveform shape during the altimeter processing. The square of the off-nadir angle, averaged in a one-cycle basis, has been plotted in figure 22. The mean values are slightly positive. This mean value is not significant in terms of actual platform mispointing. In fact squared attitude is what is retrieved from waveforms, not attitude. During the first third of the mission off-nadir angles are low and quite stable, except for cycle 69 related to a platform safehold mode. Between cycles 100 and 200, the off-nadir angle slightly increases and reaches more often strong values and since cycle 200 it is disturbed with one half of very strong values. Indeed, there are periods where the combination of low Beta angles and Sun glint or Moon in field of view significantly reduces the tracking performance of both star trackers, especially during fixed-yaw. Previously, in GDR version "a", when the off-nadir angle was larger than the 0.2 degree specification, error was introduced in the altimeter parameters as the off nadir was not taken into account in the ground processing (Vincent et al., 2003). Thus, an improvement of the retracking algorithm was made since GDR version "b" ([13]), to correct for estimations of altimeter parameters for mispointing angle errors up to 0.8 deg. (Amarouche et al. 2004 [15]).

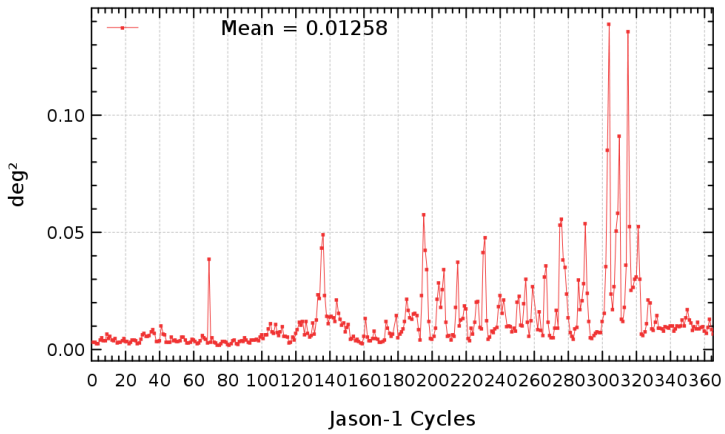

Figure 22: *Cycle mean of the square of the off-nadir angle deduced from waveforms (deg^2).*

During years 2008 and 2009, the satellite has experienced several severe mispointing cases, although the mispointing values remained within the threshold editing criteria (-0.2 to $0.64 deg^2$). This feature has been repeatedly pointed out, especially after maneuvers. Neither specific geographic pattern nor ascending/descending tracks systematism are observed. The high mispointing values are related to low star tracker availability and gyro wheels behavior. During 2010, off-nadir angles were particularly high, leading even to altimeter lost of track. Since the end of 2010 thanks to improvements of star tracker performances and switch over, mispointing is again quite low.

4.4. Significant wave height

4.4.1. Ku-band SWH

Jason-1 and T/P Ku SWH are compared in terms of global statistics in figure 23: cycle means and standard deviations of both missions are presented in a cycle basis, as well as mean differences between T/P and Jason-1. Global variations of the SWH statistics are the same on the two missions. A weak annual signal is visible. Jason-1 SWH shows almost no drift on the whole altimeter time period. The (TOPEX - Jason-1) SWH bias is about 5.4 cm. The estimate of the (Poseidon-1 - Poseidon-2) SWH difference is about 12 cm for Poseidon-2 cycle 18 not plotted here.
The standard deviation of Ku-band SWH shows an annual signal related to geophysical conditions for both Jason-1 and T/P data.

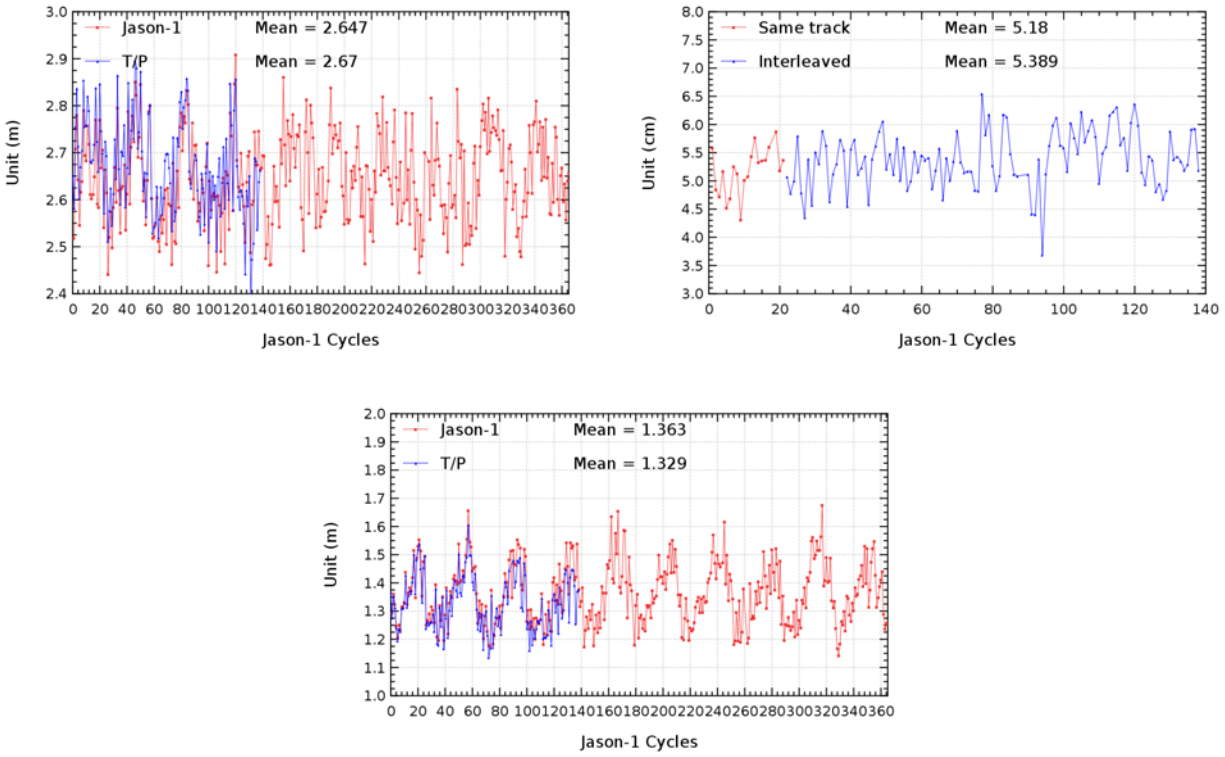

Figure 23: *Cycle per cycle mean (left), T/P−Jason mean differences (right), and standard deviation (bottom) of Ku-band SWH*

4.4.2. C-band SWH

Figure 24 shows global statistics of Jason-1 and T/P C-band SWH. The cycle per cycle mean of both missions shows a small annual signal (figure 24 top left). Jason-1 and T/P values are quite similar. The (TOPEX - Jason-1) C-band SWH mean bias is about 8 cm (figure 24 top right), with a drift of about -2 mm/yr. Moreover, the standard deviation of the C-band SWH is quite similar on both missions, showing an annual signal.

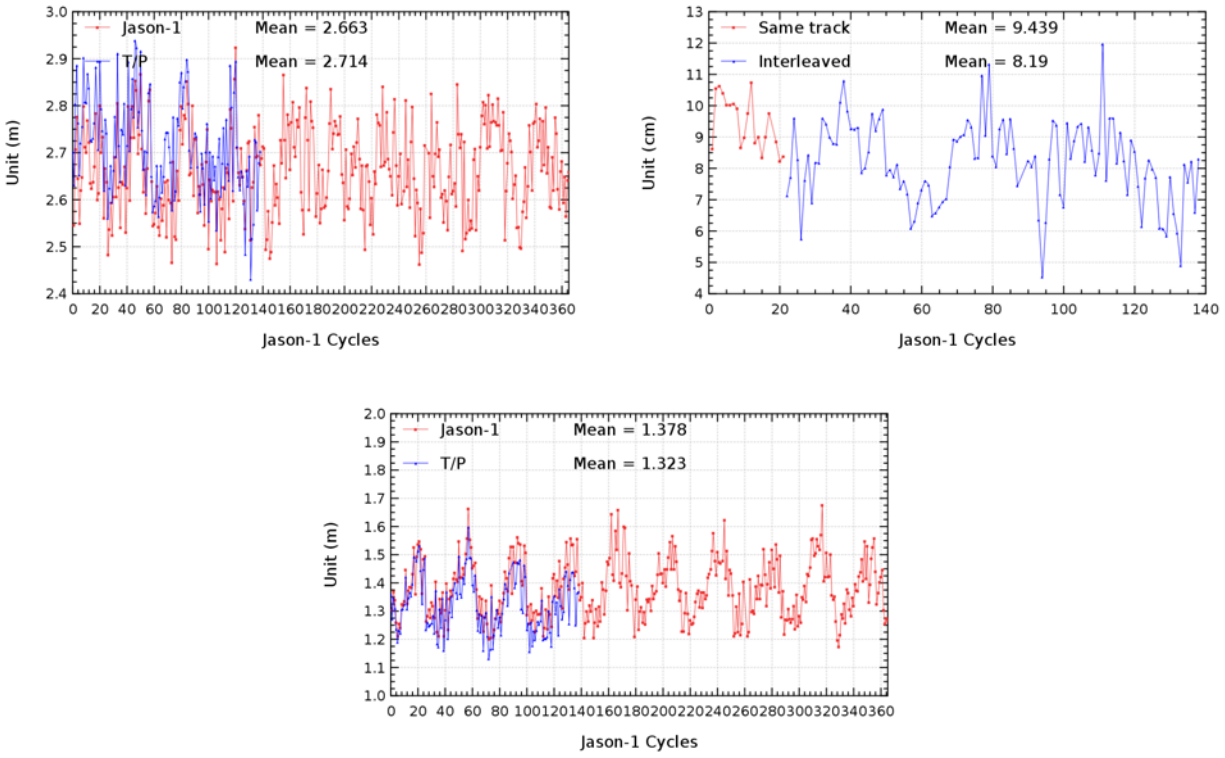

Figure 24: *Cycle per cycle mean (left), T/P−Jason mean differences (right), and standard deviation (bottom) of C-band SWH*

4.5. Backscatter coefficient

4.5.1. Ku-band Sigma0

The cycle per cycle mean (figure 25: top panel on the left) for Jason-1 (red curve) Ku-band sigma0 is coherent with the TOPEX mean (blue curve). A small drift is visible for Jason-1. It is mostly due to geophysical evolutions, but also due to small sigma0 anomalies (see also chapter 8.3. and [14]). In order to compare sigma0 parameters from both missions and keep a significant dynamic scale, TOPEX Ku-Sigma0 is biased by a 2.26 dB value to align TOPEX with the Jason-1 uncalibrated Sigma0. The bias between the two corrections (figure 25: top panel on the right) is quite stable about -2.5 dB.

Besides, the absolute bias is higher than usual from T/P cycle 433 to 437 (J1 cycles 90 to 94) by 0.1 dB : this is due to the TOPEX Sigma0. Indeed, the satellite attitude was impacted by a pitch wheel event linked to the T/P safe-hold mode occurred on cycle T/P 430 (see electronic communication : T/P Daily Status (26/07/2004)). This anomaly has probably biased the TOPEX sigma0 during this period. The T/P - Jason-1 backscattering difference is after this period slightly lower than before. This is probably also related to T/P (see figure comparing Topex altimeter wind speed and ERA-Interim wind speed in [14]). Jason-1 and T/P curves on bottom panel, showing the standard deviation differences, are very similar .

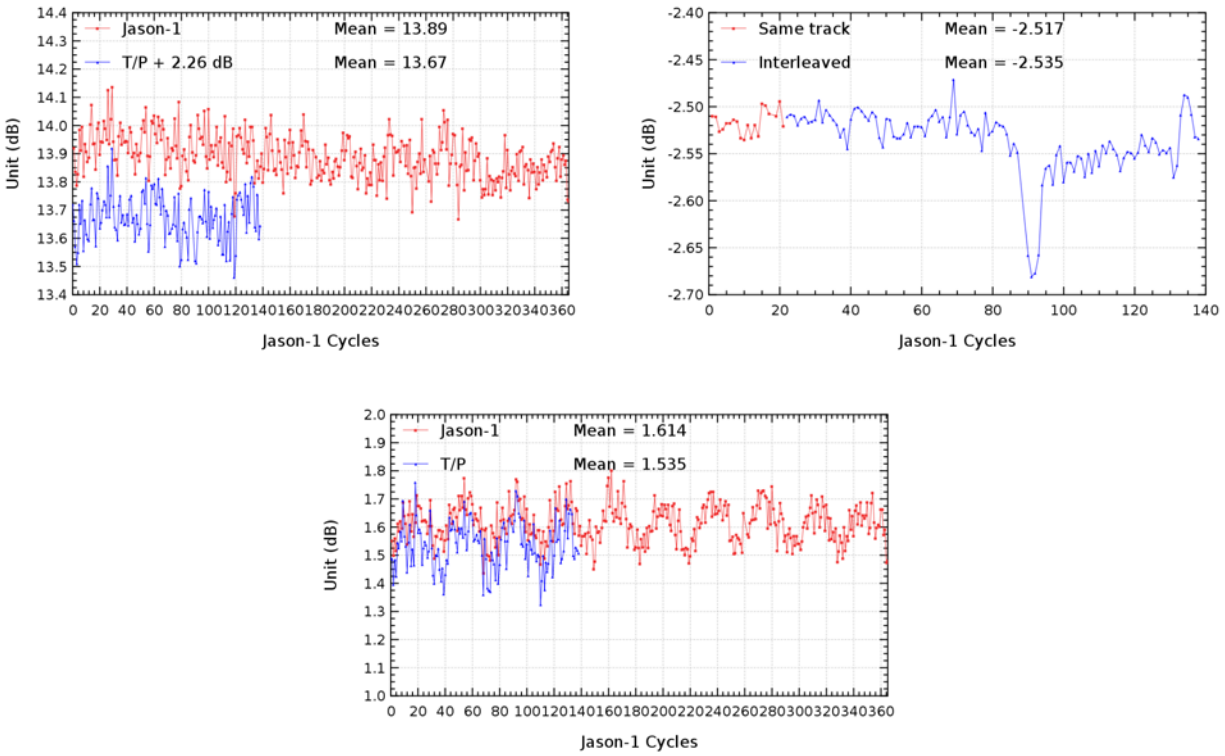

Figure 25: *Cycle per cycle mean (left), T/P−Jason mean differences (right), and standard deviation (bottom) of Ku-band SIGMA0*

4.5.2. C-band Sigma0

The cycle per cycle mean (figure 26: top panel on the left) for Jason-1 (red curve) Ku-band sigma0 is coherent with the TOPEX mean (blue curve). The bias between the two corrections (figure 26: top panel on the right) decreases from -0.6 dB to -0.8 dB. This is due to the T/P C-band Sigma0 (Ablain et al. 2004 [5]).
Note that in science processing software a bias of approximately -0.28 dB is applied to the provided C-Band Sigma0 for any geophysical algorithms that require use of sigma0. Standard deviation of C-band sigma0 (figure 26: bottom) has similar values for both missions and shows an annual signal.

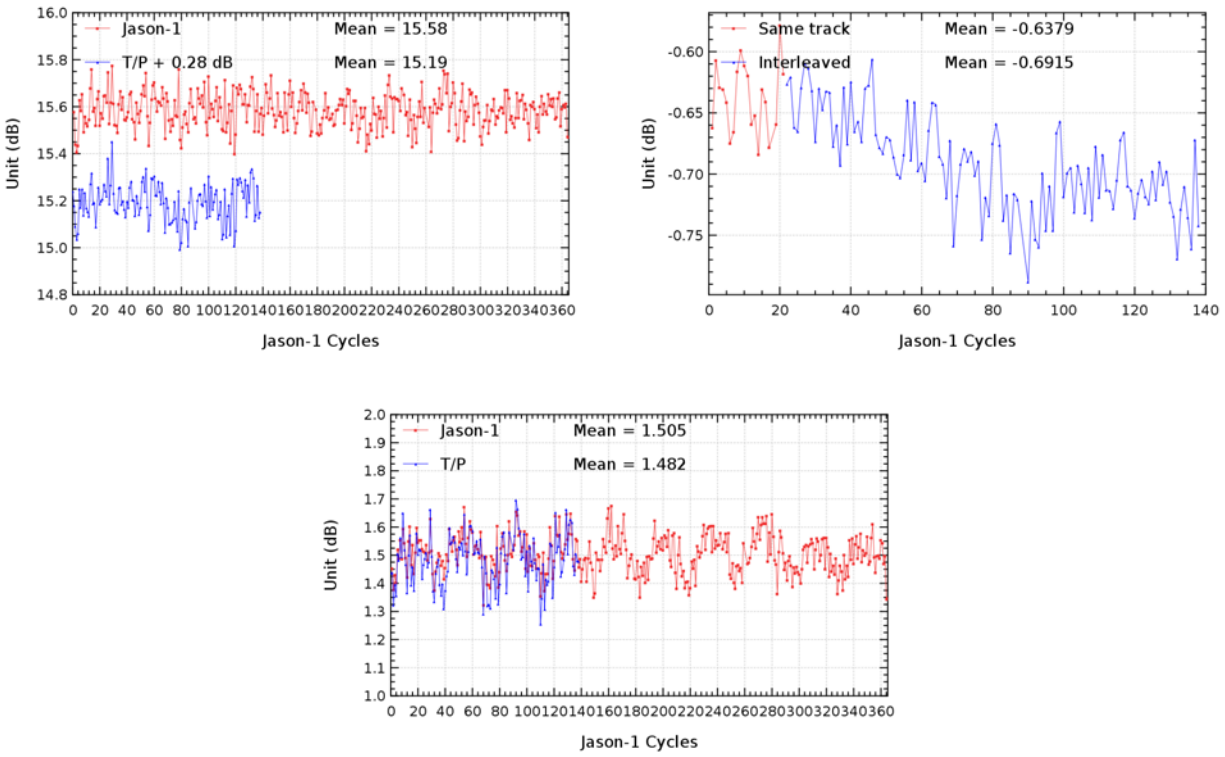

Figure 26: *Cycle per cycle mean (left), T/P−Jason mean differences (right), and standard deviation (bottom) of C-band SIGMA0*

4.6. Ionosphere correction

4.6.1. Dual-frequency ionosphere correction

The dual frequency ionosphere corrections derived from the TOPEX and Jason-1 altimeters have been monitored and compared in the same way (figure 27). The mean difference between TOPEX and Jason-1 estimates is about 1.5 mm, with cycle to cycle variations lower than 2 mm. There is nevertheless a small visible drift of 0.3 mm/yr. Both corrections are very similar and vary according to the solar activity. Note that, as for TOPEX (Le Traon et al. 1994 [66]), it is recommended to filter the Jason-1 dual frequency ionosphere correction before using it as a SSH geophysical correction (Chambers et al. 2002 [26]). A low-pass filter has thus been used to remove the noise of the correction in all SSH results presented in the following sections. Note that in GDR-C product, the DORIS ionospheric correction is no longer available. It has been replaced by the GIM ionospheric correction (model), which displays better metrics than the DORIS' one.

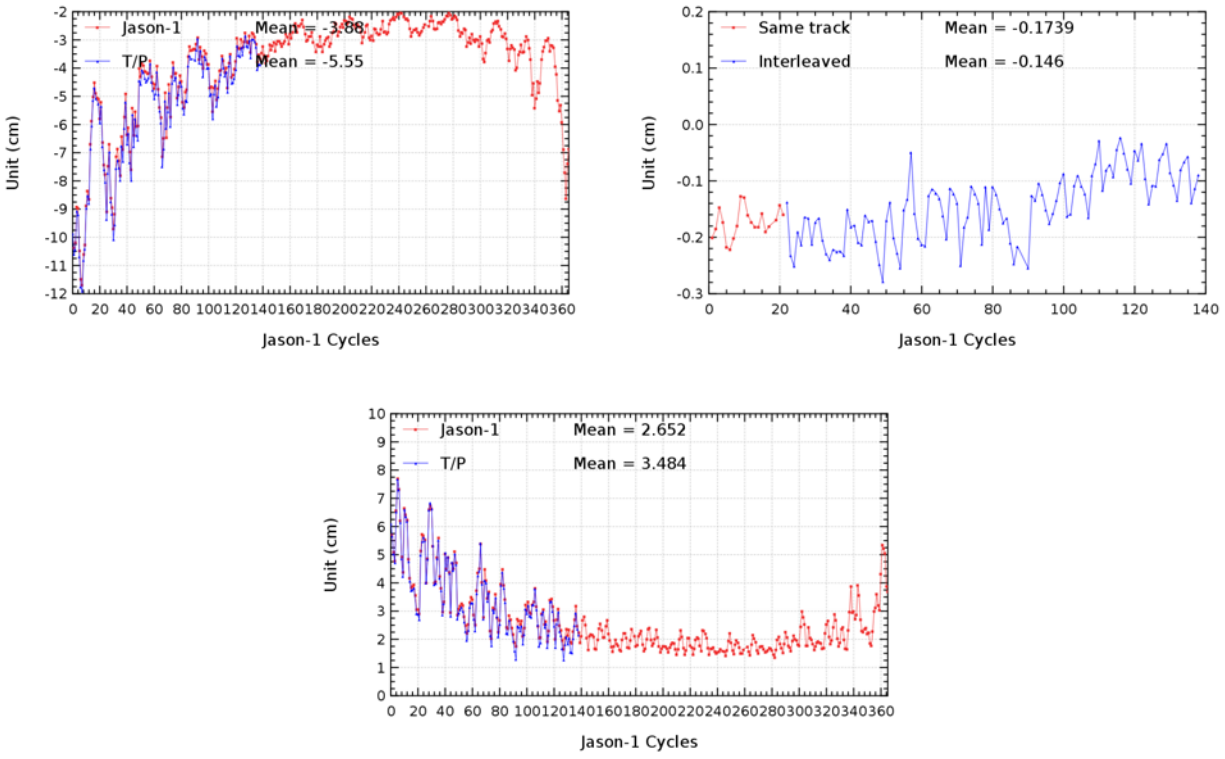

Figure 27: *Cycle per cycle mean (left), T/P−Jason mean differences (right), and standard deviation (bottom) of dual frequency ionosphere correction*

4.6.2. Comparison of GIM and filtered dual-frequency ionosphere corrections

Cycle by cycle statistics of the difference between filtered dual-frequency correction and gim correction are plotted on figure 28. The mean evolution (left part of the figure) shows first a decrease and then an increase of the correction differences with the minimum during year 2008, which is in accordance to the solar activity. The difference value stay under 1 cm over all the mission and the mean over the ten years is 0.12 cm.

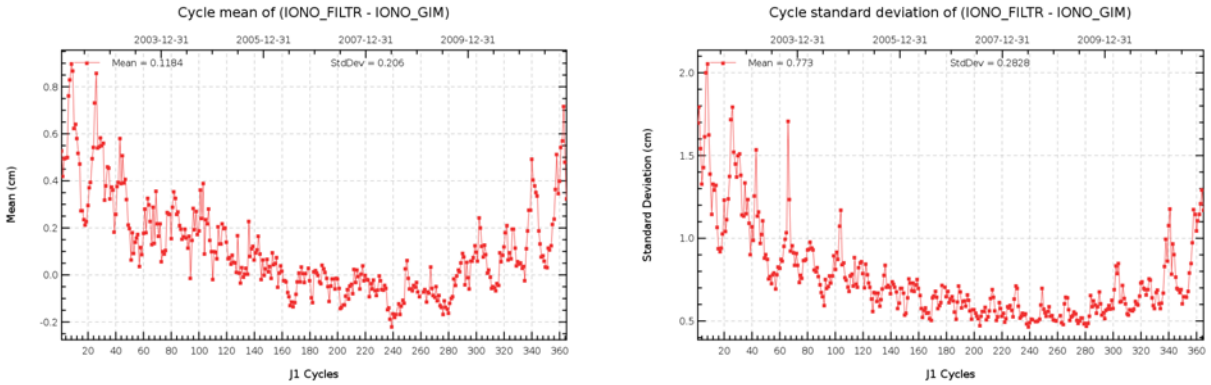

Figure 28: *Cycle per cycle mean (left), and standard deviation (right) of (filtered - gim) ionosphere correction difference*

In order to assess the evolution of the discrepancies between the two corrections, the mean differences have been computed according to several local time intervals of 4 hours. The computation has been performed through the entire mission. Each cycle gives an estimate of the mean difference between two solutions for every local time interval, it has been computed and leads to the results plotted on figure 29.
Higher level of differences is observed for local day time hours around 12:00 and differences are lower for night time hours. Furthermore, following the solar activity in both cases, the differences between corrections first decreased from the beginning of the mission and then has increased with a turn about year 2008 .

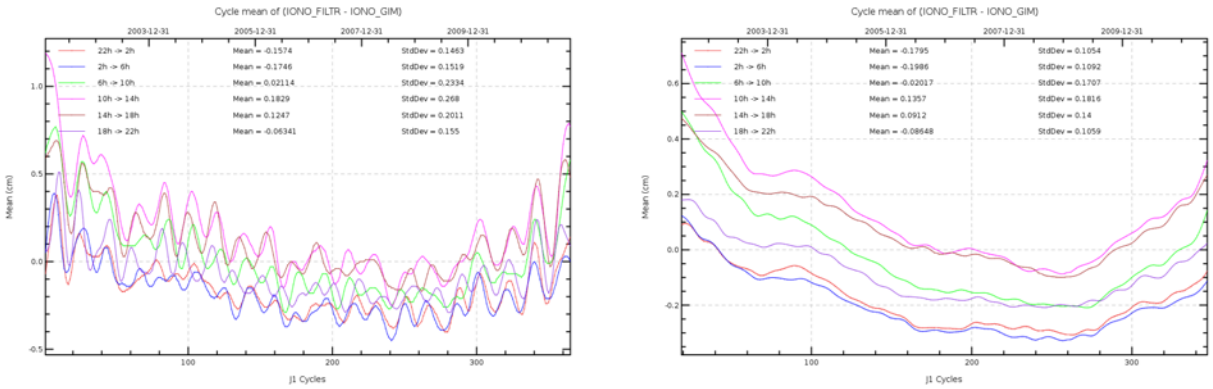

Figure 29: *Cycle per cycle mean of (filtered - gim) ionosphere correction difference as a function of local time, without smooth (left) and after smooth (right)*

4.7. JMR Wet troposphere correction comparison with ECMWF model

Wet troposphere correction is a very important variable for mean sea level trend calculation (see also [73]). Jason-1 satellite has beside the altimeter also a microwave radiometer (JMR) onboard in order to compute the radiometer wet troposphere correction. Furthermore ECMWF model wet troposphere correction is available in GDR products. Both corrections can be subject to jumps or drifts. Comparing both (as well as other radiometer corrections from e.g. Jason-2 or Envisat missions), can help to detect anomalies.
JMR is subject to jumps, or oscillations especially when thermal environment changes, such as after altimeter switch offs. Right side of figure 30 shows for instance oscillations of up to 7 mm just after August 2008 safe hold. These anomalies are generally corrected when GDR products are reprocessed. In the meanwhile, a JMR replacement product is available ([20]) which corrects for these instabilities. Furthermore, JMR continues to be sensitive to yaw maneuvers. Right side of figure 30 shows the daily monitoring of radiometer minus ECMWF model wet troposphere correction over 2011. On the other hand, ECMWF model is also subject to evolutions, which have an impact on wet troposphere correction. These evolutions are indicated by green lines in figure 30. A jump of several mm occurred after model version change of January 2002. The ECMWF model version change from 9th November 2010, induced a small jump of about 2 mm.

The improvements of the ECMWF model standards are visible on the standard deviation of wet troposphere correction difference (between radiometer and ECMWF model) which is shown on 30, left panel. At the beginning of 2003 standard deviation decreases from 1.4 cm to 1.1 cm. This corresponds to a model evolution. In the following, it continues to decrease. In 2009, an increase in standard deviation of radiometer minus ECMWF model wet troposphere differences (of about 0.1 cm) is noticeable. This corresponds to a model evolution on 10th March 2009 (see http://www.ecmwf.int/products/data/operationalsystem/evolution/evolution2009.html#10March2009). The model evolution of 9th November 2010 caused again a decrease of the standard deviation.

Behavior of wet troposphere correction is therefore continually monitored and comparison of the different radiometer and model wet tropospheric corrections are regularly done (see [63]).
On the right hand side of figure 30, a zoom is done on 2011 for the radiometer-ECMWF wet troposphere difference. It is strongly impacted by the yaw maneuvers and this impact seems to get stronger.

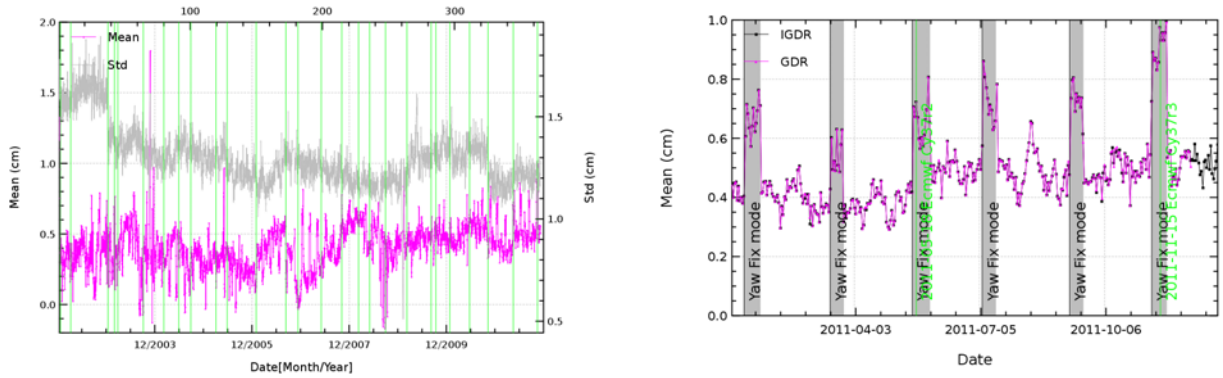

Figure 30: *Difference of radiometer and model wet tropospheric corrections. Left: daily mean and standard deviation over all the Jason-1 mission period. Right: Daily mean during 2011. Green lines indicate ECMWF model version changes, gray stripes indicate periods, where Jason-1 is in fix mode.*

5. Crossover analysis

Crossover differences are systematically analyzed to estimate data quality and the Sea Surface Height (SSH) performances. Furthermore, T/P crossover performances (as long as they were available) have been monitored in order to compare both performances. SSH crossover differences are computed on a one cycle basis, with a maximum time lag of 10 days, in order to reduce the impact of ocean variability which is a source of error in the performance estimation. The main SSH calculation for Jason-1 and T/P are defined below. For TOPEX, Jason-1 standards have been used for the tidal and atmospheric corrections.

$$SSH = Orbit - Altimeter\ Range - \sum_{i=1}^{n} Correction_i$$

with $Jason-1\ Orbit = POE\ CNES\ orbit$ and

$$\begin{aligned}
\sum_{i=1}^{n} Correction_i \;=\;& Dry\ troposphere\ correction : S1\ and\ S2\ atmospheric\ tides\ applied \\
&+ Combined\ high\ resolution\ dynamical\ atmospheric\ correction \\
&+ Radiometer\ wet\ troposphere\ correction \\
&+ Filtered\ dual\ frequency\ ionospheric\ correction \\
&+ Non\ parametric\ sea\ state\ bias\ correction \\
&+ Geocentric\ ocean\ tide\ height,\ GOT\ 2000 :\ S1\ atmospheric\ tide\ is\ applied \\
&+ Solid\ earth\ tide\ height \\
&+ Geocentric\ pole\ tide\ height
\end{aligned}$$

5.1. Mean crossover differences

The mean of crossover differences represents the average of SSH differences between ascending and descending passes. It should not be significantly different from zero. More importantly, special care is given to the geographical homogeneity of the mean differences at crossovers. The map of the Jason-1 crossover differences averaged over the whole period of available GDR (cycle 1 to 365) has been plotted in figure 31 (on the left). It is quite homogeneous. Nevertheless some geographically correlated patterns are visible (as it is also the case for Jason-2 [84]). Since GDR version "c", a new empirically correction, called pseudo_datation_bias_corr_ku is available in the products, which corrects for a bias between northern and southern hemisphere previously observable. The origin of this pseudo time tag bias was found by CNES [18].

The cycle mean of Jason-1 SSH crossover differences is plotted for the whole Jason-1 period in figure 31 (right).

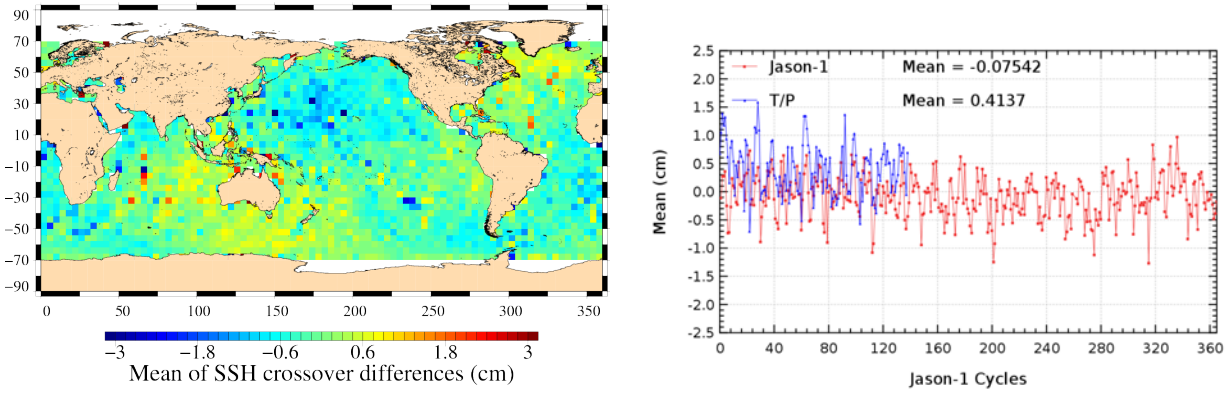

Figure 31: *Map of mean crossovers for Jason cycle 1 to 365 and cycle per cycle mean crossovers (right)*

5.2. Standard deviation of crossover differences

The cycle per cycle standard deviation of crossover differences are plotted in figure 32 (on the left) according to different crossover selections. 3 selections are applied:

- Red curve: no selection is applied. The mean value is 6.3 cm. It shows an annual signal linked to the sea ice extension variations in the Northern Hemisphere.
- Blue curve: shallow waters have been removed (bathy$\leq -1000m$). The previous annual signal has been removed by this selection even though a signal probably due to seasonal ocean variations remains.
- Green curve: the last selection allows monitoring the Jason-1 system performance. Indeed, areas with shallow waters (1000 m), of high ocean variability ($\geq 20cm$) and of high latitudes ($abs(lat) \geq 50$ degrees) have been removed. The standard deviation then provides reliable estimates of the altimeter system performances. In that case, no trend is observed in the standard deviation of Jason-1 SSH crossovers: good performances are obtained, with a standard deviation value of about 5.1 cm all along the mission.

The map of standard deviation of crossover differences overall the Jason-1 period, in figure 32 (on the right) shows usual results with high variability areas linked to ocean variability.

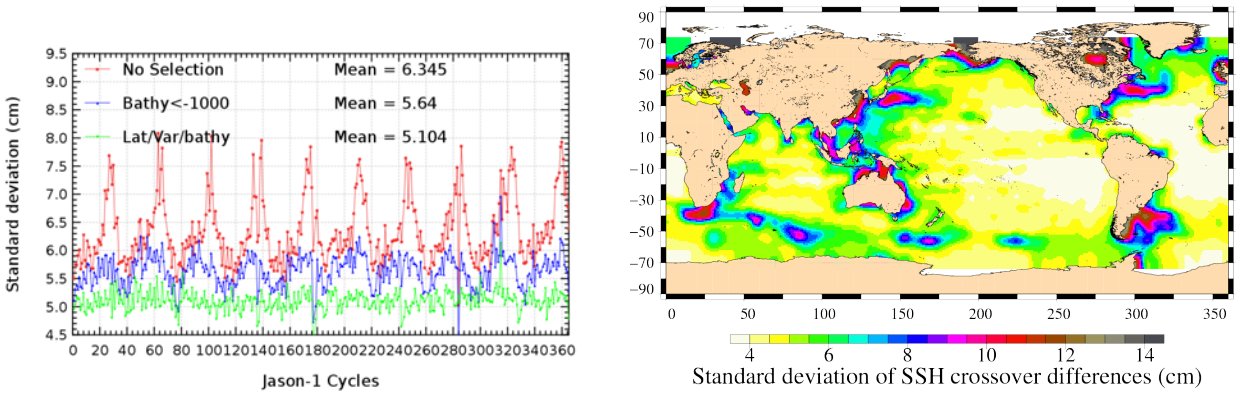

Figure 32: *Cycle per cycle standard deviation crossovers with different selections and map of Jason-1 standard deviation crossovers*

6. Along-track analysis

This analysis is used to compute Sea Level Anomalies (SLA) variability and thus to estimate data quality; it is used to determine the SSH bias between Jason-1 and T/P and the trend in the Mean Sea Level (MSL).

6.1. Along-track performances

6.1.1. Along-track performances on sea level anomaly

Along track analyzes are also used to assess the altimeter system performances, by computing Sea Level Anomalies (SLA). The SLA variance gives an estimate of the errors of the system, even though the ocean variability fully contributes in this case. A comparison between Jason-1 and T/P has been performed computing the variance of SLA relative to the MSS (CLS01). This allows global and direct calculations.
The SLA standard deviation is plotted in left side of figure 33 for Jason-1, Jason-2 and T/P. It exhibits similar and good performances for the satellites. After flight formation phases, SLA standard deviation increases for the satellite which is put on the interleaved ground track (T/P in 2002, Jason-1 in 2009). For TOPEX this is less visible, as its ground processing is different from the Jason's. Dorandeu et al. 2004 ([43]) shows that a clear increase in SLA standard deviation is visible for T/P interleaved ground-track when looking at wavelength shorter than 500km. This SLA standard deviation increase is due to the use of MSS CLS01 ([54]), as errors of this MSS are higher outside the historical T/P-Jason ground track ([43],[9]). Using a newer MSS, such as CNES/CLS 2011 ([97]) which also used data from the interleaved ground track, decreases Jason-1 SLA standard deviation significantly for interleaved period.

During summer and fall 2010 (around cycle 320), the SLA standard deviation has increased, not only for Jason-1, but also for Jason-2 and Envisat (not shown here). A part of this increase is probably related to "La Niña" episode occuring in Pacific ([107]). Focus on Pacific Ocean data (right side of figure 33) shows indeed an increase in SLA standard deviation until fall 2010, but also for second semester of 2011.

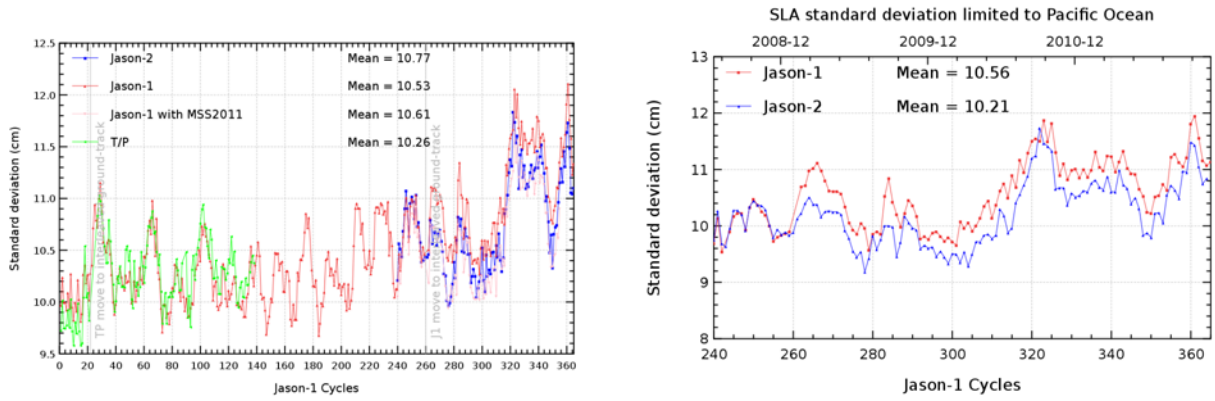

Figure 33: *Cycle per cycle SLA standard deviation. Left: showing T/P, Jason-1 and Jason-2 over whole Jason-1 period. Right: showing Jason-1 and Jason-2 over Jason-2 period and only for Pacific Ocean.*

6.2. Jason-1 Mean sea level

6.2.1. Sea surface height estimate

The assessment of the mean sea level trend is important for climate change studies. MSL estimation from Jason-1 and T/P are plotted in figure 34 (on the left), after reduction of the relative bias between the two time series.
Several error sources can influence MSL evolution, one of them is the choice of wet troposphere correction. On the one hand ECMWF model wet troposphere correction might be influenced by model evolutions, on the other hand radiometer wet troposphere correction is influenced by yaw mode transitions or thermal instabilities after altimeter switch-off. Therefore MSL calculated with radiometer correction (red curve) and with model correction (green curve) are shown in figure 34. The results are obtained after area weighting (Dorandeu and Le Traon 1999 [38]). The figure shows good agreement between the two missions and demonstrates that the Jason-1 mission ensures continuous precise MSL monitoring as it was done for more than a decade by the T/P mission. On both missions, seasonal signals are observed. Moreover (on right side of figure 34 after adjusting annual and semi-annual signals), almost 60-day signals are also detected on Jason-1 and T/P series, with nearly the same amplitude. A source of error could be from the largest tidal constituents at twice-daily periods which alias at periods close to 60 days for Jason-1 and T/P (Marshall et al. 1995 [69]). Orbit errors in T/P altimeter series used to compute the tide solutions could also have contaminated these models (Luthcke et al. 2003 [68]). In this way, a study on the 58.74-day signal observed on the MSL derived from Jason-1&2 and TOPEX data has been performed in 2010 (see also chapter 8.1.). Moreover, using JMR or model wet troposphere correction has a slight impact on the slope of about 0.2 mm/year.

On figure 34 (right panel), annual and semi-annual signals have been adjusted. This allows to decrease the adjustment formal error for both satellites. The global MSL slopes for Jason-1 is almost 0.4mm/year lower than for T/P, but for Jason-1 the shown time period is more than six years longer than for T/P. Also, the MSL slope of Jason-1 shows a flattening at the end of 2006 and during 2007 (between cycles 183 and 219). Calibration with in-situ data (see section 7.5. and

more detailed in annual reports [113] and [64]) shows no drift of altimeter MSL. Therefore this flattening might be due to "La Niña" active during this period. It also shows a strong flattening during year 2011 (between cycles 326 and 359).

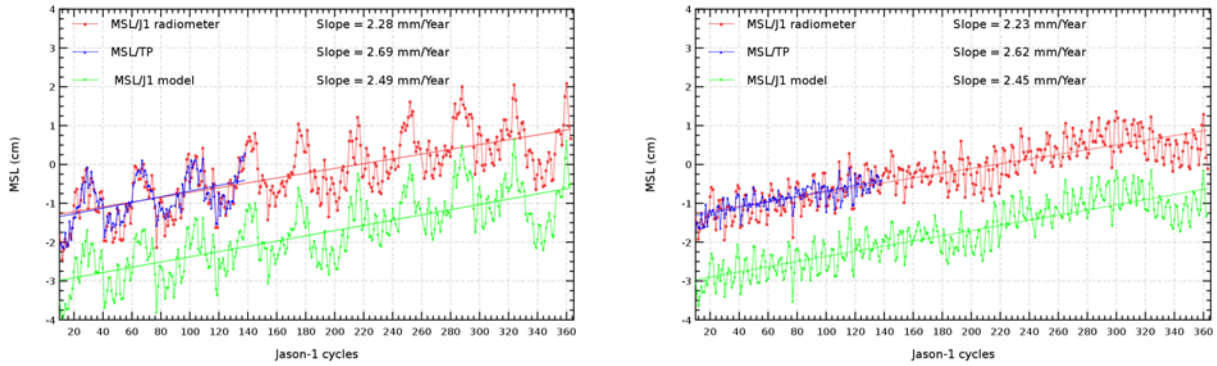

Figure 34: *Jason-1 and T/P mean sea level (on the left) with annual and semi-annual adjustment (on the right)*

The shown MSL trends were computed using as well ascending and descending passes, but when computing Jason-1 MSL slope separately for ascending and descending passes, differences are noticed. Figure 35 shows SLA slopes using Jason-1 GDRs (with ECMWF model wet troposphere correction) and T/P MGDRs.

Jason-1 SLA slopes are similar:

- 2.43 mm/yr using descending passes
- 2.41 mm/yr using ascending passes

Indeed, the difference between msl with ascending or descending passes is very dependant of the considered period. Here it represents a difference of 0.02 mm/yr, which differs from T/P (see35 right) and from the 0.23mm/yr value calculated until the end of 2010 - from cycle 1 to 331 - in 8.2.2.. There is no explanation concerning differences between ascending and descending passes. Indeed, ascending and descending passes cover the same geographical regions, so there is no reason why SLA slope should rise differently. A study using several orbit solutions showed, that use of different orbits has an impact on difference of SLA slope noticed between ascending and descending passes (see for example 8.2.2.).

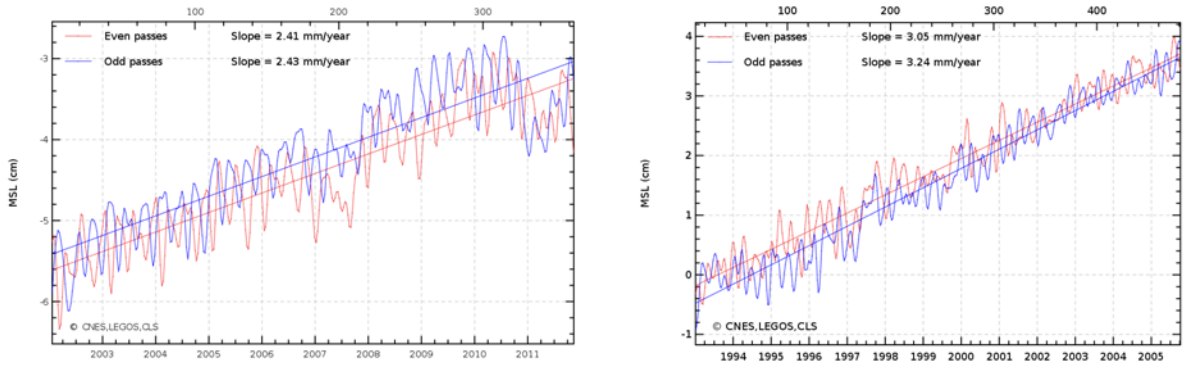

Figure 35: *J1 (left) and T/P (right) SLA slopes using only ascending (odd) or descending (even) passes.*

6.2.2. SSH bias between Jason-1 and T/P

6.2.2.1. Temporal evolution of SSH bias between Jason-1 and T/P

The ECMWF wet troposphere correction is also used in figure 36 which represents the temporal evolution of the SSH bias between T/P and Jason-1. This prevents from errors due to radiometer biases, as the model correction is the same for the two missions. When using radiometer wet troposphere correction, the bias differs by 7 to 8 mm. The impact of all geophysical corrections is also displayed in the figure. Results differ by 1.3 cm when applying or not corrections but signals seem to be homogeneous all over the time period. Notice that present results have been obtained using a dedicated TOPEX SSB estimation. Apart from higher variability for Jason-1 cycle 18 (Poseidon-1 was switched on for T/P cycle 361), the T/P to Jason-1 SSH bias nearly remains constant through the Jason-1 mission period.

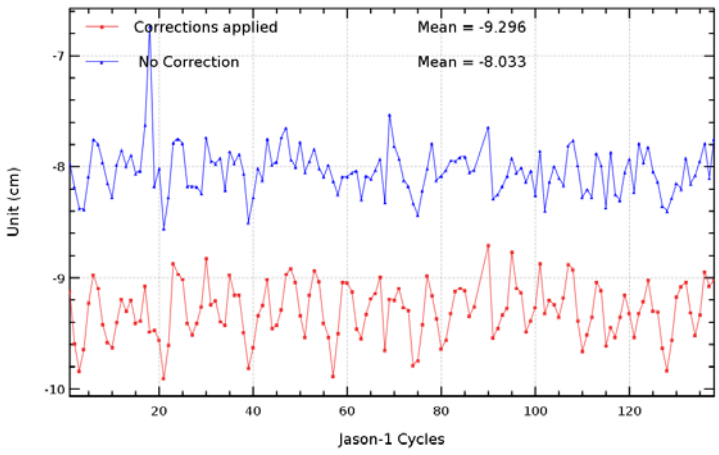

Figure 36: *Cycle per cycle mean of (T/P−Jason-1) SSH differences*

6.2.2.2. Spatial distribution of SSH bias between Jason-1 and T/P

Jason-1 and T/P have not been on the same track from cycle 21 onward. Consequently, the SSH differences can not be obtained directly as a result of the ocean variability. Thus, the map of the SSH differences between Jason-1 and T/P is obtained at the Jason-T/P crossovers in figure 37. The figure was generated using Jason-1 GDR version "c" (cycle 1 to 138) and updated corrections on T/P (GSFC orbit, Sea State Bias, ionospheric bias). The global map is much more homogeneous with these new standards, though there are still some visible structures, they are now much more consistent and have less amplitudes (generally less than ± 1 cm).
Using the official MGDR T/P standard (which was modified the last time in 1996, see handbook **??**), large differences were also visible, when looking on the verification phase of Jason-1 (cycles 1 to 21) (figure 38, left panel). Both satellites (T/P and Jason-1) were on the same ground track, which makes direct measurement comparison possible. For OSTST meetings in 2006 and 2007 retracked (new range,...) TOPEX cycles for the Jason-1 verification phase were already available (called RGDR). They contained also an orbit based on GRACE gravity model. This reduces the differences, as visible on figure 38 (right panel). The data of both missions are much more homogeneous, when looking at global maps. Indeed, when separating ascending and descending passes during computing T/P - Jason-1 SLA differences, large hemispheric biases appear (see figure 39).

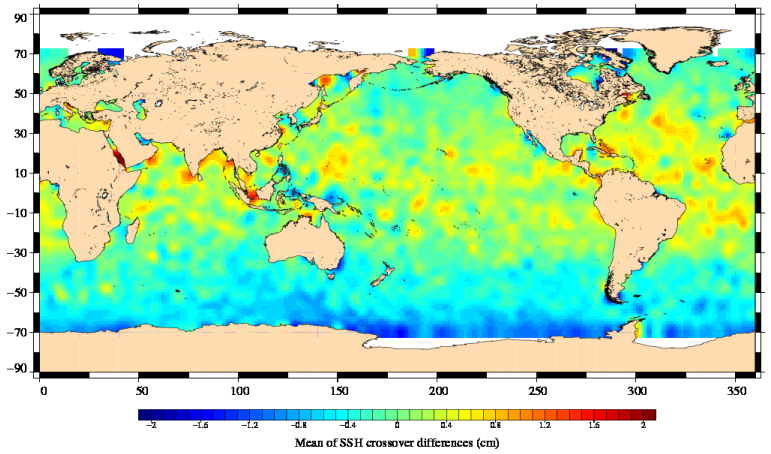

Figure 37: *Map of (T/P−Jason-1) SSH differences for Jason-1 GDR version "c" (cycles 1 to 138).*

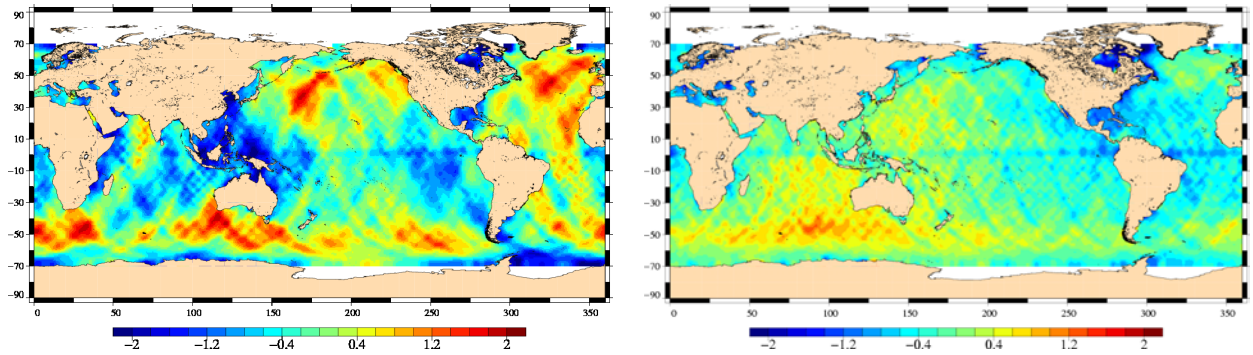

Figure 38: *Map of (T/P−Jason-1) SSH differences for Jason-1 cycles 1 - 21, using orbit of MGDR (left) and GSFC orbit based on GRACE gravity model (right) for T/P.*

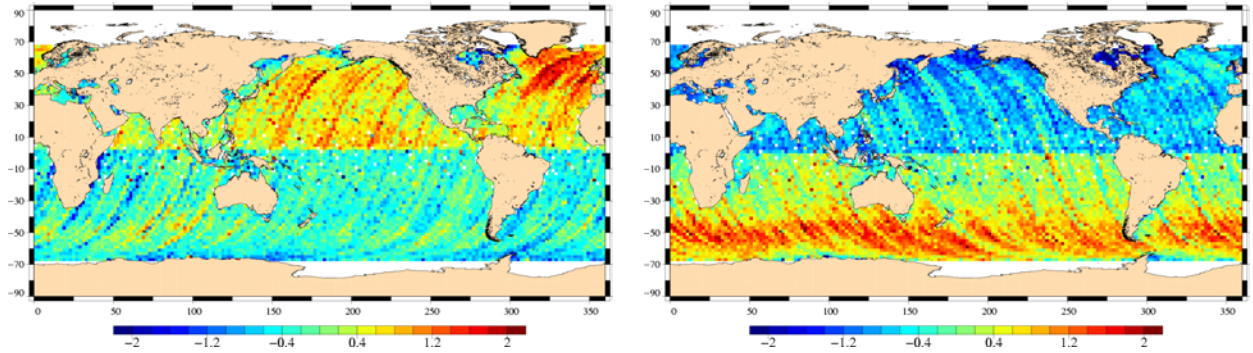

Figure 39: *Map of (T/P−Jason-1) SSH differences separating ascending and descending passes for cycles 1 - 21, using orbit based on GRACE gravity model for T/P.*

Finally new SSB corrections have been computed on cycles 1-21 for TOPEX using RGDR, with the collinear method. For J1 the Venice SSB was used ([59]). These new TOPEX and J1 SSB models are now much closer than before. When applying them in the SLA calculation in addition to the new orbits and the new ranges (Figure 40), the discrepancies between J1 and T/P are reduced. However, an East/West patch (< 1cm) remains, but it is not correlated with SWH. The origin of this signal is explained by CNES and GSFC orbit, used respectively for J1 and TOPEX. Indeed, using GSFC orbit for Jason-1 similar to those used in RGDR TOPEX data, allows to remove this East/West signal (see [7]).

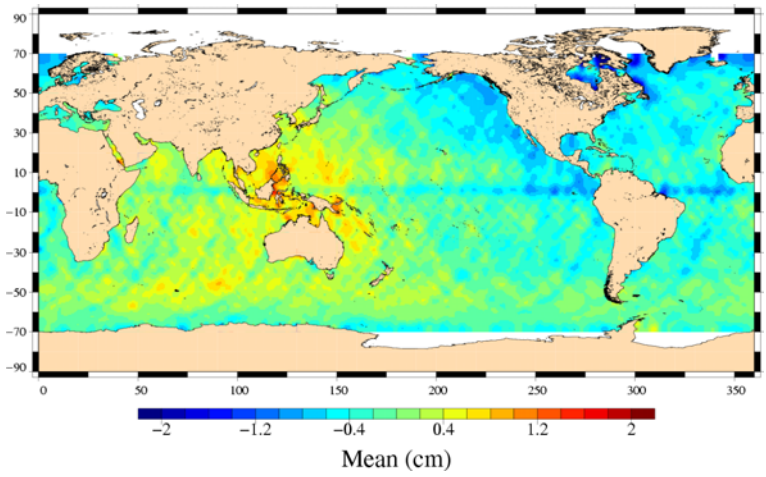

Figure 40: *Map of (T/P−Jason-1) SSH differences for Jason-1 cycles 1 - 21, using GSFC orbit based on GRACE gravity model for T/P, as well as recomputed Sea State Bias.*

6.2.2.3. Hemispheric SSH bias between Jason-1 and T/P

In order to further investigate hemispheric (T/P−Jason-1) SSH biases, its temporal evolution is presented in figure 41. It shows hemispheric differences between T/P and Jason-1, when separating northern and southern hemisphere. From the northern hemisphere to the southern hemisphere the (T/P−Jason-1) SSH bias estimates can thus differ by up to 1.5 cm. These hemispheric differences seem consistent from one cycle to another. The use of more homogeneous altimeter standards between Jason-1 and T/P has considerably lowered the difference between northern and southern hemisphere on the whole time period. Indeed, using orbits with ITRF 2005 reference system for both Jason-1 and T/P reduced these hemispheric differences.

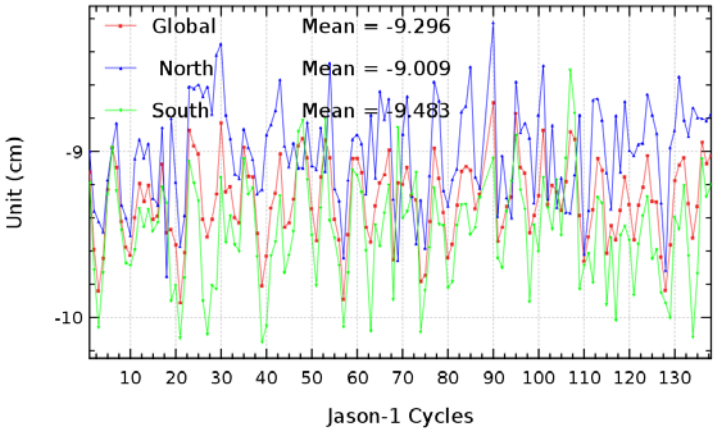

Figure 41: *Cycle per cycle mean of (T/P−Jason-1) SSH differences by hemisphere*

6.3. Sea level seasonal variations

From Sea Level Anomalies computed relative to the Mean Sea Surface CLS 2001 (Hernandez et al, 2001), the surface topography seasonal variations have been mapped from figure 42 to 51 for the overall Jason-1 data set. Major oceanic signals are showed clearly by these maps: it allow us to assess the data quality for oceanographic applications. The most important changes are observed in the equatorial band with the development of an El Niño in 2002-2003. The event peaked in the fourth quarter of 2002, and declined early in 2003. Conditions indicate an event of moderate intensity that is significantly weaker than the strong 1997-1998 El Niño (McPhaden,2003, [80]). End of 2007, a La Niña event is visible in Eastern Pacific on figure 47. It lasted till the mid 2008 (see [105]). From mid 2009 to spring 2010 a moderate El Niño event occured (see [106]). In second half of 2010 a moderate to strong La Niña event developped (see [108]) until spring 2011.

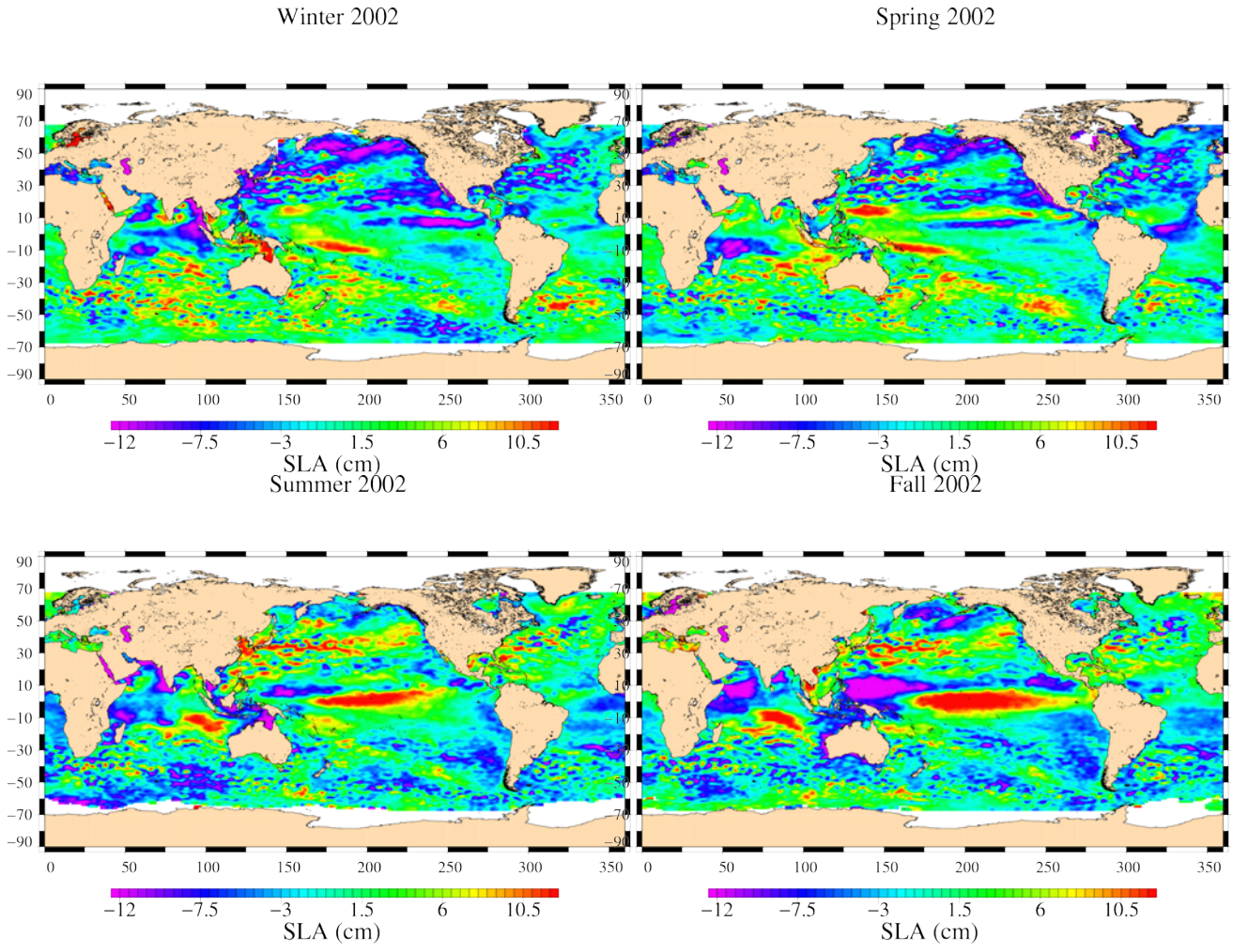

Figure 42: *Seasonal variations of Jason SLA (cm) for year 2002 relative to a MSS CLS 2001*

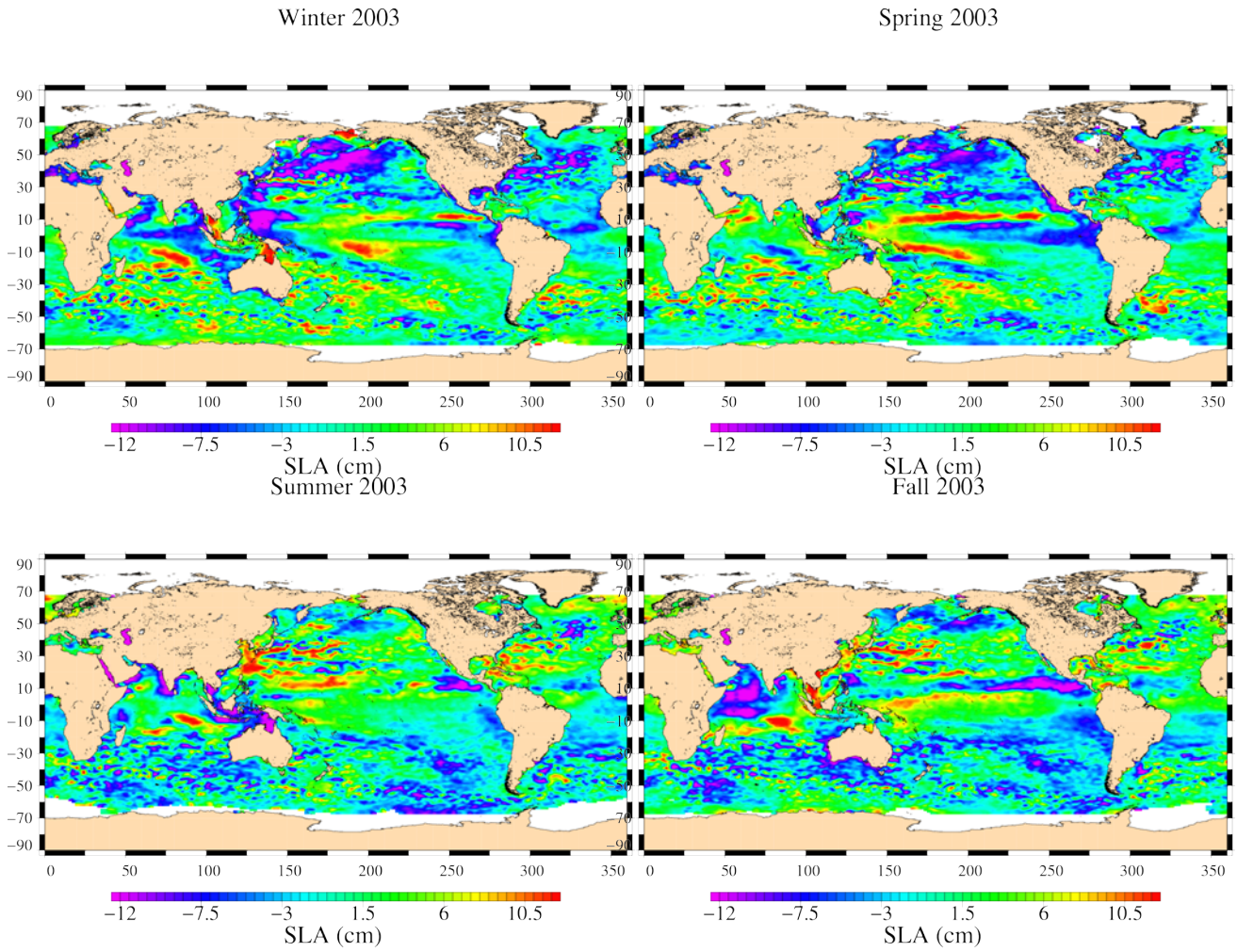

Figure 43: *Seasonal variations of Jason SLA (cm) for year 2003 relative to a MSS CLS 2001*

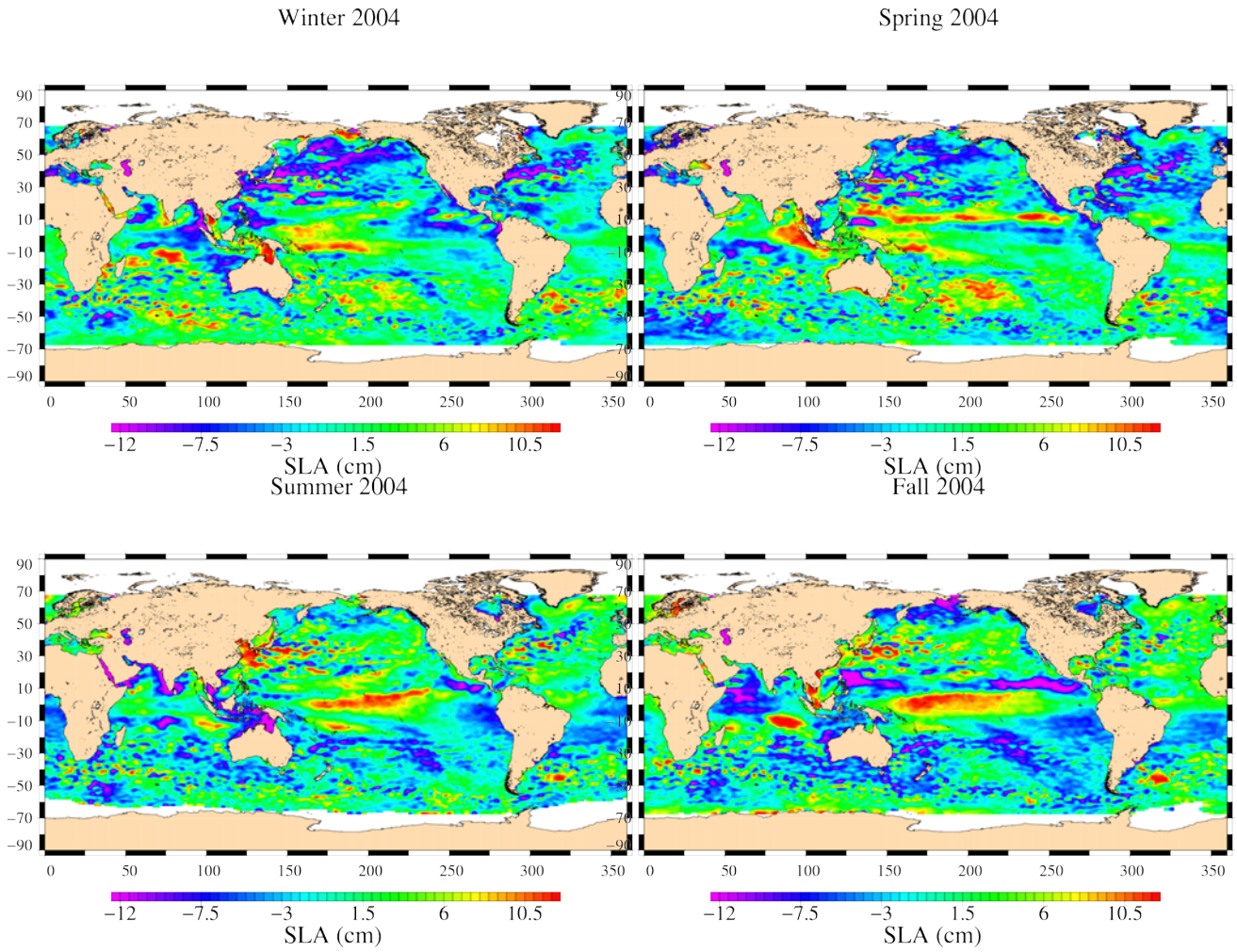

Figure 44: *Seasonal variations of Jason SLA (cm) for year 2004 relative to a MSS CLS 2001*

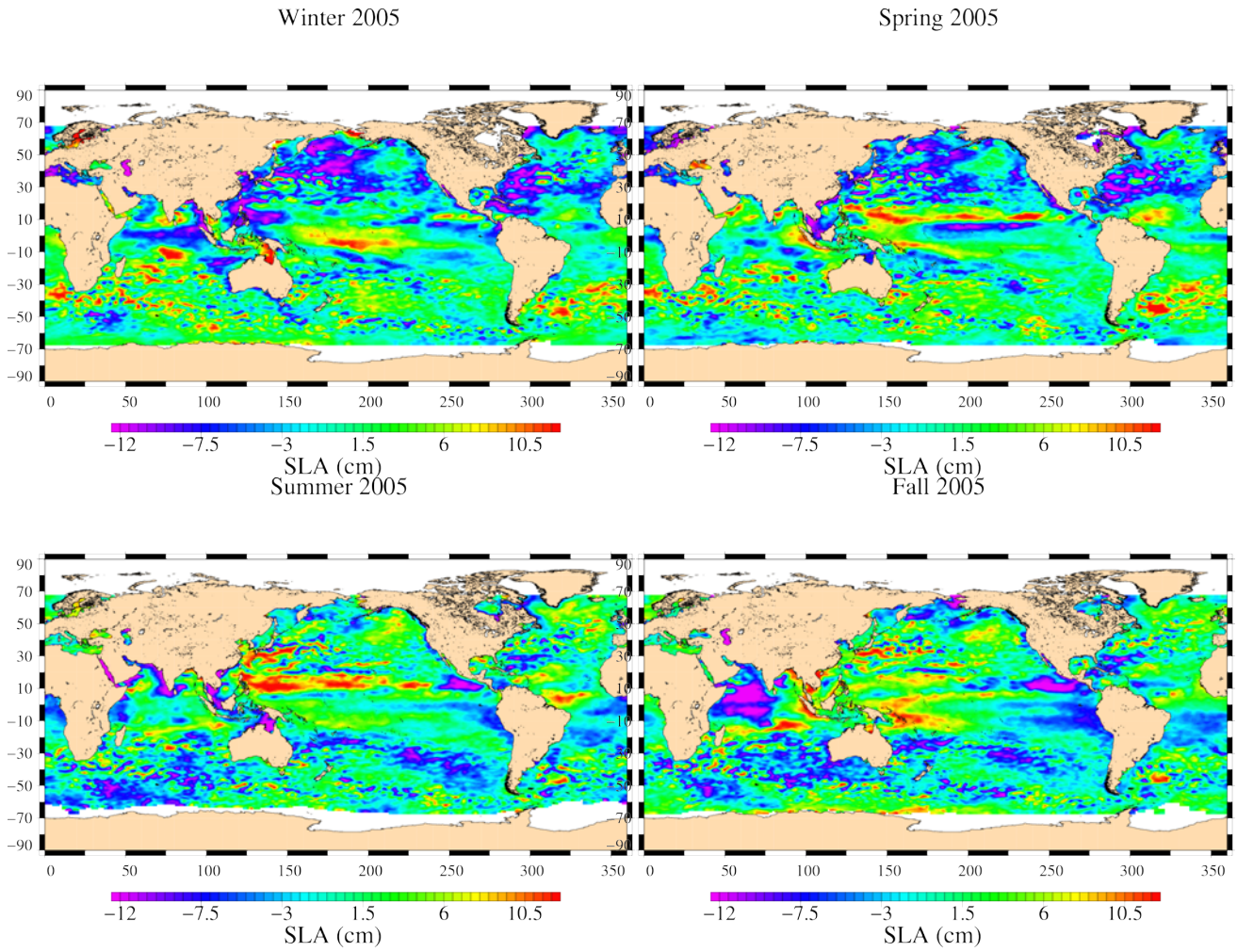

Figure 45: *Seasonal variations of Jason SLA (cm) for year 2005 relative to a MSS CLS 2001*

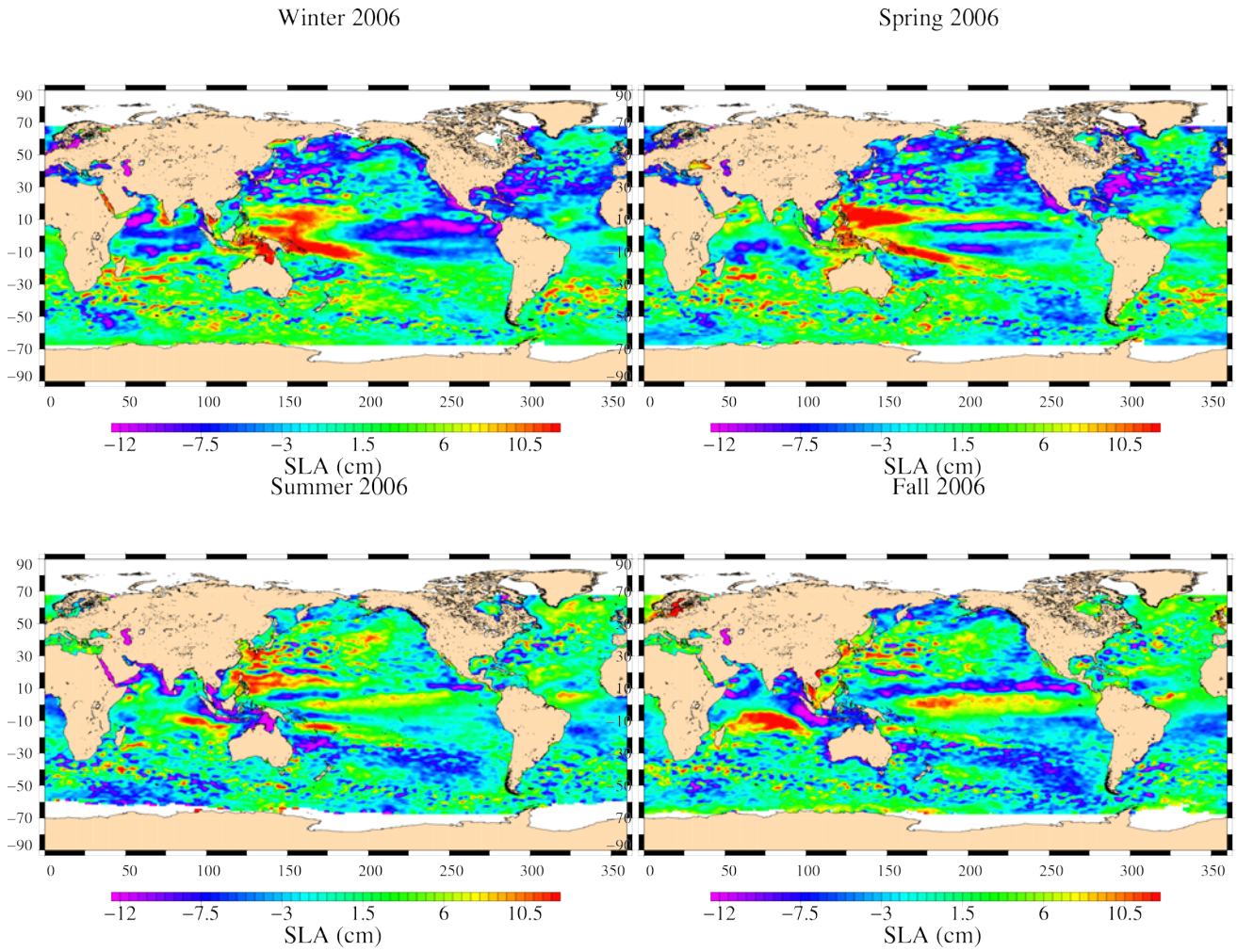

Figure 46: *Seasonal variations of Jason SLA (cm) for year 2006 relative to a MSS CLS 2001*

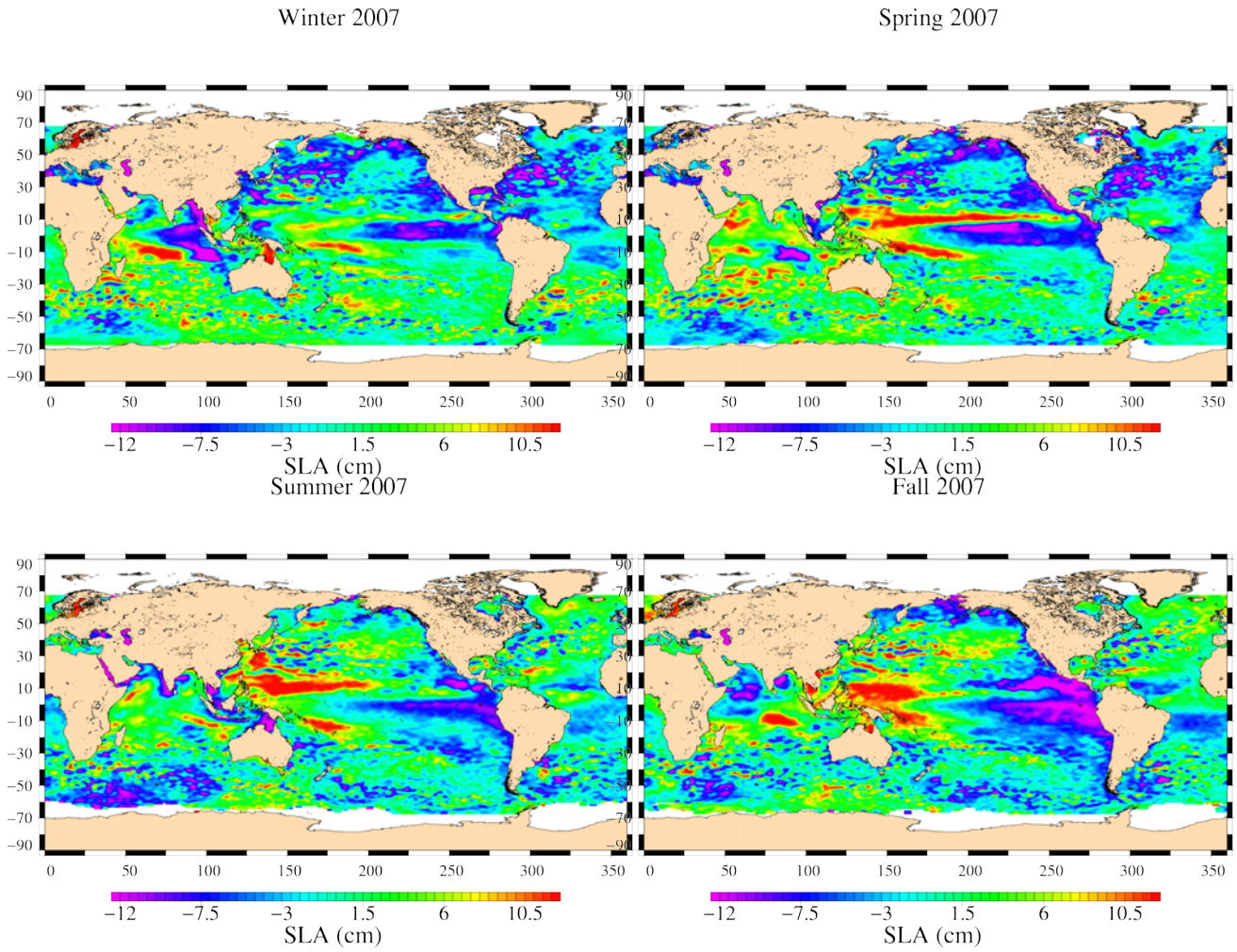

Figure 47: *Seasonal variations of Jason SLA (cm) for year 2007 relative to a MSS CLS 2001*

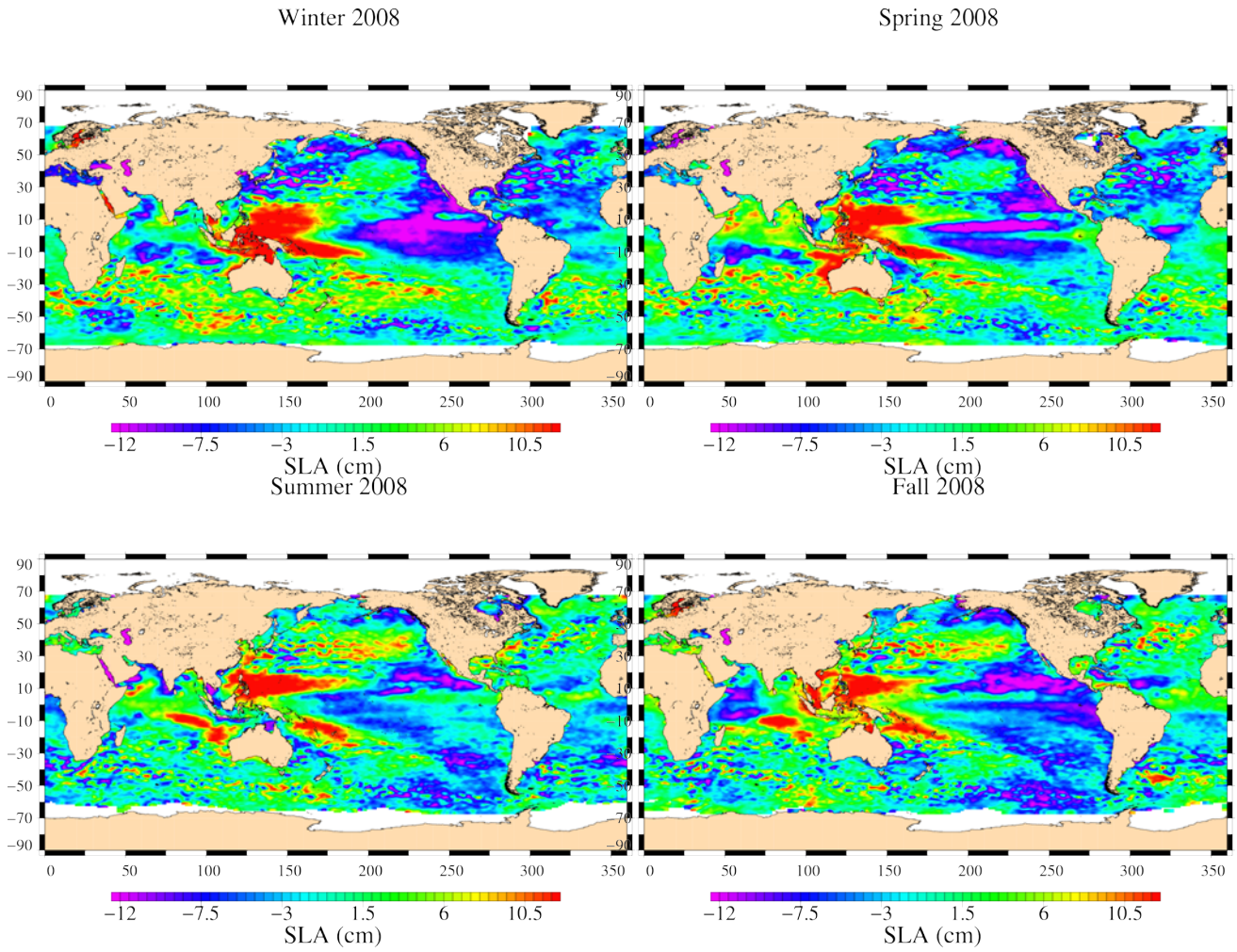

Figure 48: *Seasonal variations of Jason SLA (cm) for year 2008 relative to a MSS CLS 2001*

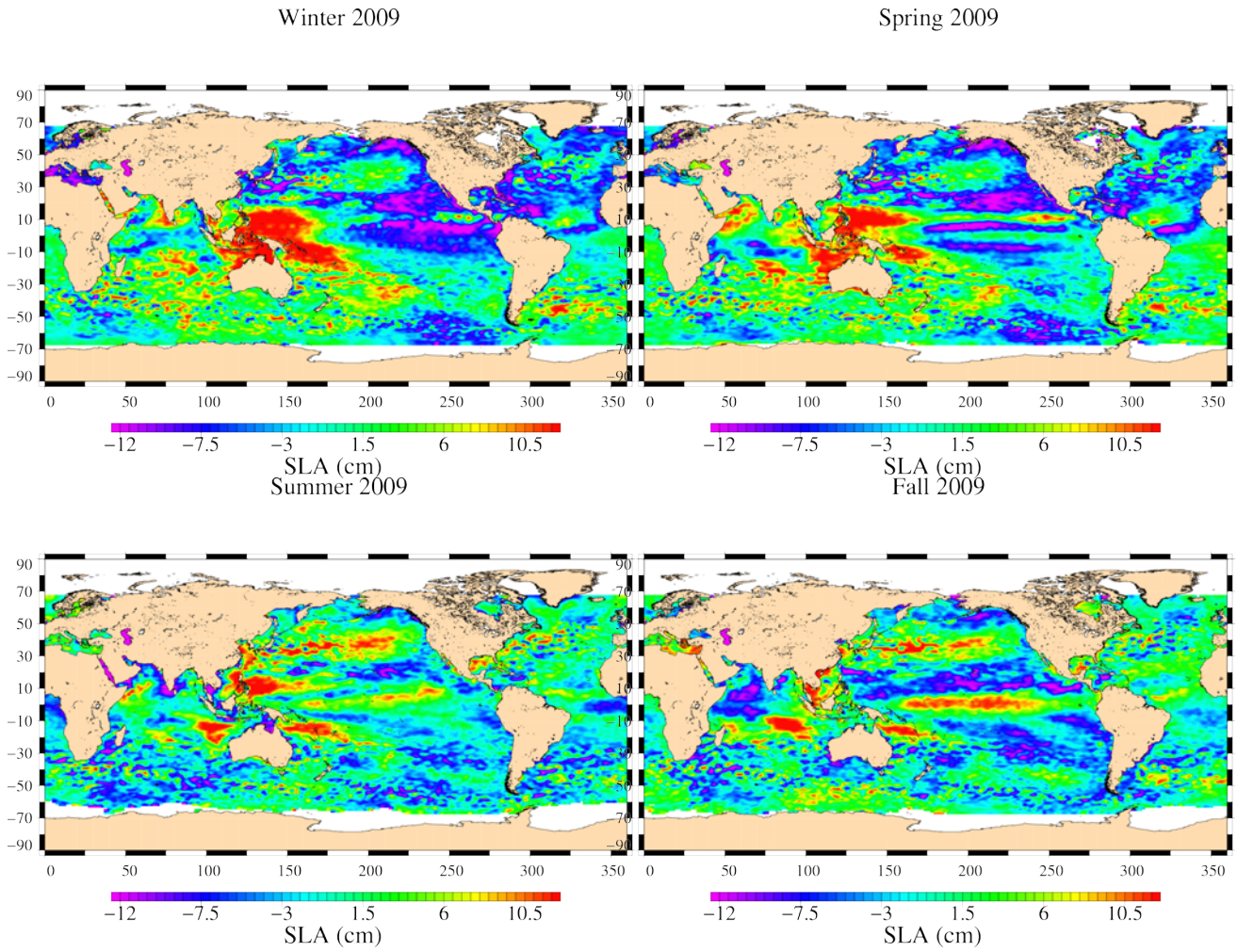

Figure 49: *Seasonal variations of Jason SLA (cm) for year 2009 relative to a MSS CLS 2001*

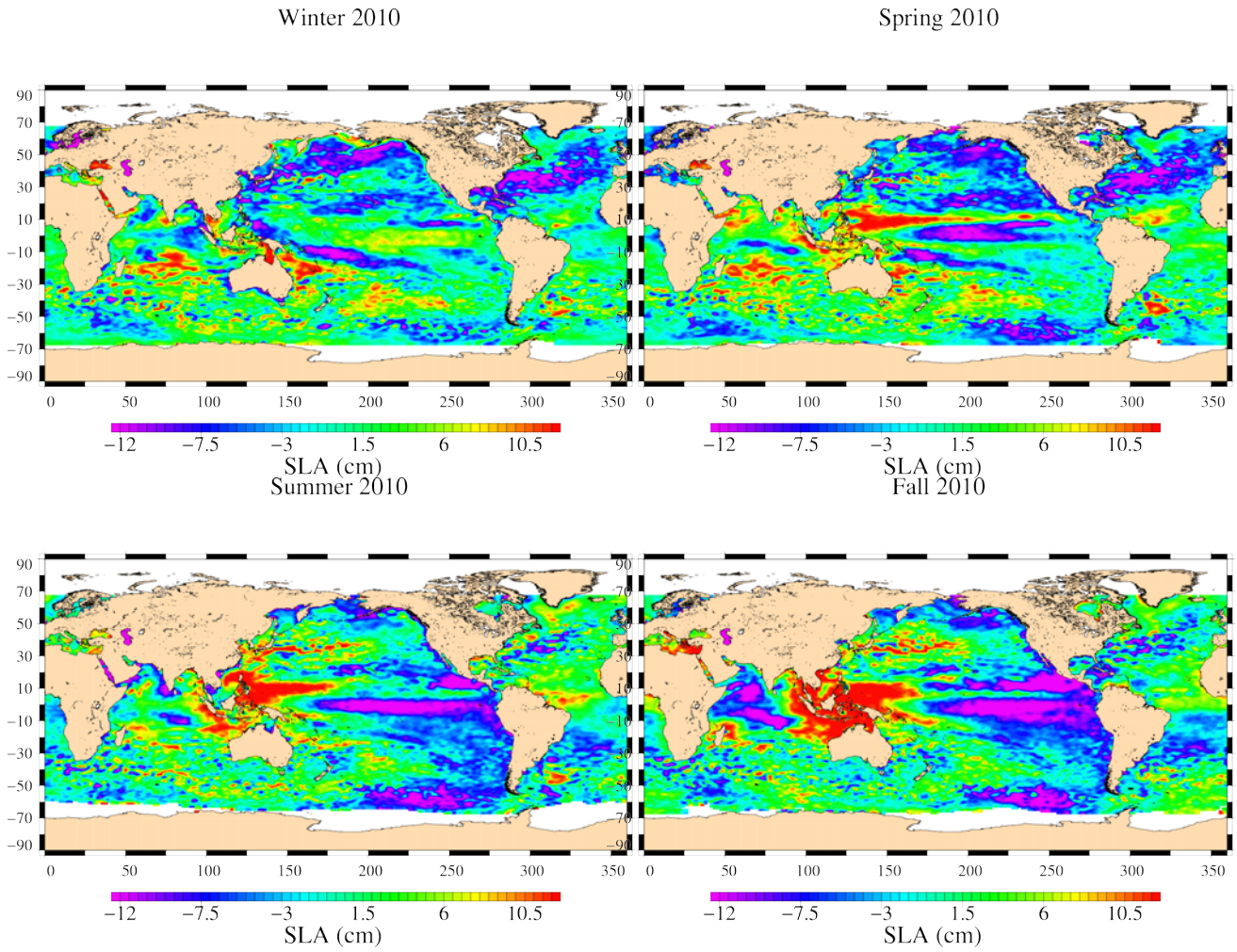

Figure 50: *Seasonal variations of Jason SLA (cm) for year 2010 relative to a MSS CLS 2001*

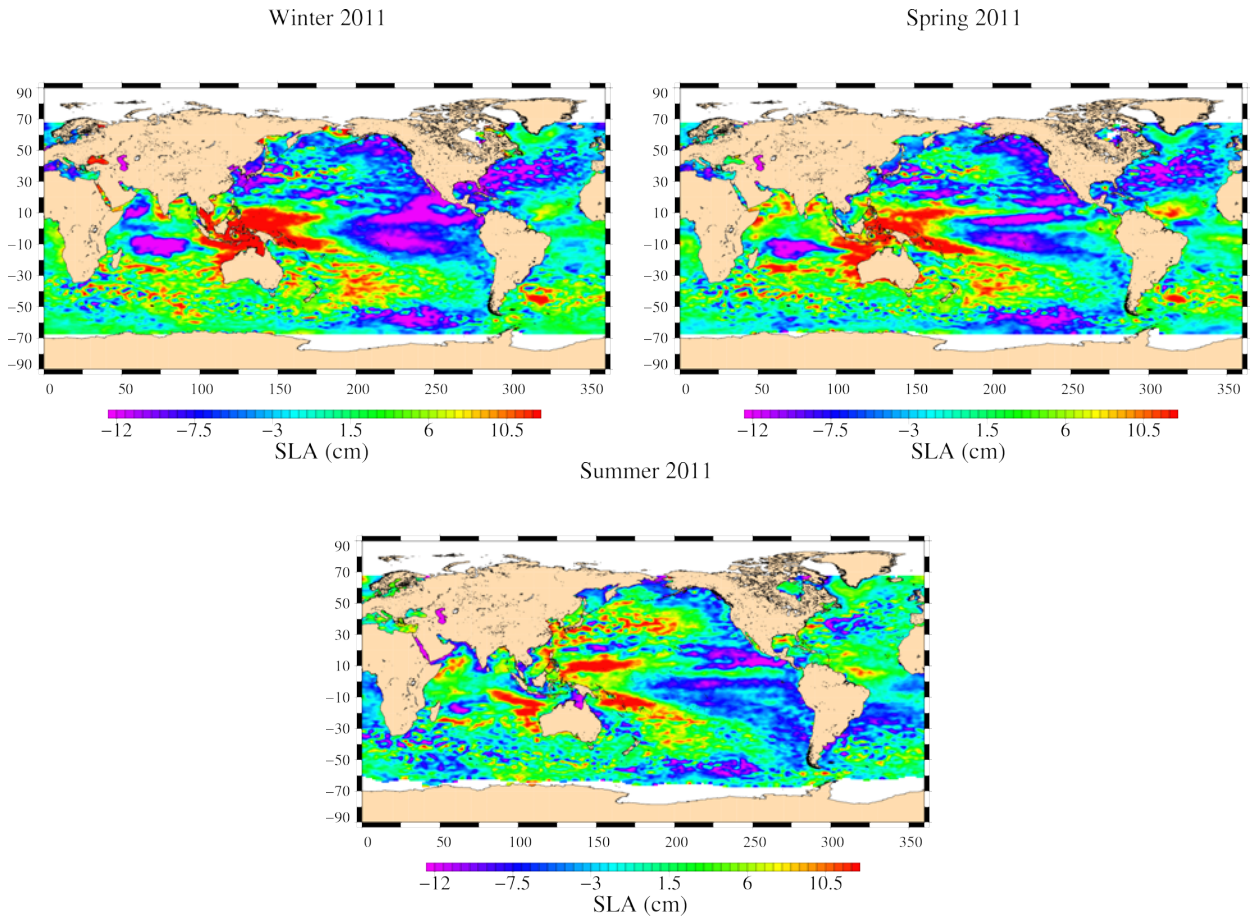

Figure 51: *Seasonal variations of Jason SLA (cm) for year 2011 relative to a MSS CLS 2001*

7. Global and regional Mean Sea Level (MSL) trends

7.1. Overview

Long-term MSL change is a variable of real interest in the studies of global climate change. Thus, a lot of works have been performed on the one hand to survey the mean sea level trend and on the other hand to assess the consistency between the MSL derived from all operational altimeter missions. Besides, external data sources such as tide gauges and Argo Temperature/Salinity (T/S) profiles have been used to assess the altimeter MSL evolution and thus detect potential MSL drift. The main results works are summarized here. In addition, the Reynolds SST is also monitored over the global ocean to analyze the MSL trend.

7.2. SSH applied for the MSL calculation

The SSH formula used to compute the MSL is defined for all the satellites as below :

$$SSH = Orbit - Altimeter\ Range - \sum_{i=1}^{n} Correction_i$$

with :

$$\begin{aligned}
\sum_{i=1}^{n} Correction_i &= Dry\ troposphere\ correction : S1\ and\ S2\ atmospheric\ tides\ applied \\
&+ Combined\ high\ resolution\ dynamical\ atmospheric\ correction \\
&+ Wet\ troposphere\ correction\ (radiometer\ or\ ECMWF\ model) \\
&+ Filtered\ dual\ frequency\ ionospheric\ correction \\
&+ Non\ parametric\ sea\ state\ bias\ correction \\
&+ Geocentric\ ocean\ tide\ height,\ GOT\ 4.7 \\
&+ Solid\ earth\ tide\ height \\
&+ Geocentric\ pole\ tide\ height
\end{aligned}$$

The SSH formula has been modified or updated for each satellite in order to calculate the best MSL. Especially, stability problems of the radiometer wet troposphere correction have been taken into account :

- For Jason-1 : the radiometer wet troposphere correction is used although 60-days signals are still detected since 2006.
- For Envisat : the ECMWF model wet troposphere correction is used to remove the effects of abnormal changes or trends observed on the radiometer wet troposphere correction, the USO correction has been applied (drift and anomaly : see Envisat yearly report [48]). A reprocessed orbit (GdrC standard) was used.

- For T/P : the radiometer wet troposphere correction drift has been corrected with Scharroo's correction (Scharroo R., 2004 [95]), the relative bias between TOPEX and Poseidon and between TOPEX A and TOPEX B has been taken into account, the drift between the TOPEX and DORIS ionosphere corrections has been corrected on Poseidon cycles. GSFC std0809 was used as well as a recomputed sea state bias (Tran et al., 2010 [104]).
- For Geosat Follow-On: the ECMWF model wet troposphere correction is used, the GIM model has been used for the ionospheric correction. Furthermore, GSFC std0809 orbits and an updated sea state bias were used.

7.3. Analyses of the MSL trend

7.3.1. Global MSL trend derived from Jason-1&2 and T/P data

The global MSL trend derived from satellite altimetry - T/P, Jason-1 and Jason-2 - is now used as the reference for climate studies. A SSH bias of 8.45 cm has been applied on Jason-1 data to be linked to TOPEX/Poseidon and of 7.46 cm between Jason-1 and Jason-2 (see also Aviso web site http://www.aviso.oceanobs.com/en/news/ocean-indicators/mean-sea-level/). These biases were accurately estimated during the verification phase where Jason-1 and T/P (respectively Jason-2 and Jason-1) were on the same orbit. This MSL plotted on figure 52 highlights a global trend of 3.19 mm/yr (post glacial rebound of -0.3 mm/yr was taken into account (Peltier, 2004 [78])). However, the MSL rise is lower and very weak from the end of 2005 to the end of 2007. During this period, only Jason-1 measurements are available, thus the comparisons with T/P MSL is not possible to confirm this behavior. However, comparisons with other satellites and in-situ data, do not highlight any abnormal drift on Jason-1. This MSL trend change might be explained by the very strong "La Niña" event which occurred in 2007 and beginning of 2008. Indeed, the MSL started to rise again in 2008. Note that the same behavior is observed in 2011 on the global MSL.

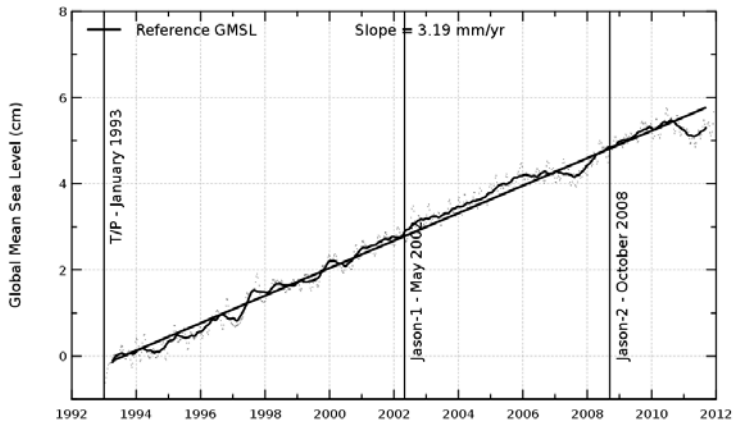

Figure 52: *Global MSL trend derived from Jason-2, Jason-1 and T/P data*

7.3.2. Regional MSL trends derived from AVISO merged products

The AVISO merged products are used to compute the regional MSL trends. Thanks to the high resolution of their grids (0.5 degrees), the MSL regional trends are accurate enough to assess the variability of regional slopes as plotted on map 53. Local slopes range between ±10mm/yr with large structure in main oceans, especially in Pacific Ocean. This kind of map brings a lot of information about the regional MSL evolution, which have to be further studied for the long term evolution of oceanic circulation as well as the intensity of geostrophic currents and interannual oscillations (decadal, Madden-Julian oscillations for example).

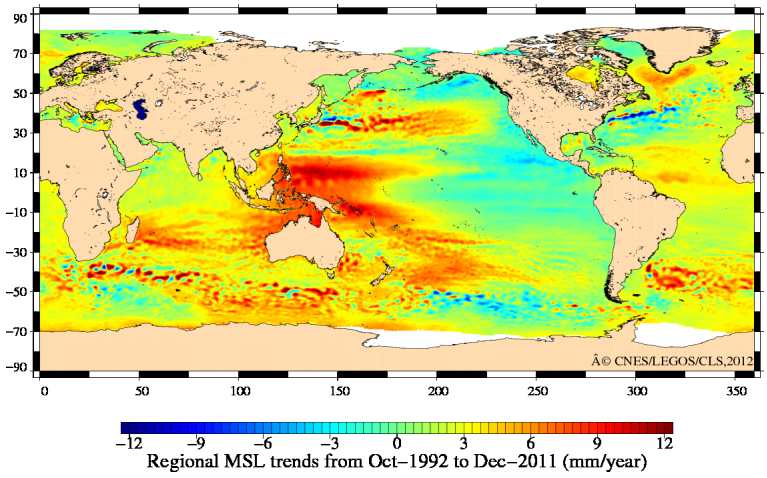

Figure 53: *Regional MSL trends derived from AVISO merged products*

7.4. Multi-mission comparisons of global MSL trends

The MSL has been monitored for each satellite altimeter over global ocean in order to assess the global MSL trend and also to detect any anomalies or any drifts on each MSL series. These different MSL have been plotted in figure 54, after removing annual and semi-annual signals, and filtering out signals lower than 60 days. Considering both T/P and GFO, the trends of global MSL are quite the same on their entire time period, around 3.1 mm/yr (figure 54 left). Moreover, since the beginning of Jason-1 (figure 54 right), results deduced from Jason-1 and GFO are in agreement with each other and slightly different from T/P, with respective slopes of 2.3 mm/yr, 2.2 mm/yr and 2.7 mm/yr). However, differences on the trends are partly explained by the different time periods considered, which is demonstrated on figure 54 bottom considering these 3 missions on the same time period. Indeed,between 2002 and 2006, Jason-1 is 0.3 mm/yr higher than T/P, which is 0.6 mm/yr higher than GFO. Finally, concerning Envisat mission, the global MSL behavior is quite different with a global slope of about 0.5 mm/yr on its whole time period. Next to the reprocessing of Envisat during 2011, the new global MSL trend is now around 2.7 mm/year, in better agreement with all altimeter missions (see Envisat annual report 2011 [76]).

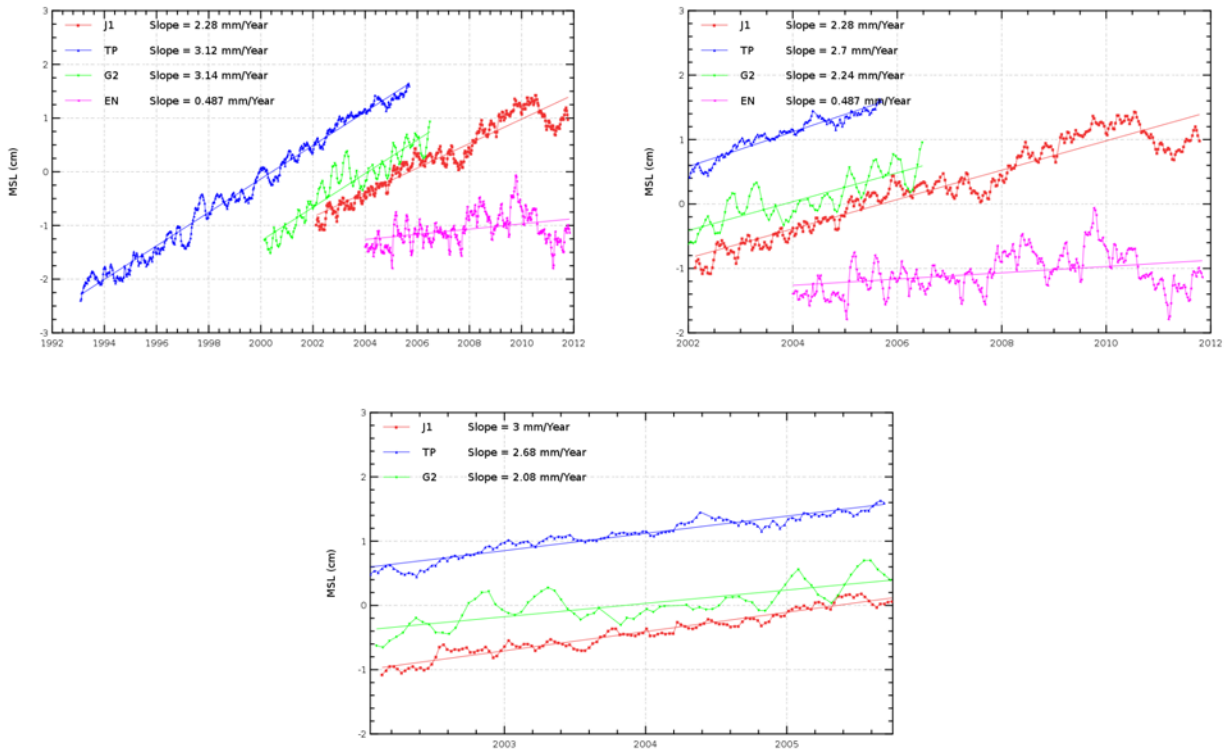

Figure 54: *Multi-mission MSL over global ocean since the beginning of T/P mission on the left and the beginning of Jason-1 mission on the right after removing annual and semi-annual signals. Post glacial rebound was not applied.*

7.5. External data comparisons

7.5.1. Comparison with tide gauges

In order to assess the global MSL trend, comparisons to independent in-situ datasets are of great interest. Two methods have been developed in the frame of in-situ Calval studies and thoroughly described in both altimeter / tide gauges ([113]) and altimeter / Argo T/S profiles ([64]) annual reports. Firstly, Jason-1 altimeter data is compared with tide gauge measurements thanks to a dedicated method which aims at detecting potential drifts in sea surface heights (SSH). The tide gauge network processed is the GLOSS/CLIVAR "fast" sea level database, formerly known as the WOCE network.

Regarding tide gauges, the SSH bias has been computed and is shown on figure 55, which indicates that no altimeter drift is observed with Jason-1 data (0.1 mm/yr), with a formal adjustment error of 0.1 mm/yr. Again, on almost 10 years of consistent altimeter data delivery, the coherence with in-situ measurements along coastal areas is pretty good, and rms differences are lower than 3.7 cm. Although the drift is close to zero, some misunderstood signals are observed, especially in 2004 with a small jump of few millimeters. Currently, the accuracy of the method of comparison between altimetry and tide gauge is not able to determine if these signals are due to errors on Jason-1 data

or intrinsic uncertainties of the method.

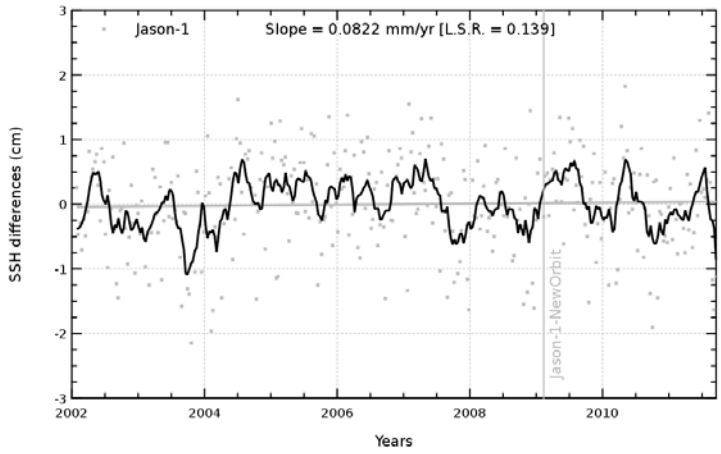

Figure 55: *Jason-1 altimeter MSL drifts compared with tide gauges measurements*

7.5.2. Comparison with Argo T/S profiles

The Argo network provides an almost coverage of the whole global ocean with Temperature and Salinity (T/S) profiles. More than 500 000 profiles are available since 2004 and the Dynamic Height Anomalies derived from these profiles are used as a reference to study the regional altimeter MSL trend discrepancies observed between Jason-1 and Envisat data.

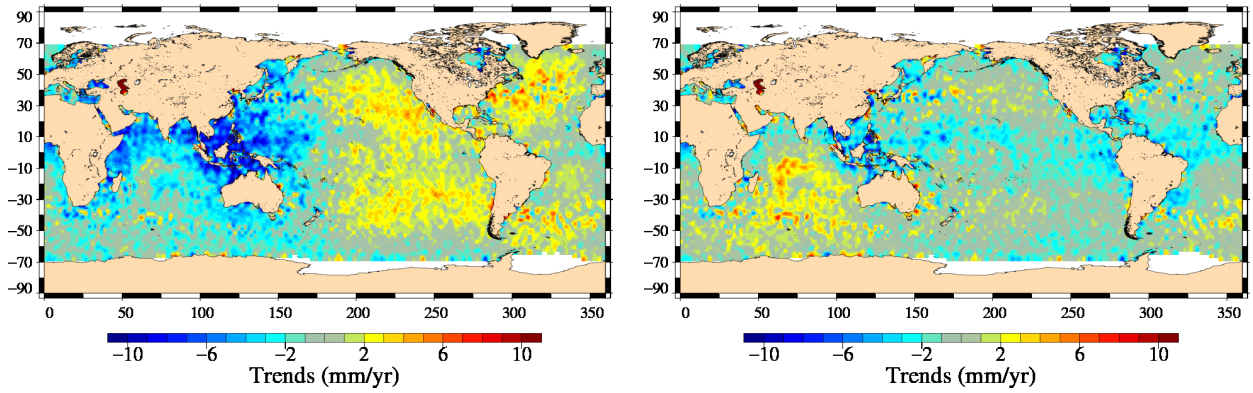

Figure 56: *MSL trend differences (mm/yr) between Envisat and Jason-1 missions computed with GDR-C (left) and CNES preliminary GDR-D orbit (right) (Envisat cycles 10-93 and Jason-1 cycles 28-323).*

The map of the MSL trend differences between both missions underlines a large longitudinal discrepancies of ± 3 mm/yr between the eastern (0°, 180°) and the western (180°, 360°) part of the global ocean (figure 56, left). But the mission at the origin of this regional bias can not be detected with this cross-calibration. Therefore, the Argo in-situ profiles are used as an external and independent reference to compare both altimeter missions. Time series of sea surface heights differences

between altimetry and in-situ data are computed for both Jason-1 and Envisat missions. Then, the drifts of these differences are estimated separating east (0°/180°) and west (180°/360°) parts in order to detect which mission is closest to the in-situ reference. The analysis with Jason-1 data (figure 57, left) indicates that the MSL trends difference between west and east hemispheres is of -0,9 mm/yr whereas the same approach with Envisat data reveals a trends difference of up to 3,8 mm/yr (figure 57, right). Considering the associated precision (± 0.5 mm/yr), it indicates that both Envisat and Jason-1 altimeter SSH are affected by the regional difference but the anomaly is strongly enhanced with Envisat measurements. Further analysis has shown that this anomaly is in relationship with the calculation of the GDR-C orbit standard. Indeed Envisat, as well as Jason orbits are concerned, but Envisat orbit is more impacted. This has been solved with the preliminary version of the GDR-D orbit whose impact is described below. These results demonstrate that the use of Argo in-situ data to compute relative estimations of the altimeter MSL trend makes possible the detection of regional relative drifts in altimeter measurements. However such differences observed between two hemispheres indicate that the error associated with the regional altimeter MSL trend currently strongly affect climate studies at the spatial scale of a single ocean basin.

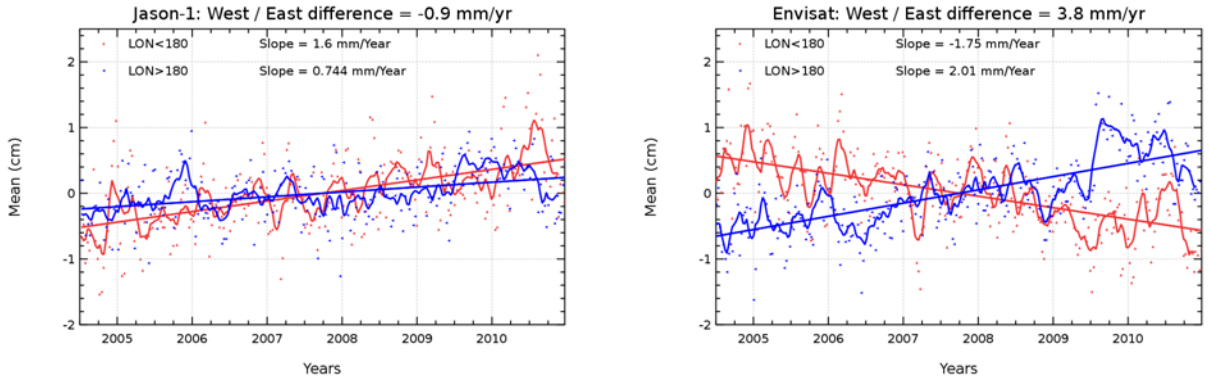

Figure 57: *SSH difference (cm) between altimeter data and Argo in-situ measurements for Jason-1 (left) and Envisat (right) computed with GDR-C orbit, separating east (<180°) and west (>180°) longitudes. Corresponding annual and semi-annual signals are removed. Trends of raw data are indicated and the 2-month filtered signal is added.*

A new preliminary CNES GDR-D orbit solution has been developed (Cerri et al., 2011: [24]) where the long term evolution of the gravity field has been improved. Its use in the SSH calculation reduces the observed regional discrepancy since the previous longitudinal structures using GDR-C orbit solution (figure 56, left) are now removed (figure 56, right). Altimeter data with the new orbit solution are compared with Argo in-situ measurements in order to detect potential remaining errors. Indeed errors with similar impact on both missions would not be detected without a comparison with external data as in-situ Argo profiles. It has a strong impact on the East / West difference observed with Envisat: initially +3.8 mm/yr (figure 57, right), the difference is now reduced to +1.0 mm/yr (figure 58, right). In addition, the new orbit solution makes both missions more homogeneous since the East / West difference observed with Jason-1 is increased from -0.9 mm/yr (figure 57, left) to +0.7 mm/yr (figure 58, left), which is similar to the Envisat result within the ±0.5 mm/yr uncertainty on the precision. Note that the East/West MSL trend differences are enhanced with Envisat mission because the satellite is closer to the Earth and thus more affected by the gravity field than Jason-1 (Cerri et al., 2011: [24]). Thus the comparison of

altimeter measurements with Argo profiles makes possible the estimation of the impact of a new altimeter standard in the SSH calculation.

These results have been submitted for publication in Marine Geodesy 2012.

Both in-situ comparison methods complement each other since the first one using tide gauges only concerns coastal areas while the second one using T/S profiles is well widespread to get a regional assessment of the MSL.

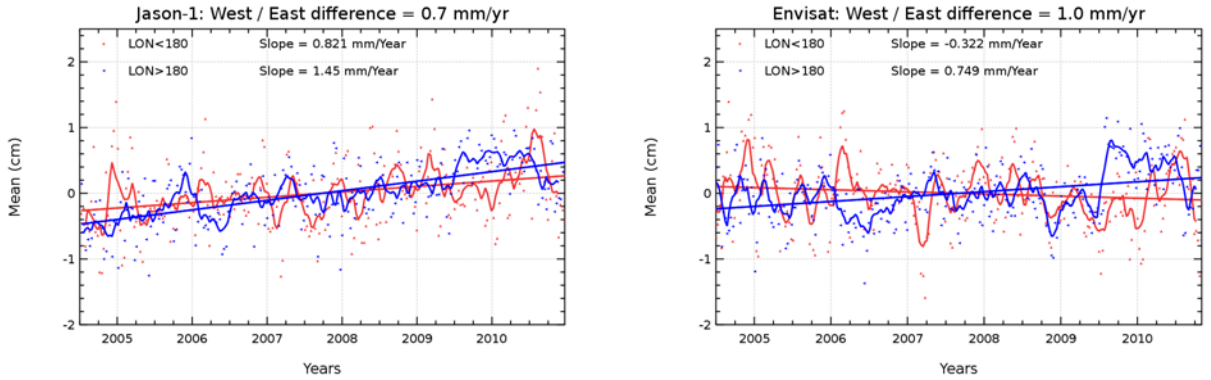

Figure 58: *SSH difference (cm) between altimeter data and Argo in-situ measurements for Jason-1 (left) and Envisat (right) computed with CNES preliminary GDR-D orbit, separating east ($< 180^\circ$) and west ($> 180^\circ$) longitudes. Corresponding annual and semi-annual signals are removed. Trends of raw data are indicated and the 2-month filtered signal is added.*

7.5.3. Reynolds's SST

The Reynold's Sea Surface Temperature (SST) has been monitored over the 19 year period from 1993 to 2011 along the T/P and Jason-1 tracks and compared with the reference MSL in figure 59 (after removing annual signal and semi-annual signal). Indeed, the SST is strongly related with the steric contribution of the sea level, which represents a part of the total elevation of the water column (steric and mass contributions gives the total altimeter sea level). Both trends are positive (figure 59, the SST scale has been adjusted so that they can be compared) which reveals that the sea level rise as seen by altimetry is partly explains by the steric content of the water column. The SST rise in 1998 is to be related with the El Niño event whereas its decreases in 2008 and 2011 are the consequence of a La Niña event, as warmer or colder temperature events correspond to the movements of water masses in the Pacific ocean. The mean SST rises by less than 0.01 Celsius degree/yr with a dynamic much stronger than the MSL. In Particular, the signatures of the 1998 El Niño and the 2008 and beginning 2011 La Niña / ENSO events are more visible than with altimetric data.

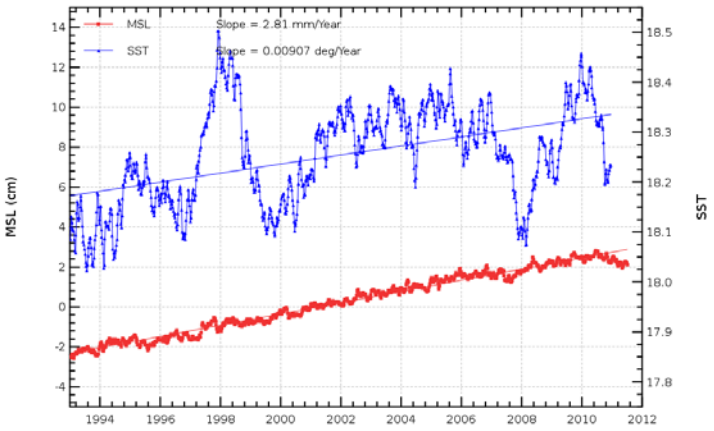

Figure 59: *Comparison of MSL and SST trend over global ocean for the T/P / Jason-1 period*

8. Particular Investigations

This sections contains some investigations led on Jason-1 data in 2011 such as

- Analysis of the 59-day signal on the MSL (see also [10])
- Comparison between preliminary GDR-D orbit and GDR-C orbit
- Investigations on σ_0 / altimeter wind speed stability
- Impact of fuel depletion maneuvers

8.1. Analysis of 58.74-day signal observed on the MSL derived from Jason-1&2 and TOPEX data

To date, the global Mean Sea Level (MSL) curve derived from Jason-1 and Jason-2 data highlights a periodic signal close to 60-days with amplitude significantly stronger than for the TOPEX MSL curve (4 mm for Jason-1 or Jason-2 and 1.5 mm for TOPEX) whereas similar altimeter standards are used for all satellites (figure 60). In fact, the exact period of this signal is 58.74 days. It corresponds to the aliasing of a semi-diurnal periodic signal (12 hours) with the ground repetitivity of Jason-1 and TOPEX missions (9.91 days).

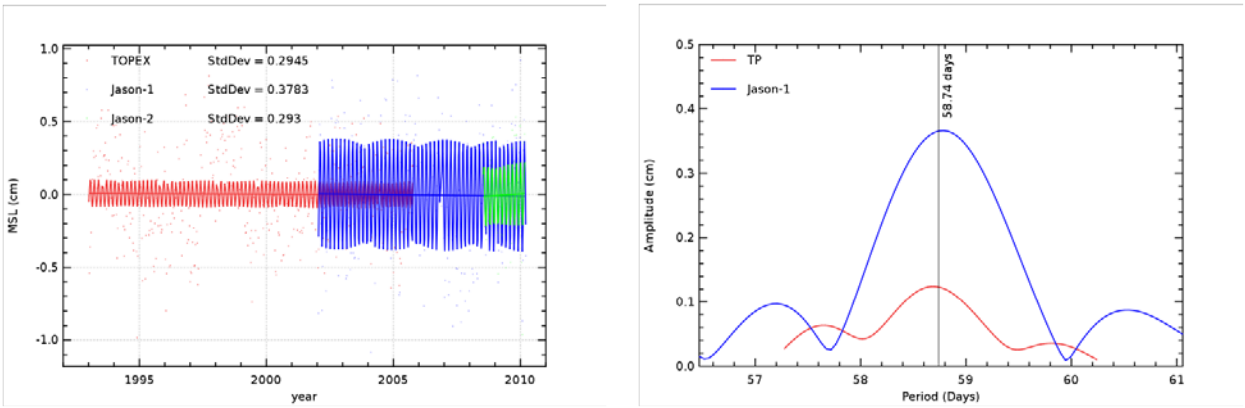

Figure 60: *Left: 58.74-day signal on global MSL after removing the global trend. Right: Periodogram on Jason-1 and TP MSL focused on 58.74-day signal.*

The first objective of this study is to describe accurately this 58.74-day signal observed on the MSL, estimating its global and local amplitudes and testing its sensitivity to the period. As shown on figure 61, the map of the 58.74 amplitude signal of the difference between Jason-1 and TOPEX shows a stronger amplitude of the signal for Jason-1 ($>$ 5 mm) generally between -40° and 40° of latitude. Moreover, the SSH differences between altimetry and tide gauges highlight a 58.74-day signal of about 3-4 mm for Jason-1&2 and 1 mm for TOPEX. Note that similar results are obtained when comparing altimeter data with tide gauges measurements (figure 62). This result is in agreement with previous analyses and proves that the 59-day signal is not a physical signal but an error on altimetry data.

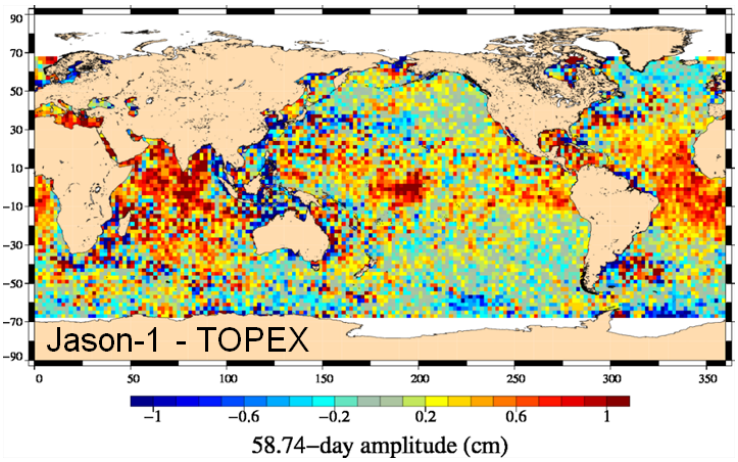

Figure 61: *Map of 58.74-day signal on the difference between Jason-1 and TOPEX.*

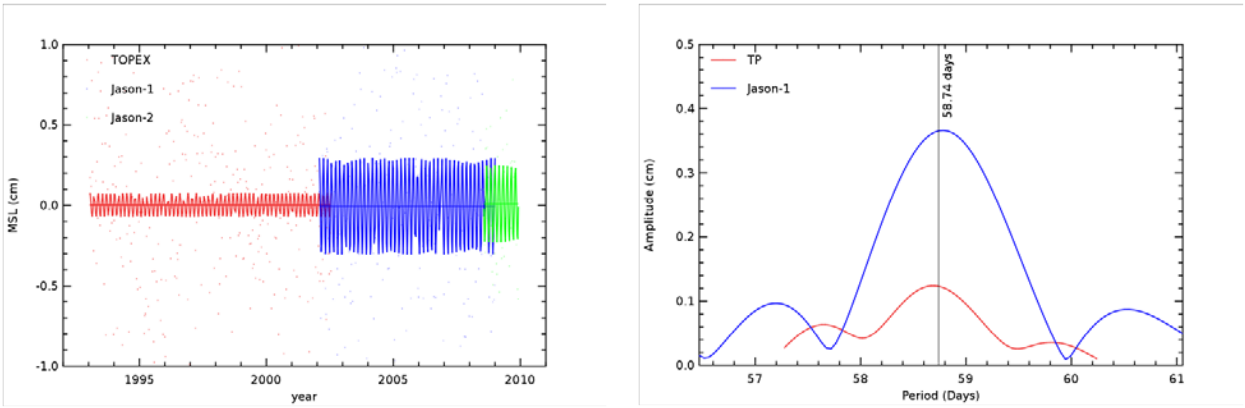

Figure 62: *Left: 58.74-day signal on altimetry/tide gauges SSH differences after removing the global trend. Right: Periodogram on altimetry/tide gauges SSH differences focused on 58.74-day signal.*

The second objective is to analyze the impact of changing corrections applied in the MSL calculation. We especially pay a great attention to oceanic tidal models which contain a strong semi-diurnal signal (S2 wave) and compare the impact of using GOT and FES tide solutions.
As shown on figure 63, the main part of the 58.74-day signal observed on the Jason-1 MSL is due to the use of GOT models in the SSH calculation while FES04 model allows us to significantly reduce down to 0.5 mm the 58.74-day signal on Jason-1 MSL.

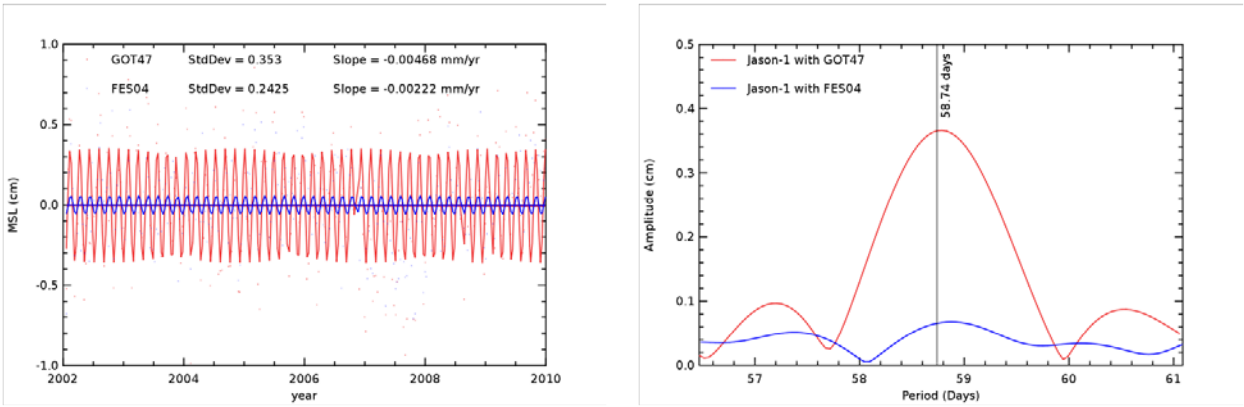

Figure 63: *Left: 58.74-day signal on Jason-1 global MSL after removing the global trend. Right: Periodogram on Jason-1 MSL focused on the 58.74-day signal.*

Using a hydrodynamical model without altimetry assimilation, a 3 mm stronger 58.74-day signal is highlighted on TOPEX MSL than in Jason-1 MSL (figure 64). The main result is that MSL errors on TOPEX for the 58.74-day signal have been likely assimilated by GOT. However, FES04 may have also assimilated TOPEX data with the same errors but this model is less sensitive to altimetry data assimilation than GOT (stochastical model), explaining its better behavior concerning the 58.74-day signal.

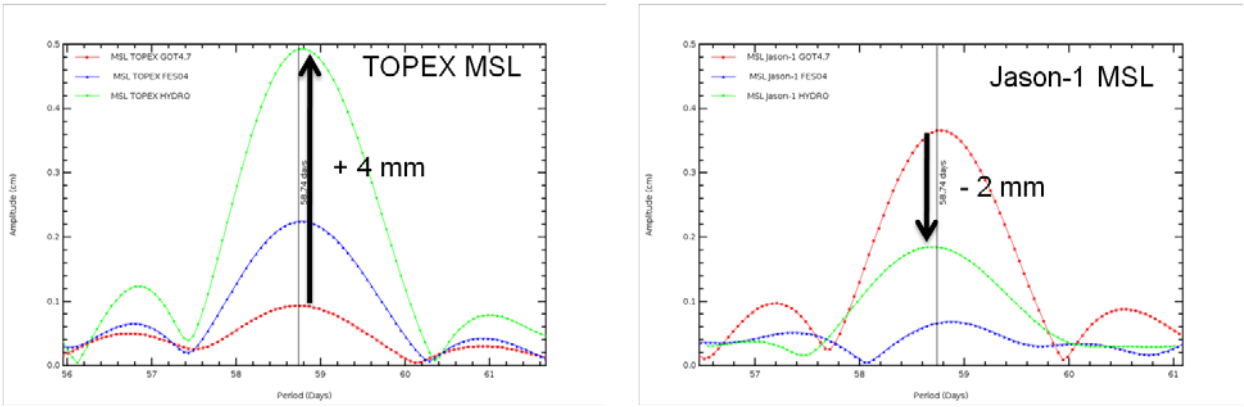

Figure 64: *Sensitivity of oceanic tide models on the 58.74-day signal. Left: TOPEX. Right: Jason-1.*

For TOPEX, a CG_RANGE_CORR correction is available in MGDR. It provides a correction to altimeter tracker range for center of mass movement caused by solar array motion and satellite roll and pitch. This correction has to be either added to the range to correct it or subtracted from Sea Surface height. Figure 65 shows Orbit - range - MSS differences between Jason-1 and TOPEX during Jason-1 verification phase when direct comparison was possible. Difference is plotted in function of local time. A 12 h signal is visible. Applying the CG_RANGE_CORR correction as advised in the Handbook, increases the observed signal (blue curve), whereas applying it with the opposite sign (green curve), reduces the signal. This seemed to indicate that the CG_RANGE_CORR correction has been applied with a bad sign.
Nevertheless, at 2010 OSTST meeting, Zelensky ([118]) showed that CG_RANGE_CORR correc-

tion is valid. It might be that other thermal effects are correlated at the same frequency (12h) and are not yet corrected for.

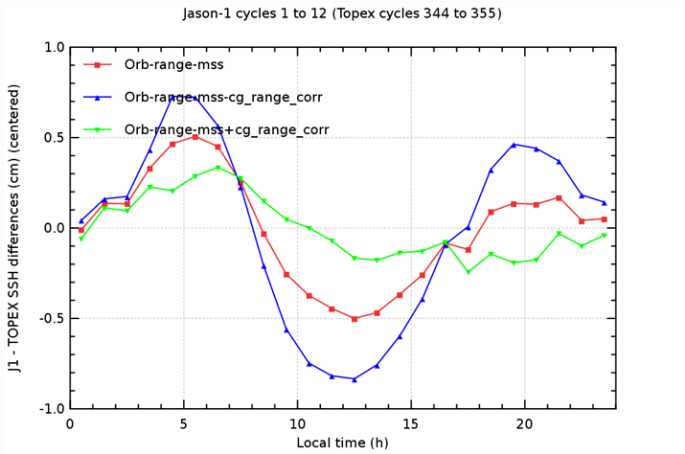

Figure 65: *[Orbit -Range -MSS] differences between Jason-1 and TOPEX applying CG_RANGE_CORR with its current sign (blue curve), its opposite sign (green curve) or without applying it (red curve).*

8.2. Comparison between preliminary GDR-D orbit and GDR-C orbit

Quality of Precise Orbit Ephemeris is crucial for quality of altimeter data products and the studies based upon these data. Inversely, studies using Sea Surface Height (SSH) calculation from altimeter or in-situ data enable to give insight in orbit quality for the different missions, to compare different orbit solutions for one mission, and to give hints which mission is impacted by suspicious behavior, when comparing several missions.

Preliminary GDR-D orbit standard from CNES has been tested over the period from cycle 1 to 331. It has been compared to GDR-C orbit standard (currently used for Jason-1 GDR-C, Jason-2 GDR-T, Envisat GDR V2.1) with the objective to characterize the spatial and temporal differences between the two orbit solutions by temporal evolution of mean and variance and geographical differences of mean. So, this investigation contains SSH crossovers and along-track SLA comparisons, in order to study the impact of using the future GDR-D orbit standard instead of GDR-C orbit standard to compute SSH and SLA and to evaluate global msl trends.

	GDR-C	Preliminary GDR-D
Gravity field	EIGEN-GL04S Drift: Annual + Semiannual 50x50 from EIGEN-GL04SANNUAL	EIGEN-GRGS_RL02bis_MEAN-FIELD : a new mean model from CNES/GRGS spanning 8 years of Grace data
ITRF	2005	2008

Table 5: *O*rbit: GDR-D vs GDR-C

8.2.1. SSH crossovers results comparison

Figure 66 represents the temporal evolution of SSH crossovers statistics (mean and standard deviation) calculated from a cyclic way, using successively both altimetric components in the SSH calculation. The metrics are similar.

The localisation of the main differences in SSH crossovers mean is represented on figure 67. Geographically correlated patterns are already small using GDR-C POE. Mean are slightly reduced in Pacific ocean when using preliminary GDR-D orbit instead of GDR-C one. Little evolutions can be noticed around Australia and in South Atlantic too.

Figure 68 shows the differences between temporal evolution of SSH crossovers variance. During the first part of the mission, the SSH crossovers variances are similar for both orbit solutions. But for the second part of the mission, a SSH variance reduction is observed when using preliminary GDR-D orbit. This reduction increases over time. This is related to the fact that the EIGEN-GRGS_RL02bis_MEAN gravity field benefits from a longer time period of GRACE measurements. A similar behavior is observed with SLA calculation (see figure 70).

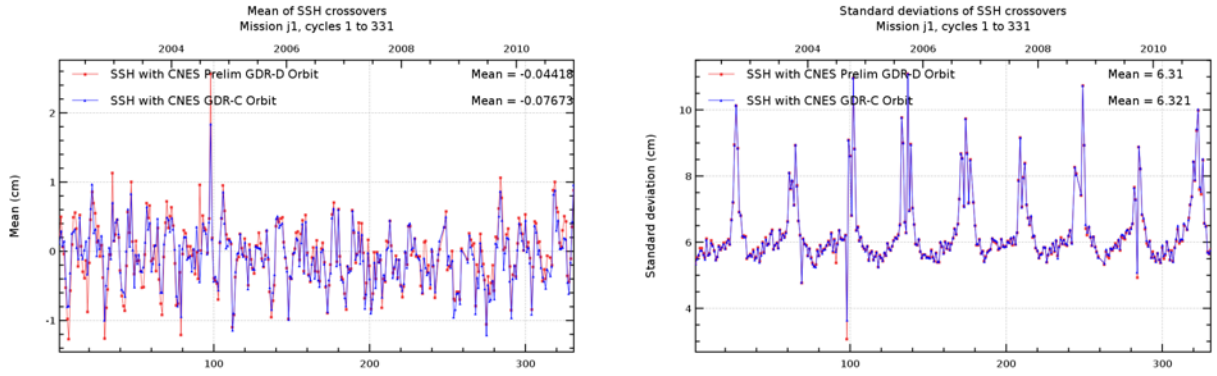

Figure 66: *Cycle mean (left) and standard deviation (right) of SSH crossovers using GDR-C orbit (blue) or preliminary GDR-D orbit (red)*

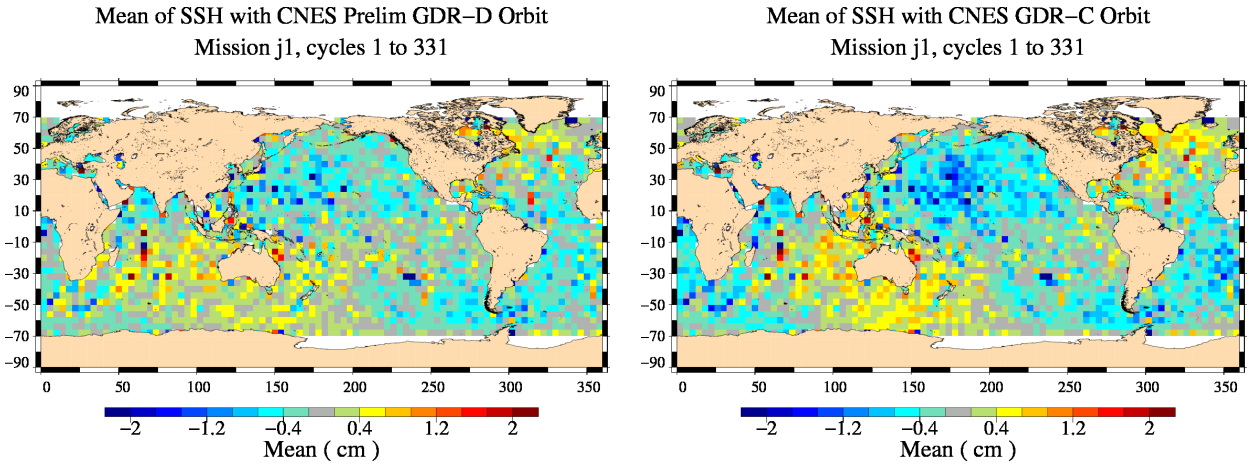

Figure 67: *Localisation of mean of SSH crossovers computed with preliminary GDR-D orbit (left) or with GDR-C orbit (right)*

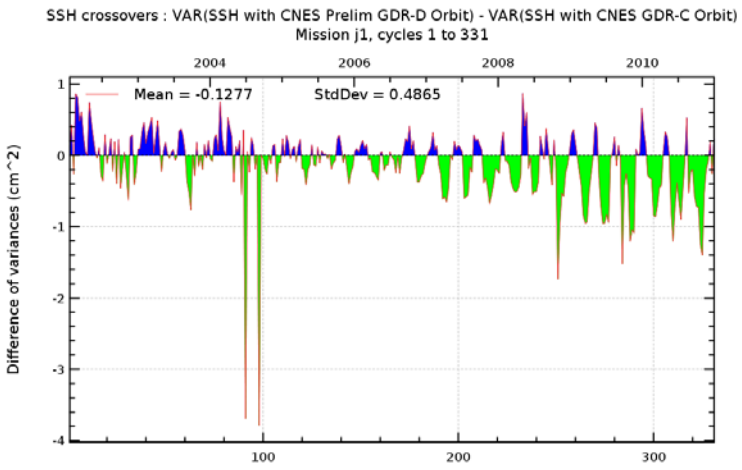

Figure 68: *Cycle SSH crossovers variance difference (X_SSH computed with preliminary GDR-D orbit variance - X_SSH computed with GDR-C orbit variance)*

8.2.2. Sea Level Anomaly evolution

Using preliminary preliminary GDR-D POE instead of GDR-C POE has negligible impact on Jason-1 and Jason-2 global sea level trends. The difference of trends for global msl between even and odd passes decreases from 0.23 mm with GDR-C orbit to 0.16 mm using GDR-D orbit. (See Figue 69)

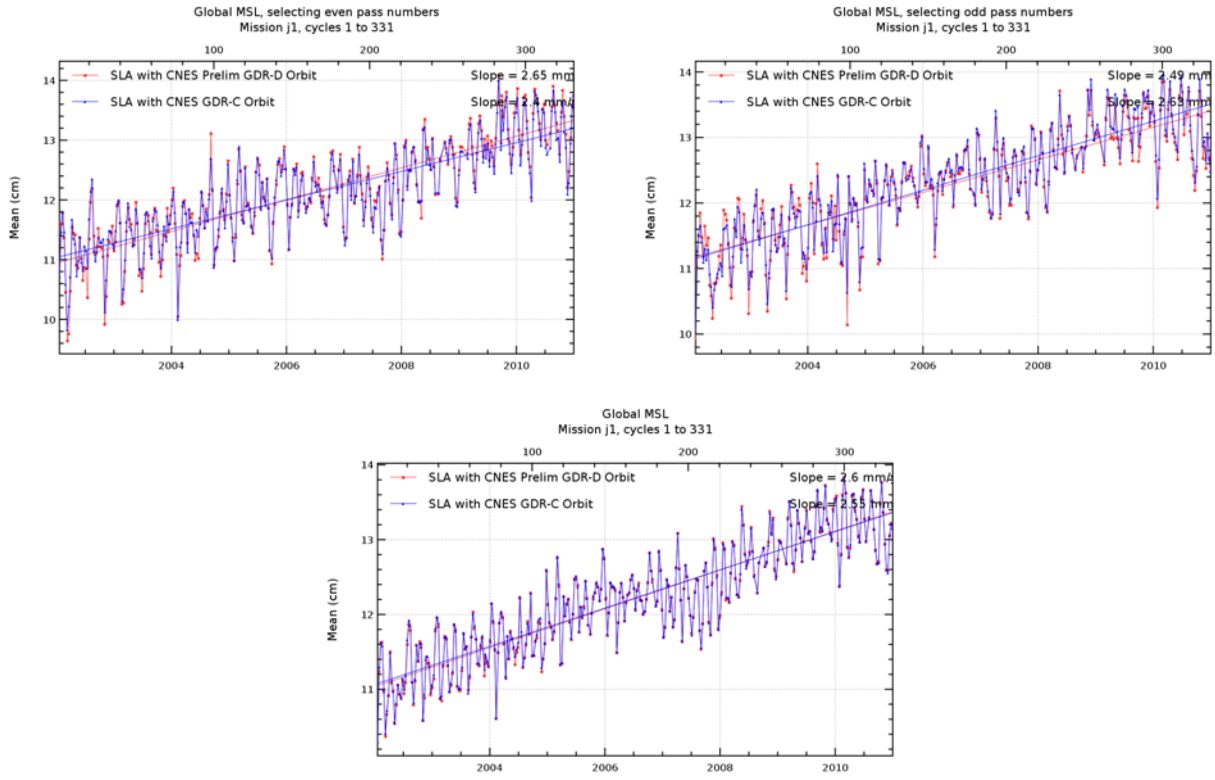

Figure 69: *Global MSL trends (bottom), even pass number (top left), odd pass numbers(top right)*

As for SSH variance differences, the difference of variance for along track SLA computed with GDR-C orbit and with preliminary GDR-D orbit increses at the end of the studied period (see figure 70)

Several authors ([35],[75]) reported an East-West bias between Jason-1 and Envisat when using GDR-C orbits for both missions, which increased from 2007 onwards. This was related to the gravity field used for orbit computation. Using the preliminary GDR-D orbits on both missions, removes this East-West bias (see figure 56, or also Envisat yearly report 2011 [76] or [77]).

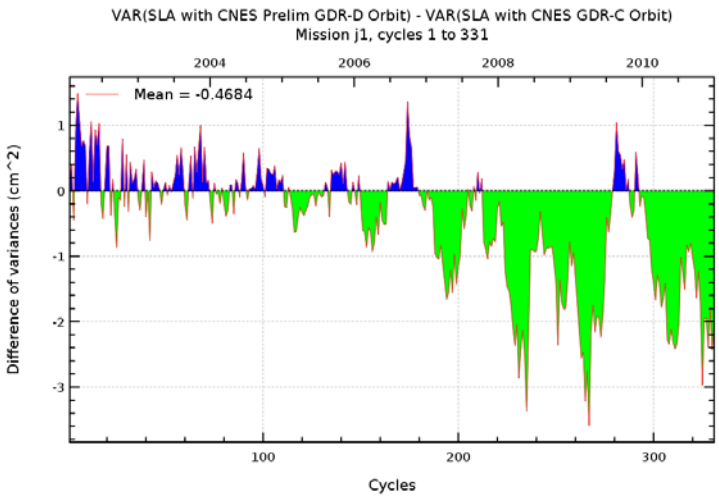

Figure 70: *Cycle SLA variance difference (SLA computed with GDR-D orbit variance - SLA computed with GDR-C orbit variance)*

8.3. Investigations on long-term instabilities on altimeter backscattering coefficient via wind speed comparison

As long-term stability of altimeter backscatter coefficient (σ_0) can impact the accuracy of the global Mean Sea Level (MSL) trend through the Sea State Bias (SSB) correction, it is important to accurately monitor its evolution in order to detect instability such as drifts or jumps. This study aims to characterize long-term σ_0 uncertainties from Jason-1 and Envisat altimeter missions.
Until now, small σ_0 variations lower than 0.1 dB over a year-period have been considered as insignificant since they are within the altimeter missions requirements. Nevertheless, a light σ_0 drift of 0.02 dB/yr has an impact on the global MSL trend close to 0.25 mm/yr via the SSB correction. Such impact is significant for the MSL stability since the scientific requirement on the global MSL stability is of 0.3 mm/yr over a decadal period ([60]).
A lot of effort has already been put into monitoring and checking the long-term stability of the σ_0 parameter. For instance, the long term analyses of the altimeter electronic stability is regularly performed thanks to dedicated calibrations in order to monitor the onboard altimeter power. Another approach is the cross-comparison between altimeter missions data as performed between TOPEX/Poseidon, ERS-2, Jason-1, Jason-2 and Envisat in the frame of calibration and validation activities. By this way, relative σ_0 biases between sets of two missions are commonly estimated which is essential to correctly calibrate wind speed estimations between missions and in the end calculate a good SSB correction. A third way is to monitor the long-term σ_0 parameter stability indirectly via the altimeter-retrieved marine wind speed evolution derived from the main altimeter missions. The interest of the approach developed here is to compare altimeter wind speeds with winds derived from a model (ERA-interim reanalyzes produced by ECMWF).

8.3.1. Analysis of the long-term stability of backscatter coefficient via crossover analyses

The temporal evolution of global mean σ_0 differences between Jason-1 and Envisat derived from 3-hour crossovers has been performed and plotted on left side of figure 71 from 2003 to 2011. It highlights a significant drift from 2003 to 2006 whereas the differences are more stable after this period. This drift corresponds to a jump close to 0.06 dB with an error of $\pm$ 0.01 dB due to the high-frequency signals observed on σ_0 differences. The analysis of the Jason-2 σ_0 stability is less relevant than for Jason-1 and Envisat due to the relative short period: 3 years from mid-2008 to mid-2011. But, three satellites are available during this period which provide σ_0 and wind speed cross-comparisons more reliable to detect anomalies on wind speed evolution. The evolution of σ_0 differences derived from 3-hour crossovers between Envisat and Jason-2 as well as between Jason-1 and Jason-2 has been plotted in right side of figure 71. No drift or jump is detected between Envisat and Jason-2 with small σ_0 differences of 0.012 dB rms. Over the same period, Jason-1 and Jason-2 display stronger σ_0 differences close to 0.023 dB rms, in 2010 the difference reaches even values lower than -0.05 dB. This result highlights Jason-1 σ_0 instabilities. They are due to the strong mispointing values observed on Jason-1 especially in 2010.

8.3.2. Analysis of the long-term stability of backscatter coefficient via wind speed comparison

As mentioned previously, another way to monitor long-term stability of backscatter coefficient is to do wind speed comparison between altimeter and model wind speeds. Several wind speed algorithms exist which compute altimeter wind speed from σ_0 (1-parameter algorithm) or from σ_0 and significant wave height (2-parameter algorithm). For this study, only 1-parameter algorithms

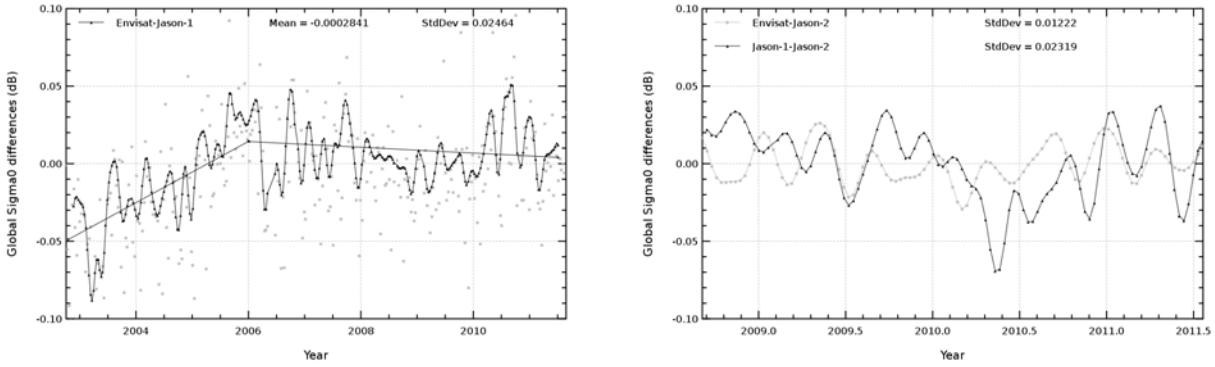

Figure 71: *Evolution of global mean σ_0 differences derived from 3-hour crossovers between Jason-1 and Envisat (left). Evolution of global mean σ_0 differences derived from 3-hour crossovers between Envisat and Jason-2 and between Jason-1 and Jason-2.*

have been applied in order to avoid taking into account potential SWH drifts on altimeter missions. For Jason-1 and Jason-2 (where the product wind speed is derived from a 2-parameter wind speed algorithm) wind speeds have been recomputed using the 1-parameter Abdalla algorithm ([2]) for this study. For Envisat, the very recent reprocessed GDR release (version 2.1) has been used from cycles 9 to 107 (September 2002 to September 2011) where the wind speed is derived from the Abdalla algorithm. Altimeter wind speeds have been compared with winds produced by the European Centre for Medium-Range Weather Forecasts (ECMWF). For this study in order to prevent inhomogeneities due to model version changes, reanalyzed data from ERA-interim product ([33]) were used, instead of operational ECMWF model version.
For this study, altimeter and model wind speed (after interpolating at position and time of altimeter data) were processed similary, involving calculation of global mean wind speed (MWS) time series from a mean grid of valid wind speed (2°x2°) every 10 days and limited to $\pm$ 66° latitude. The global mean for each grid is calculated by weighting each box according to its area in order to give less significance to boxes at high latitudes which cover a smaller area.
The second step consists in comparing the global MWS time series between altimetry and model by calculating directly 10-day differences for each altimetry mission. The global MWS time series differences are then obtained and filtered with a low-pass filter in order to remove high frequency signals lower than 2 months. Residual annual periodic signals due to not explained differences between altimetry and models are also adjusted using a least square method. The interest of this second diagnosis lies in the very good temporal correlation between altimeter and model MWS. Correlations close to 0.9 are obtained between Jason-2 and ERA-interim and between Jason-1 and ERA interim (figure 72) without applying any smoothing over the global MWS time series.

After calculating differences between both altimetry and model, the average rms is reduced to less than 3 cm/s for all the missions. Therefore, thanks to this approach, small drifts or jumps in the global MWS time series are potentially detectable. The minimal threshold to be able to detect such anomalies is likely 3 or 4 cm/s over a year. As a +10 cm/s MWS jump (considering that the global MWS value is close to 7.5 m/s) is approximately equivalent to a σ_0 jump of -0.03 dB, the method developed here allows the detection of σ_0 instabilities close to 0.01 over a year period, which is well below the mission requirement.

Figure 71 showed a significant drift from 2003 to 2006 in σ_0 3-hour crossovers differences between

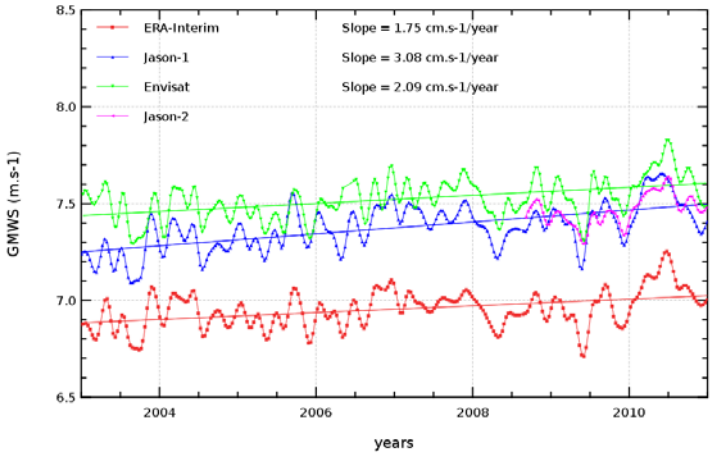

Figure 72: *Evolution of Global mean wind speed derived from Envisat, Jason-1, Jason-2 and ERA-Interim from 2003 onwards (left).*

Envisat and Jason-1. In order to know which mission contains this drift, the temporal evolutions of global MWS differences have been plotted in figure 73 between Jason-1 and ERA-interim, and between Envisat and ERA-interim. Focusing on the analysis of the 2003 to 2006 period, a first drift is clearly detected on Jason-1/ERA-interim MWS differences from mid-2004 to late 2005. Another one is also detected on Envisat/ERA-interim MWS differences during year 2003. These both drifts correspond to a jump of about +10 cm/s for Jason-1 and -10 cm/s for Envisat. As they are not observed on the same period, they are very likely due to altimeter missions and not to the ERA-interim model. Therefore the σ_0 drift previously described between Envisat and Jason-1 from 3-hour crossovers is explained by 2 similar anomalies on both missions corresponding to an Envisat σ_0 jump of +0.03 dB in 2003 and a Jason-1 σ_0 jump of -0.03 dB from mid-2004 to 2005. From 2006 onwards, larger oscillations are observed on Jason-1/ERA-interim MWS differences. They reach 15 cm/s of amplitude in 2010 preventing the detection of drifts during this period. For Envisat, the MWS differences with ERA-interim are more homogeneous at small temporal scales allowing the detection of variations at larger scales with a low increase from 2006 to 2010 and a decrease after. Due to the strong oscillations observed on Jason-1, it is not possible to determine if these variations are due to Envisat or to the ERA-interim model. Cross-comparisons with Jason-2 from mid-2008 (described in next paragraph) provide additional information useful to construe the evolution of MWS differences from 2010 onwards. The origin of these σ_0 instabilities for both missions remains unknown. However, some potential sources of error can be proposed. For Jason-1, the rise of mispointing values due to the low availability of star-trackers ([110]) could have an impact on the global mean σ_0 value. It likely explains the large oscillations observed in 2010 where mispointing values are especially strong ([110]). But the relationship between the σ_0 drift from mid-2004 to 2005 and the apparent mispointing rise during the same period is not demonstrated. For Envisat, the σ_0 evolution detected in 2003 could be in relationship with the global Envisat MSL drift already detected on this period ([77]), but the origin of this MSL drift remains currently unknown.

For the Jason-2 data period, comparisons with ERA-interim have been plotted in figure 74 for Jason-2, Jason-1 and Envisat. As already mentioned, a decrease of global MWS is observed between Envisat and ERA-interim from mid-2009 to 2011 close to -5 cm/s, followed by a +5 cm/s rise after 2011 (on bottom of figure 74). It is interesting to observe that similar global MWS vari-

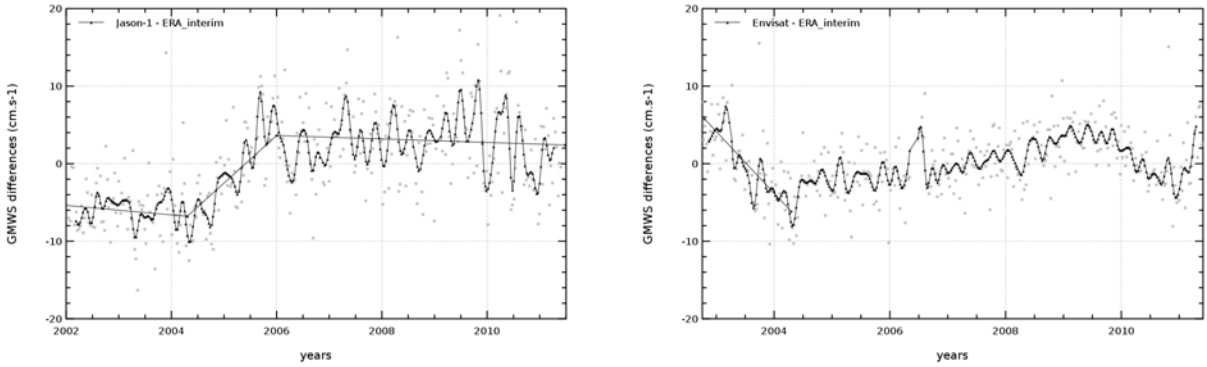

Figure 73: *Evolution of global mean wind speed differences between Jason-1 and ERA-interim after filtering out signals lower than 2 months and removing residual annual and semi-annual signals.*

ations are observed between Jason-2 and ERA-interim (on top left of figure 74). Between Jason-1 and ERA-interim (on top right of figure 74), this signal seems still visible although oscillations at smaller time scales due to the Jason-1 σ_0 instabilities prevent its good detection. Therefore, this cross-comparison analysis derived from 3 satellites indicates that these variations on global MWS between mid-2009 and mid-2011 do not result from altimeter instabilities but they are likely due to the ERA-interim model. To check this analysis, the comparison with NCEP model has also been performed (not shown here). The evolution of global MWS differences with the 3 altimetry missions does not reveal any similar variation confirming that the ERA-interim wind speed is not as stable as altimetry at global time scale over the Jason-2 period. Due to these instabilities, the detection of σ_0 drifts on this period is thus not as relevant as from 1993 to 2009.

8.3.3. Conclusion

The main result of this study is the detection of long-term σ_0 instabilities on altimetry missions. Thanks to thorough cross-comparisons between global MWS derived from altimetry and models, σ_0 drift or abnormal variations have been detected and described accurately. The major interest of estimating these instrumental errors concerns their impact on the global MSL evolution. For the global MSL trend, the impact of the small σ_0 drifts (+0.03 dB in 2003 for Envisat, -0.03 dB for Jason-1 from mid-2004 to 2005 and -0.1 dB from 1993 to 2002 for TOPEX) is low but not negligible since they translate to an overestimation of the global MSL trend (AVISO approach) of about 0.1 mm/yr from 1993 to 2011.
This study, completed with analyses for TOPEX and ERS-2 data and estimation of impact on MSL, is submitted to Marine Geodesy.

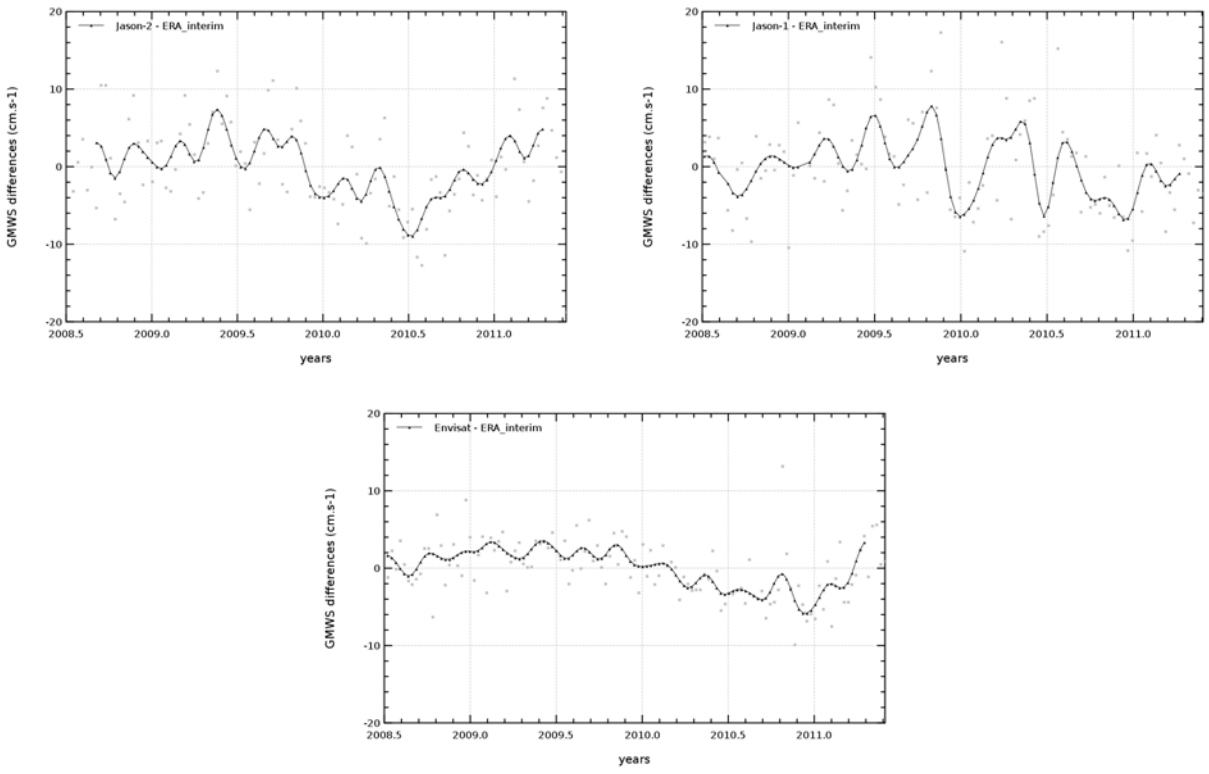

Figure 74: *Evolution of global mean wind speed differences between Jason-2 and ERA-interim (top left), Jason-1 and ERA-interim (top right) and Envisat and ERA-interim (bottom) after filtering out signals lower than 2 month and removing residual annual and semi-annual signals.*

8.4. Events during 2010

During 2010, the Jason-1 satellite experienced several events, which had an impact on its data availability and quality. Several events are indicated by colored lines in figure 75.

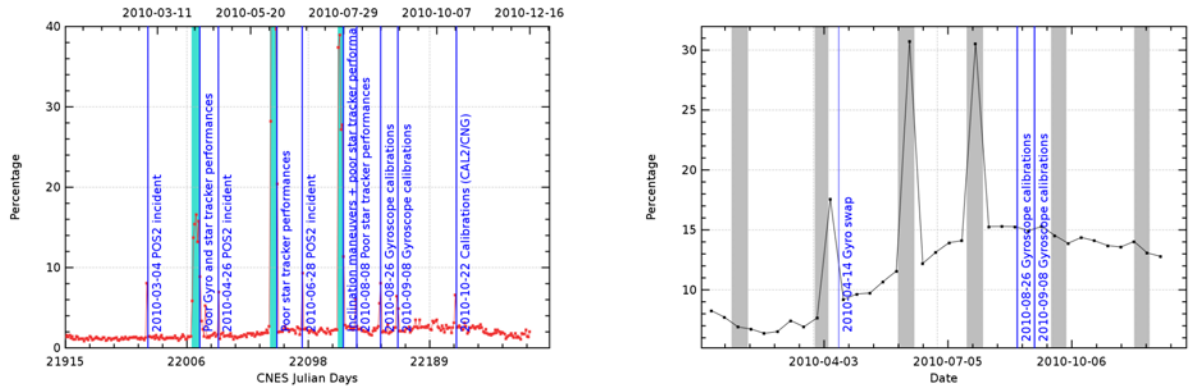

Figure 75: *Daily monitoring of missing ocean measurements (left) and cyclic monitoring of edited measurements (right) for Jason-1 during 2010. Gray stripes indicate periods, where Jason-1 is in fix mode.*

Due to poor star tracker performances related to beta angle values and also poor gyro wheel performances, Jason-1 experienced several periods of high off-nadir angles of the platform, especially when the satellite was in fix mode (see figure 76). End of July / beginning of August, several inclination maneuvers were performed in order to deplete fuel. This had an impact on data quality, but also on data availability, as star tracker performances were poor.

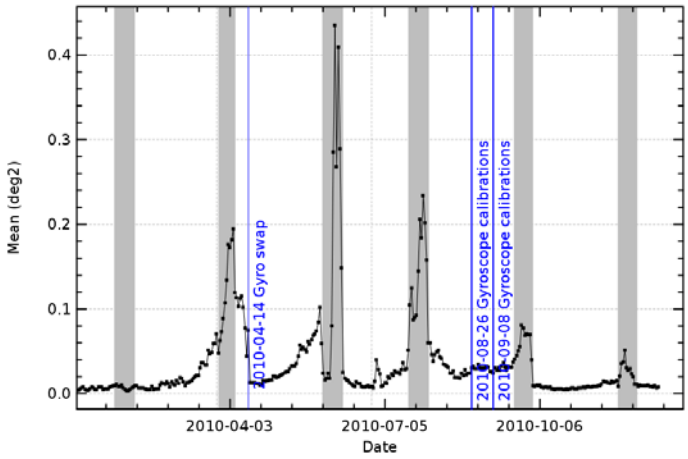

Figure 76: *Daily monitoring of Jason-1 apparent squared misponting from waveforms for 2010. Gray stripes indicate periods, where Jason-1 is in fix mode.*

8.4.1. Events of high mispointing

Since mid-march 2010, off-nadir angles of the platform were increased for Jason-1, which affected especially OSDR data, as they still use on-bord MLE3 tracking (which needs off-nadir angles < 0.4 deg). Therefore, when this threshold was exceeded, several passes had altimeter data at default value. In April (during cycle 304), off-nadir angles were such high, that altimeter lost several times tracking. Therefore, data gaps appeared, which also impacts IGDR and GDR data. Furthermore, gyroscope 1 showed poor performances during March and April. Therefore, a swap of gyroscopes was done on 2010-04-14.
Mispointing reached several times between April and October 2010 high values. During fall 2010, upload of new tables to the star trackers were done. For the last months of 2010, mispointing values were on an usual level again.

Relationship between mispointing and missing measurements, is shown for cycle 304 as an example. High mispointing values occurred especially for local hours around 12h as shown in figure 77.

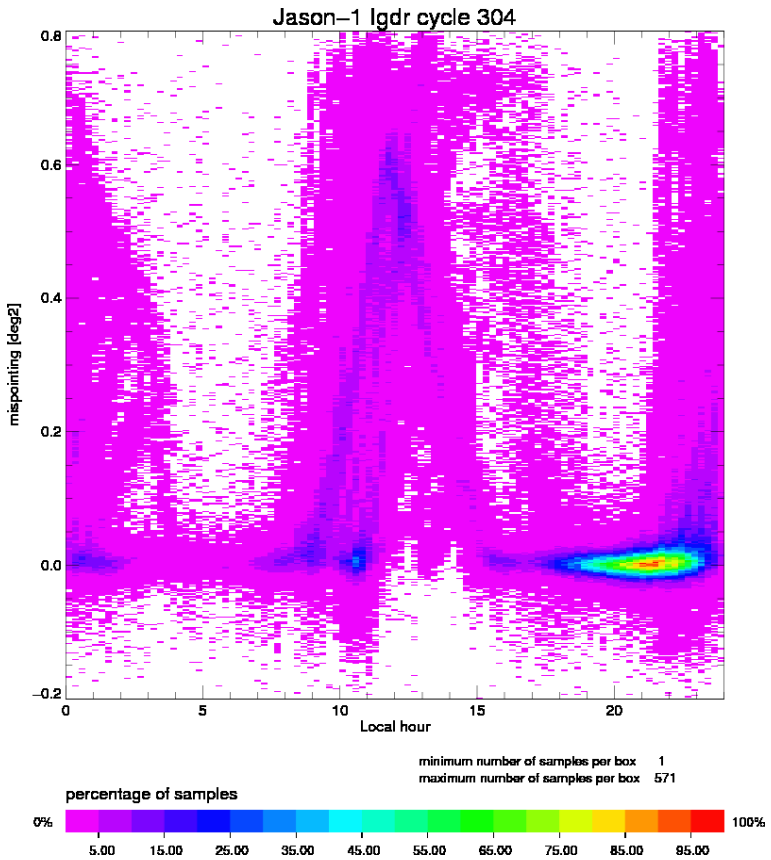

Figure 77: *Dispersion diagram between local hours and mispointing values for Jason-1 cycle 304.*

When looking at a particular pass (124), one observe, that:

- Over land (till 12h15), number of elementary range measurements and mispointing is disturbed.
- Over ocean (between approximatively 12h15 and 12h31), number of elementary range measurements is close to 20 (highest possible value) and apparent squared mispointing increases rapidly from about 0 deg2 to 0.6 deg2.

- For mispointing values higher than 0.64 deg2 (threshold for validation), data are edited. Furthermore number of elementary range measurements decreases rapidly.
- From about 12h36, mispointing values are at default value (as well as other altimeter parameters, such as range, significant wave height, backscattering coefficient), whereas number of elementary range stay at zero till 12h44. These measurements are therefore edited by the several threshold criteria.
- From 12h44 onwards, till almost the end of the pass, measurements are missing.

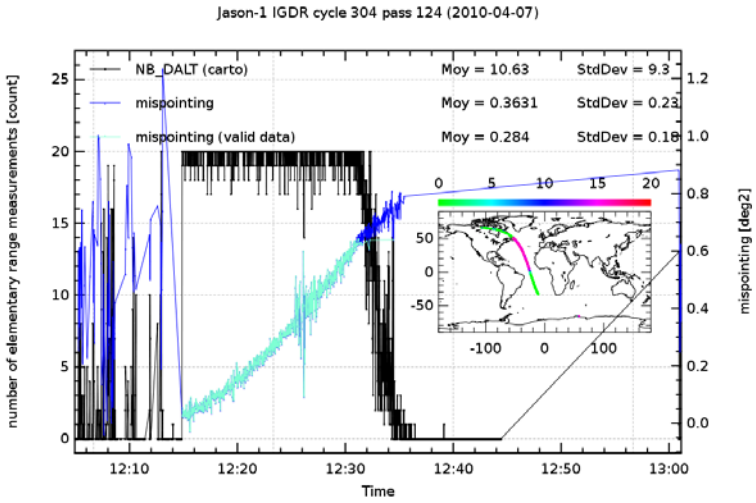

Figure 78: *Apparent squared mispointing (blue) and number of elementary Ku-band range measurements (black) for pass 124, cycle 304.*

As pass 124, many other passes of cycle 304 were impacted by high off-nadir angles. Indeed percentage of missing and edited measurements is high for this cycle, as shown on figure 79.

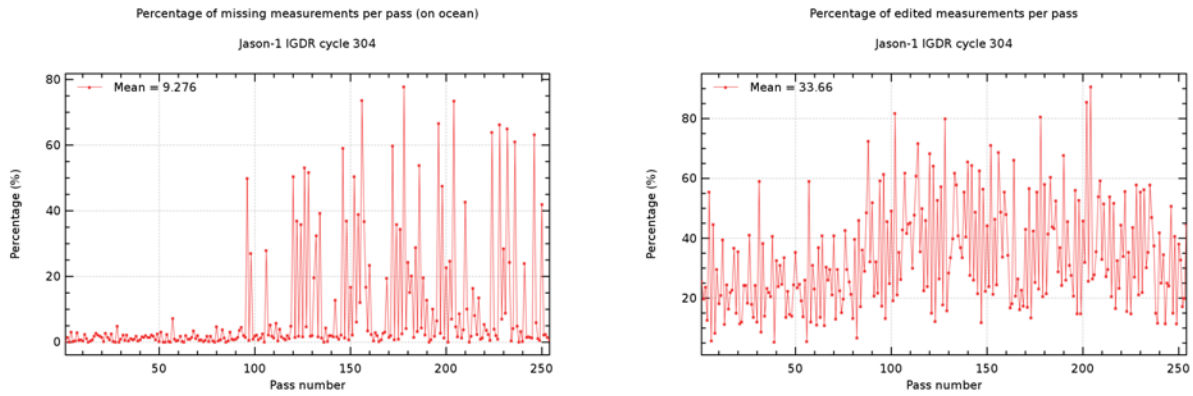

Figure 79: *Pass by pass montitoring of missing ocean measurements (left) and edited measurements (right) for Jason-1 cycle 304.*

8.4.2. Fuel depletion maneuvers

In order to reduce the risk of an explosion in the event of any type of collision, the fuel tank of Jason-1 was partially depleted. Between 10 to 12 out of plane maneuvers were scheduled to burn about half of remaining propellant (about 11 kg), but only 6 inclination maneuvers took place, as a problem was detected on thrust number 4. The out of plan maneuvers began on the 20th of July around 19:00 UTC (start of cycle 315) and ended on 28th of July. The impact on the orbit inclination was 0.04° max, this changes slightly the ground track. Each maneuver consisted of 2 propulsions. One day, this modified the orbit inclination by about 0.04°, the next day the maneuvers put the orbit back to nominal inclination. During the first days of August, several OCM2 maneuvers were necessary in order to put the satellite back in its station keeping box.

8.4.2.1. Cross-track distance

Cross-track distance was monitored over the period of maneuvers, showing important variations to be linked with different maneuvers (figure 80). Departure up to 7 km were observed in the firsts maneuvers period. Finally cross-track distance came back to its nominal value (less than 1 km). As far as altimetry processing are concerned, the risk associated to this configuration is a degradation of the SLA from a subpar cross-track geoid gradient correction (or CTGG, see Dorandeu et al, 2003 [41]) or inadequate mean profile (time reference used for the computation of Sea Level Anomalies).

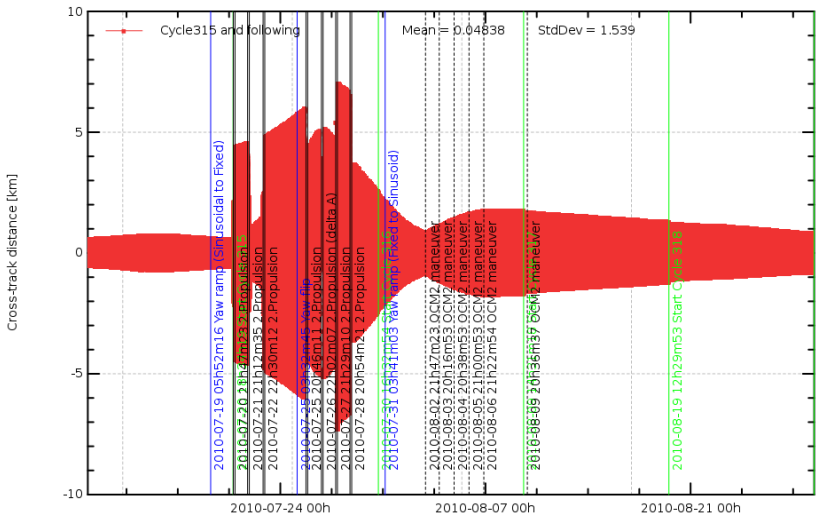

Figure 80: *Monitoring of cross-track distance from nominal ground-track for cycles 314 to 318.*

8.4.2.2. Data quality during cycle 315

During the first couples of out of plan maneuvers there were no missing measurements. But following Yaw flip maneuver, mispointing increased and several data gaps appeared, which coincide with maneuver periods (see left side of figure 81). Data during maneuver periods are edited, as orbit quality is degraded (see right side of figure 81). Following Yaw flip maneuver, number of

edited measurements increases as mispointing is very high and altimeter parameters are often at default values.
In the light of the many out of plan maneuvers (which are difficult to take into account for precise orbite computation), note that the POE for cycle 315 was not recomputed, but is an assembled MOE. Performances of SSH differences at cross-over points are therefore not as good as usual (see also figure 32).

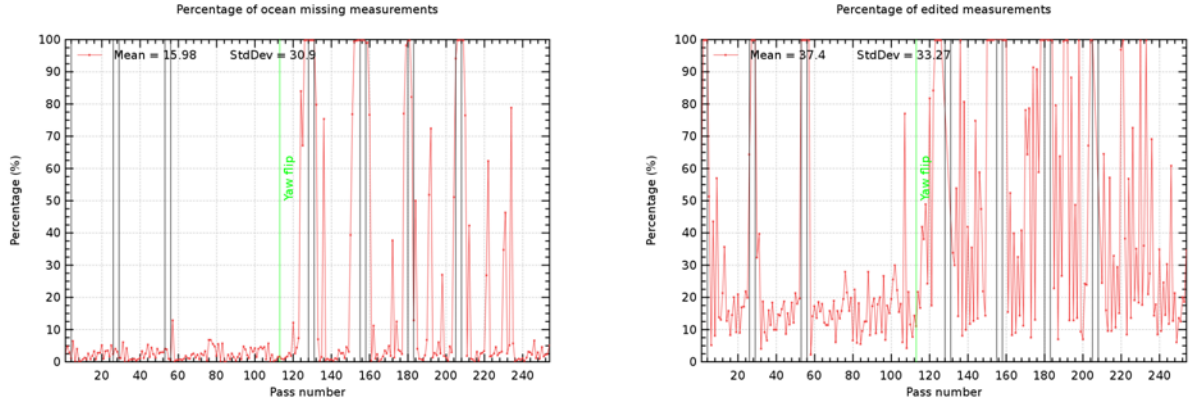

Figure 81: *Pass by pass monitoring of missing ocean measurements (left) and edited measurements (right) for Jason-1 cycle 315. Orbit maneuvers are indicated by black lines. Yaw maneuver is indicated by green line.*

8.5. Events during 2011

During 2011, the Jason-1 satellite experienced several events, which had an impact on its data availability and quality. Several events are indicated by colored lines on left side of figure 82. The events which lead to missing measurements are :

- long calibrations.
- data loss due to imprecise datation during an autoinit diode.

After uploading a safety patch, which works also during OCM4 maneuvers, the fuel depletion maneuvers of Jason-1 resumed in September and October 2011 (during cycles 356, 358, 359, and 360). The maneuvers are listed in table 6. They consisted in inclination maneuvers, which are quite strong and long maneuvers. During these cycles, more measurements than usual are edited, as shown on the right side of figure 82. During this fuel depletion campaign, precise orbit determination was computed, but it was quite difficult for these cycles and needed a special processing. Often, this special POE processing gave better results than MOE processing (orbit available in the IGDR product), as can be seen on figure 83

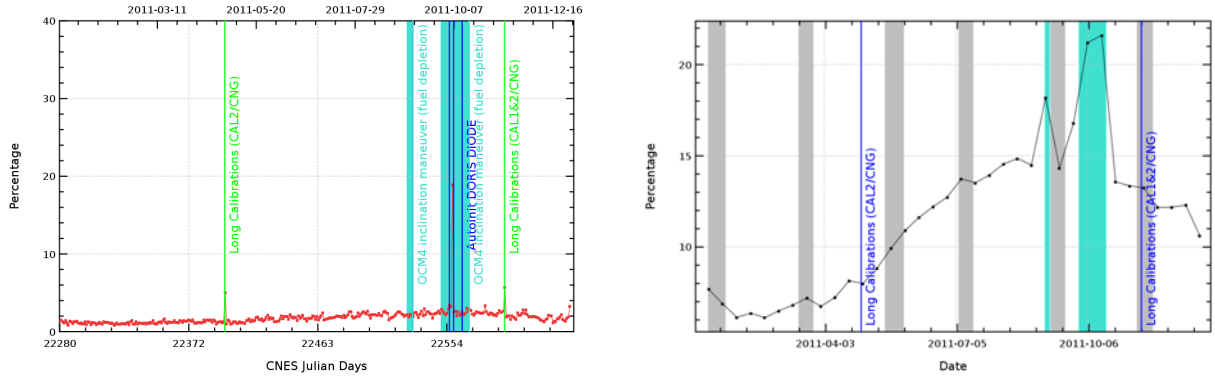

Figure 82: *Daily montitoring of missing ocean measurements (left) and cyclic monitoring of edited measurements (right) for Jason-1 during 2011. Gray stripes indicate periods, where Jason-1 is in fix mode. Turquoise stripes indicate periods where fuel depletion maneuvers took place.*

Nevertheless, SLA of GDR products is still impacted by maneuvers. It is therefore advised to use orb_state_flag, in order to invalidate POE estimated during maneuver periods.

Due to the out of plane maneuvers, the cross-track distance departed from nominal theoretical track (outside of the ± 1km station keeping box). Figure 84 shows the cross-track distance of Jason-1 for September and October 2011. For OSDR and IGDR products it is generally less than 3 km. This are better values than during 2010, when cross-track distance could depart up to 7 km. Nevertheless for GDR product, cross-track distance departs for a couple of maneuvers up to 10 km from nominal ground-track. This is very likely related to the special treatment for POE computation. But as these high cross-track distances occur between 2 maneuver thrusts, their measurements are already invalidated by orb_state_flag.

Apparent squared mispointing was generally very low during 2011. Daily statistics show values less than 0.03 deg2 (see figure 85). This is an huge improvement compared to mispointing values during mid-2010.

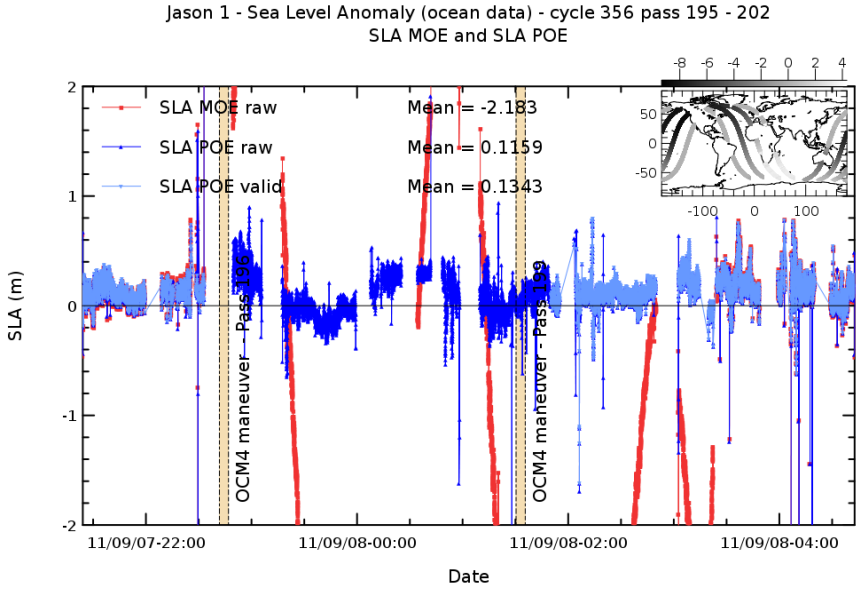

Figure 83: *Along-track SLA for IGDR (red) and GDR (blue) for cycle 356, passes 195 to 202. inclination maneuvers took place on pass 196 and 199.*

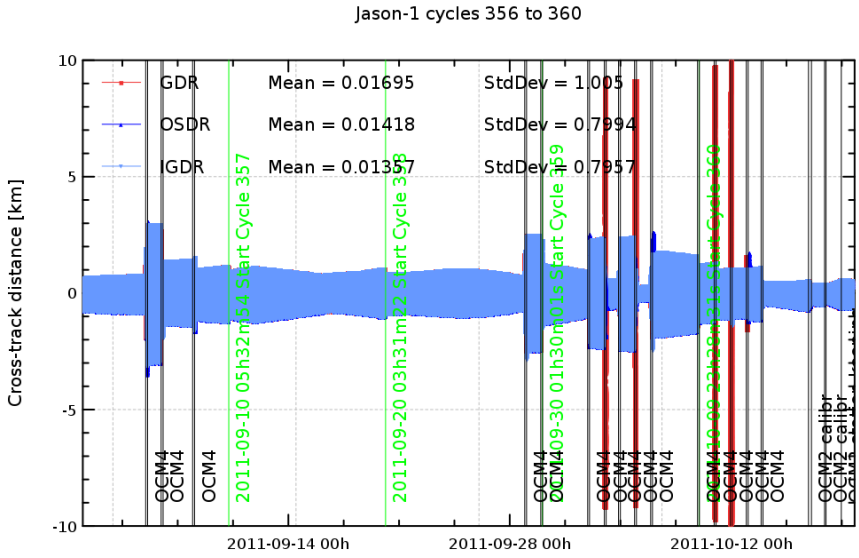

Figure 84: *Monitoring of cross-track distance from nominal ground-track for cycles 356 to 360.*

Maneuver type/Event	Period	Cycle/Pass
OCM4 inclin. man (fuel depletion)	2011-09-04 from 23:29:35 to 23:34:26	C356/P120
OCM4 inclin. man (fuel depletion)	2011-09-05 from 02:18:13 to 02:23:07	C356/P123

.../...

Maneuver type/Event	Period	Cycle/Pass
OCM4 inclin. man (fuel depletion)	2011-09-05 from 22:52:34 to 23:02:15	C356/P145
OCM4 inclin. man (fuel depletion)	2011-09-06 from 01:41:06 to 01:50:59	C356/P148
OCM4 inclin. man (fuel depletion)	2011-09-07 from 22:41:45 to 22:46:55	C356/P196
OCM4 inclin. man (fuel depletion)	2011-09-08 from 01:30:22 to 01:35:36	C356/P199
OCM4 inclin. man (fuel depletion)	2011-09-28 from 22:45:21 to 22:50:17	C358/P226
OCM4 inclin. man (fuel depletion)	2011-09-29 from 01:33:59 to 01:38:58	C358/P229
OCM4 inclin. man (fuel depletion)	2011-09-29 from 23:04:32 to 23:14:19	C358/P252
OCM4 inclin. man (fuel depletion)	2011-09-30 from 01:53:06 to 02:03:03	C359/P001
OCM4 inclin. man (fuel depletion)	2011-10-02 from 22:16:49 to 22:26:40	C359/P074
OCM4 inclin. man (fuel depletion)	2011-10-03 from 01:05:24 to 01:15:23	C359/P077
OCM4 inclin. man (fuel depletion)	2011-10-03 from 23:34:38 to 23:44:28	C359/P101
OCM4 inclin. man (fuel depletion)	2011-10-04 from 02:23:12 to 02:33:10	C359/P104
OCM4 inclin. man (fuel depletion)	2011-10-04 from 21:07:32 to 21:17:25	C359/P124
OCM4 inclin. man (fuel depletion)	2011-10-04 from 23:56:08 to 2011-10-05 00:06:08	C359/P127
OCM4 inclin. man (fuel depletion)	2011-10-05 from 21:29:07 to 21:39:00	C359/P150
OCM4 inclin. man (fuel depletion)	2011-10-06 from 00:17:44 to 00:27:42	C359/P153
OCM4 inclin. man (fuel depletion)	2011-10-06 from 21:50:42 to 22:00:35	C359/P176
OCM4 inclin. man (fuel depletion)	2011-10-07 from 00:39:18 to 00:49:17	C359/P179
OCM4 inclin. man (fuel depletion)	2011-10-09 from 21:03:01 to 21:12:55	C359/P252
OCM4 inclin. man (fuel depletion)	2011-10-09 from 23:51:37 to 2011-10-10 00:01:37	C360/P001
OCM4 inclin. man (fuel depletion)	2011-10-10 from 22:20:49 to 22:30:44	C360/P025
OCM4 inclin. man (fuel depletion)	2011-10-11 from 01:09:24 to 01:19:23	C360/P028
OCM4 inclin. man (fuel depletion)	2011-10-11 from 22:42:24 to 22:52:19	C360/P051
OCM4 inclin. man (fuel depletion)	2011-10-12 from 01:30:59 to 01:40:59	C360/P054
OCM4 inclin. man (fuel depletion)	2011-10-12 from 23:04:52 to 23:13:00	C360/P077
OCM4 inclin. man (fuel depletion)	2011-10-13 from 01:53:28 to 02:01:39	C360/P080
OCM4 inclin. man (fuel depletion)	2011-10-13 from 21:35:27 to 21:40:43	C360/P101
OCM4 inclin. man (fuel depletion)	2011-10-14 from 00:24:04 to 00:29:21	C360/P104
OCM2 calibr. man	2011-10-16 from 21:28:30 to 21:29:32	C360/P178

.../...

Maneuver type/Event	Period	Cycle/Pass
OCM2 calibr. man	2011-10-17 from 01:59:06 to 02:00:02	C360/P182,183
OCM2 calibr. man	2011-10-17 from 21:52:46 to 21:53:46	C360/P204
OCM2 calibr. man	2011-10-18 from 00:03:49 to 00:04:45	C360/P206
OCM2 station keeping man	2011-10-18 from 23:13:20 to 23:13:33	C360/P231
autoinit DORIS DIODE	2011-09-08 from 03:03:50 to 04:25:50	C359/P103,104
autoinit DORIS DIODE	2011-10-04 from 01:44:40 to 02:47:10	C359/P103,104
autoinit DORIS DIODE	2011-10-07 from 02:49:00 to 04:00:50	C359/P181,182
autoinit DORIS DIODE	2011-10-13 from 05:07:10 to 06:02:10	C360/P083,084

Table 6: *F*uel depletion maneuvers during 2011 (cycles 356 to 360)

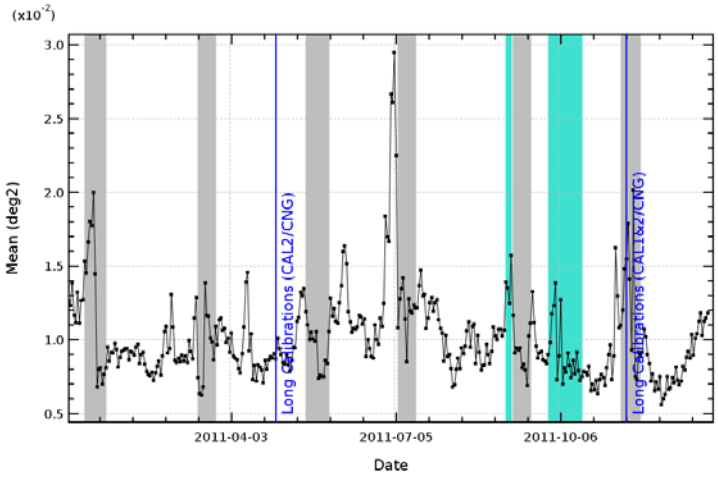

Figure 85: *Daily monitoring of Jason-1 apparent squared misponting from waveforms for 2011. Gray stripes indicate periods, where Jason-1 is in fix mode. Turquoise stripes indicate periods where fuel depletion maneuvers took place.*

9. Conclusion

Jason-1 celebrated its 10th anniversary in December 2011. Since the beginning of the Jason-1 mission and until the end of the T/P mission in October 2005, T/P and Jason-1 overflew the ocean over 2 parallel passes except the 21 first cycles, when they were on the same pass. Thanks to this long flight configuration, performances comparisons between both missions have been performed with success during 4 years, proving that the major objective of the Jason-1 mission to continue the T/P high precision has been reached.
The good quality of Jason-1 data has been shown in this report : the main altimeter parameters are stable and have the same behaviors as T/P ones, the crossover and along-track performances remain very good. Since mid-2008 Jason-1 flies in tandem with Jason-2. After the flight formation phase with Jason-2, Jason-1 was moved in February 2009 on its interleaved orbit. This is the same ground track as Topex/Poseidon during its tandem phase with Jason-1, but there is a time shift of 5 days. Cross-over and along-track performances remain good.

In 2010 and 2011, fuel depletion maneuvers have been performed, in order to reduce the risk of explosion in case of a collision with debris or other satellites. This allows to continue operating on Jason-1 on its current orbit until 2013.
Finally, Jason-1 continues to gather valuable altimeter data. Comparisons between both Jason missions are consistent, which is a good indicator of the performance of both satellites.

10. References

References

[1] Abdalla, S., P. A.E.M. Janssen, and J.-R. Bidlot, 2010: Jason-2 OGDR Wind and Wave Products: Monitoring, Validation and Assimilation. *Mar. Geod.*, **33 (S1), 239-255.**

[2] Abdalla, S.: Ku-band Altimeter Surface Wind Speed Algorithm. Proc. Envisat Symposium 2007, Montreux, Switzerland 23-27 April 2007 (ESA SP-636)

[3] Ablain, M., J. Dorandeu, Y. Faugère, F. Mertz, B. Soussi, F. Mercier, P. Vincent, and N. Picot, 2003a: SSALTO/CALVAL Jason-1 data quality assessment and Jason-1 / TOPEX cross-calibration using GDRs. *Paper presented at the Jason-1 and TOPEX/Poseidon Science Working Team Meeting, Arles (France), November.*

[4] Ablain, M., J. Dorandeu, Y. Faugere, F. Mertz, 2004: Jason-1 Validation and Cross-calibration activities Contract No 731/CNES/00/8435/00. Available at: http://www.jason.oceanobs.com/documents/calval/validation_report/j1/annual_report_j1_2004.pdf

[5] Ablain, M. and J. Dorandeu, 2005: TOPEX/Poseidon validation activities, 13 years of T/P data (GDR-Ms), Available at: http://www.jason.oceanobs.com/documents/calval/validation_report/tp/annual_report_tp_2005.pdf

[6] Ablain, M., S. Philipps, P. Thibaut, J. Dorandeu, and N. Picot, 2009: Jason-1 GDR Quality Assessment Report. Cycle 273. SALP-RP-P2-EX-21072-CLS273,. http://www.jason.oceanobs.com/fileadmin/documents/calval/validation_report/J1/Bilan_Calval_J1_Cycle_273.pdf

[7] Ablain, M., S. Philipps, S. Labroue, J. Dorandeu, and N. Picot, 2007: SSALTO CALVAL Consistency assessment between Jason-1 and TOPEX. poster presented at OSTST meeting, Hobart, Australia, 12-15 march 2007. Available at: http://www.jason.oceanobs.com/documents/swt/posters2007/ablain_J1TP.pdf

[8] Ablain, M., S. Philipps, J. Dorandeu, and N. Picot, 2007: SSALTO CALVAL Performance assessment Jason-1 data. Poster presented at OSTST meeting, Hobart, Australia, 12-15 march 2007. Available at: http://www.aviso.oceanobs.com/fileadmin/documents/OSTST/2007/ablain_J1.pdf

[9] Ablain, M., S. Philipps, N. Picot, and E. Bronner, 2010: Jason-2 Global Statistical Assessment and Cross-Calibration with Jason-1. *Marine Geodesy*, **33(S1), 162-185**. Available at http://pdfserve.informaworld.com/807580__925506316.pdf

[10] Ablain, M., S. Philipps, L. Carrere, G. Valladeau, J.-F. Legeais, E. Bronner, and N. Picot, 2010: Analysis of 58.74-day signal observed on the MSL derived from Jason-1&2 and TOPEX data. Oral presentation at OSTST meeting, Lisbon, Portugal, 18-20 October 2010. Available at: http://www.aviso.oceanobs.com/fileadmin/documents/OSTST/2010/oral/20_Wednesday/morning/Ablain.pdf

[11] Ablain, M., M. Urvoy, N. Tran, E. Bronner, and N. Picot, 2010: Analysis of wind speed evolution over ocean derived from altimeter missions and models. Oral presentation at OSTST meeting, Lisbon, Portugal, 18-20 October 2010. Available at: http://www.aviso.oceanobs.com/fileadmin/documents/OSTST/2010/oral/19_Tuesday/Tuesday_afternoon/ABLAIN.pdf

[12] Ablain, M., G. Valladeau, S. Philipps, P. Thibaut, and N. Picot, 2011: Jason-1 GDR Quality Assessment Report. Cycle 363. SALP-RP-P2-EX-21072-CLS363,. http://www.aviso.oceanobs.com/fileadmin/documents/calval/validation_report/J1/BilanCalval_J1_Cycle_363.pdf

[13] Ablain, M., S. Philipps, J. Dorandeu, P. Thibaut and N. Picot, 2006: SSALTO CALVAL Performance assessment Jason-1 GDR 'B'/ GDR 'A'. Poster presented at OSTST meeting, Venice, Italy, 16-18 march 2006. Available at: http://www.aviso.oceanobs.com/fileadmin/documents/OSTST/2006/ablain1.pdf

[14] Ablain, M., S. Philipps, M. Urvoy, N. Tran, and N. Picot, 2012: Detection of long-term instabilities on altimeter backscatter coefficient thanks to wind speed data comparisons from altimeters and models. *Mar. Geod.* Accepted for publication in Volume 3 of the Marine Geodesy special issue on Jason-2 altimetry.

[15] Amarouche, L., P. Thibaut, O.Z. Zanife, P. Vincent, and N. Steunou. 2004: Improving the Jason-1 Ground Retracking to Better Account or Attitude Effects. *Mar. Geod.***27 (1-2): 171-197.**

[16] Arnault, S., N. Chouaib, D. Diverres, S. Jaquin, and O. Coze, 2004: Comparison of TOPEX/Poseidon and JASON Altimetry with ARAMIS In Situ Observations in the Tropical Atlantic Ocean. *Mar. Geod.***27 (1-2): 15-30.**

[17] Aviso User Handbook: Merged Topex/Poseidon Products (1996). AVI-NT-02-101-CN, edition 3.0. Available at http://www.aviso.oceanobs.com/fileadmin/documents/data/tools/hdbk_tp_gdrm.pdf

[18] Boy, François and Jean-Damien Desjonqueres. 2010: Note technique datation de l'instant de reflexion des échos altimètres pour POSEIDON2 et POSEIDON3 *Reference: TP3-JPOS3-NT-1616-CNES*

[19] Brown G.S., 1977: The average impulse response of a rough surface and its application, IEEE Transactions on Antenna and Propagation, Vol. AP 25, N1, pp. 67-74, Jan.

[20] Brown, S., S. Desai, W. Lu, and A. Sibthorpe. 2009. Performance Assessment of the Advanced Microwave Radiometer after 1 Year in Orbit. *Oral presentation at OSTST meeting, Seattle, USA*. Available at: http://www.aviso.oceanobs.com/fileadmin/documents/OSTST/2009/oral/Brown.pdf

[21] Callahan, Phil., 2006: electronic communication (retrk-gdr-data-rec-r10.062.pdf) send to OSTST on 13 February.

[22] Carayon, G., N. Steunou, J. L. Courriere, and P. Thibaut, 2003: Poseidon 2 radar altimeter design and results of in flight performances. *Mar. Geod.***26(3-4): 159-165.**

[23] Carrère, L., and F. Lyard, 2003: Modeling the barotropic response of the global ocean to atmospheric wind and pressure forcing - comparisons with observations. Geophys. Res. Lett., 30(6), 1275, doi:10.1029/2002GL016473.

[24] Cerri L., A. Couhert, S. Houry and F. Mercier, 2011: Improving the long-term stability of the GDR orbit solutions. OSTST presentation, San Diego.

[25] Chambers, D. P., S. A. Hayes, J. C. Ries, and T. J. Urban, 2003: New TOPEX sea state bias models and their effect on global mean sea level. J. Geophys. Res. 108(C10): 3305.

[26] Chambers, D., P., J. Ries, T. Urban, and S. Hayes, 2002: Results of global intercomparison between TOPEX and Jason measurements and models. Paper presented at the Jason-1 and TOPEX/Poseidon Science Working Team Meeting, Biarritz (France), 10-12 June.

[27] Chambers, D. P. and B. D. Tapley, 1998: Reduction of Geoid Gradient Error in Ocean Variability from Satellite Altimetry. *Mar. Geod.*, **21, 25-39.**

[28] Choy, K, J. C. Ries, and B. D Tapley, 2004: Jason-1 Precision Orbit Determination by Combining SLR and DORIS with GPS Tracking Data. *Mar. Geod.***27(1-2): 319-331.**

[29] Commien, L., 2009: Différences entre l'orbite des GDR-C et GDR-B Jason-1, NT08.338

[30] Commien, L., S. Philipps, M. Ablain, and N. Picot, 2008: SSALTO CALVAL Performance assessment Jason-1 GDR "C" / GDR "B". Poster presented at OSTST meeting, Nice, France, 09-12 November 2008. Available at: http://www.aviso.oceanobs.com/fileadmin/documents/OSTST/2008/commien.pdf

[31] Commien, L. and S. Philipps, 2009: Reprocessing of Jason-1 GDR-C, SALP-RP-MA-EA-21731-CLS

[32] Couhert, A., L. Cerri, F. Mercier, S. Houry, 2010: Status of Jason-1 and Jason-2 GDR orbits. *Talk presented at OSTST meeting, Lisbon, Portugal.* Available at: http://www.aviso.oceanobs.com/fileadmin/documents/OSTST/2010/oral/couhert.pdf

[33] Dee, D. P., Uppala, S. M., Simmons, A. J., Berrisford, P., Poli, P., Kobayashi, S., Andrae, U., Balmaseda, M. A., Balsamo, G., Bauer, P., Bechtold, P., Beljaars, A. C. M., van de Berg, L., Bidlot, J., Bormann, N., Delsol, C., Dragani, R., Fuentes, M., Geer, A. J., Haimberger, L., Healy, S. B., Hersbach, H., Hólm, E. V., Isaksen, L., Kållberg, P., Köhler, M., Matricardi, M., McNally, A. P., Monge-Sanz, B. M., Morcrette, J.-J., Park, B.-K., Peubey, C., de Rosnay, P., Tavolato, C., Thépaut, J.-N. and Vitart, F., 2011: The ERA-Interim reanalysis: configuration and performance of the data assimilation system. *Quarterly Journal of the Royal Meteorological Society, 137: 553597. doi: 10.1002/qj.828*

*[34] Desai, S. D., and B. J. Haines, 2004: Monitoring Measurements from the Jason-1 Microwave Radiometer and Independent Validation with GPS. Mar. Geod.***27(1-2): 221-240.**

[35] Dettmering, Denise and Bosch, Wolfgang (2010) Global Calibration of Jason-2 by Multi-Mission Crossover Analysis, Marine Geodesy, **33:1, 150 - 161***. Available at http://pdfserve.informaworld.com/315039__925510361.pdf*

[36] Dibarbour, G., 2011: Bruit Jason et Analyse spectrale, March, CLS.ED/NT

[37] Dorandeu, J., M. H. De Launay, F. Mertz and J. Stum, 2001: AVISO/CALVAL yearly report. 8 years of TOPEX/Poseidon data (M-GDRs).

*[38] Dorandeu, J. and P.Y. Le Traon, 1999: Effects of Global Atmospheric Pressure Variations on Mean Sea Level Changes from TOPEX/Poseidon. J. Atmos. Technol.,***16, 1279-1283.**

[39] Dorandeu, J, M. Ablain, Y. Faugere, B. Soussi, and J. Stum, 2002a: Global statistical assessment of Jason-1 data and Jason-1/TOPEX/Poseiodn Cross-calibration. Paper presented at the Jason-1 and TOPEX/Poseidon Science Working Team Meeting, Biarritz (France), **10-12 June.**

[40] Dorandeu, J., P. Thibaut, O. Z. Zanife, Y. Faugère, G. Dibarboure, N. Steunou, and P. Vincent. 2002b. Poseidon-1, Poseidon-2 and TOPEX noise analysis. Paper presented at the Jason-1 and TOPEX/Poseidon Science Working Team Meeting, New-Orleans (USA), **October.**

*[41] Dorandeu., J., M. Ablain, P. Y. Le Traon, 2003a: Reducing Cross-track Geoid Gradient Errors around TOPEX/Poseidon and Jason-1 Nominal Tracks. Application to Calculation of Sea Level Anomalies. J. Atmos. Oceanic Technol.,***20, 1826-1838.**

[42] Dorandeu, J., Y. Faugère, and F. Mertz, 2003b: ENVISAT data quality: Particular investigations. Proposal for ENVISAT GDR evolutions. Paper presented at the ENVISAT Ra-2 & MWR Quality Working Group meeting. **October.**

*[43] Dorandeu.,J., M. Ablain, Y. Faugère, F. Mertz, 2004: Jason-1 global statistical evaluation and performance assessment. Calibration and cross-calibration results. Mar. Geod.***This issue.**

*[44] Durrant, T.H., J.M. Greenslade, I. Simmonds, 2009: Validation of Jason-1 and Envisat Remotly Sensed Wave Heights. JAOT.***26, 123-134.**

[45] Y.Faugere, J.Dorandeu, F.Lefevre, N.Picot and P.Femenias, 2005: Envisat ocean altimetry performance assessment and cross-calibration. Submitted in the special issue of SENSOR 'Satellite Altimetry: New Sensors and New Applications'

[46] Y.Faugere and J.Dorandeu, 2004: Nouvel algorithme de détection des glaces de mer pour Jason-1. SALP-PR-MA-EA-21235-CLS.

[47] Faugere Y., 2002: Estimation du bruit de mesure sur jason-1, December, CLS.ED/NT.

[48] Y.Faugere, N.Granier, and A.Ollivier, 2007: Envisat validation activities. 2007 yearly report, Available at: http://www.jason.oceanobs.com/documents/calval/validation_report/en/annual_report_en_2007.pdf

[49] Förste, C., F. Flechtner, R. Schmidt, U. Meyer, R. Stubenvoll, F. Barthelmes, R. König, K.-H. Neumayer, M. Rothacher, C. Reigber, R. Biancale, S. Bruinsma, J.-M. Lemoine, and J.C. Raimondo, 2005: A New Heigh Resolution Global Gravity Field Model Derived From Combination of GRACE and CHAMP Mission and Altimetry/ Gravimetry Surface Gravity Data. Poster presented at EGU General Assembly 2005, Vienna, Austria, 24-29 April.

[50] Fu, L. L., 2002: Minutes of the Joint Jason-1 and TOPEX/Poseidon Science Working Team Meeting, Oct. 21-23, JPL Tech. Report. JPL D-25506, edited by L. Fu, USA.

*[51] Gaspar, P., S. Labroue, F. Ogor, G. Lafitte, L. Marchal and M. Rafanel, 2002: Improving non parametric estimates of the sea state bias in radar altimeter measurements of sea level. J. Atmos. Oceanic Technol.,***19, 1690-1707.**

*[52] Haines, B., Y. Bar-Sever, W. Bertiger, S. Desai, P. Willis, 2004: One-Centimeter Orbit Determination for Jason-1: New GPS-Based Strategies. Mar. Geod.***27(1-2): 299-318.**

[53] Hamming, R. W., 1977: Digital Filter. Prentice-Hall Signal Processing Series, edited by A. V. Oppenheim Prentice-Hall, Englewood Cliffs, N. J.

[54] Hernandez, F. and P. Schaeffer, 2000: Altimetric Mean Sea Surfaces and Gravity Anomaly maps inter-comparisons AVI-NT-011-5242-CLS, 48 pp. CLS Ramonville St Agne.

[55] Hirose N., Fukumori I., Zlotnicki V., Ponte R. M. 2001: High-frequency barotropic response to atmospheric disturbances: sensitivity to forcing, topography, and friction, J. Geophys. Res. 106(C12), 30987-30996.

*[56] Keihm, S. J., V. Zlotnicki, and C. S. Ruf. 2000: TOPEX Microwave Radiometer performance evaluation, 1992-1998, IEEE Trans. Geosci. Rem. Sens.,***38(3): 1379-1386.**

[57] Labroue, S. and P. Gaspar, 2002: Comparison of non parametric estimates of the TOPEX A, TOPEX B and JASON 1 sea state bias. Paper presented at the Jason 1 and TOPEX/Poseidon SWT meeting, New-Orleans, 21-12 October.

*[58] Labroue, S. P. Gaspar, J. Dorandeu, O.Z. Zanifé, P. Vincent, and D. Choquet, 2004: Non Parametric Estimates of the Sea State Bias for Jason 1 Radar Altimeter. Mar. Geod.***This issue.**

[59] Labroue, S., Ph. Gaspar, J. Dorandeu, O.Z. Zanife, 2006: Latest Results on Jason-1 Sea State Bias with the Non-Parametric Technique. Talk presented at OSTST meeting, Venice, Italy, 16-18 March.

[60] Larnicol, G, 2011: User Requirement Document of Sea level Climate Change Initiative Project (CCI). Available on CCI website: ftp://slcci_team:%2fextcci2011-@ftp.esa-sealevel-cci.org/Documents/Technical/SLCCI-URD-004%20v1.1.pdf

[61] Legeais, J.F. and L. Carrère, 2008: Complément de validation de la DAC_HR par rapport à la DAC , en zone côtière, Technical Note CLS.DOS/08.189. July.

[62] Legeais, J.F. and M. Ablain, 2011: Validation of altimetric data by comparison with in-situ T/S Argo profiles for TOPEX/Poseidon, Jason-1, Envisat and Jason-2 (Annual report 2010). SALP-NT-MA-P2-21799-CLS, CLS.DOS/NT/10-308.

[63] Legeais, J.F., 2010: On the stability of the altimetric wet tropospheric correction. CLS.DOS/NT/11-033.

[64] Legeais, J.F. and M. Ablain, 2012: Validation of altimetric data by comparison with in-situ T/S Argo profiles for TOPEX/Poseidon, Jason-1, Envisat and Jason-2 (Annual report 2011). SALP-RP-MA-EA-22045-CLS, CLS.DOS/NT/11-305.

*[65] Lemoine, F. G., S. B. Luthcke, N. P. Zelinsky, D. S. Chinn, T. A. Williams, C. M. Cox, and B. D. Beckley, 2003: An Evaluation of Recent gravity Models Wrt to Altimeter Satellite Missions.Paper presented at the Jason-1 and TOPEX/Poseidon Science Working Team Meeting,***Arles (France), November.**

*[66] Le Traon, P.-Y., J. Stum, J. Dorandeu, P. Gaspar, and P. Vincent, 1994: Global statistical analysis of TOPEX and POSEIDON data. J. Geophys. Res.,***99, 24619-24631.**

*[67] Le Traon, P. Y., and G. Dibarboure, 2004: An Illustration of the Contribution of the TOPEX/Poseidon-Jason-1 Tandem Mission to Mesoscale Variability Studies. Mar. Geod.***27(1-2) 3-13.**

*[68] Luthcke. S. B., N. P. Zelinsky, D. D. Rowlands, F. G. Lemoine, and T. A. Williams, 2003: The 1-Centimeter Orbit: jason-1 Precision Orbit Determination Using GPS, SLR, DORIS, and Altimeter Data. Mar. Geod.***26(3-4): 399-421.**

[69] Marshall, J. A., N. P. Zelinsky, S. B. Luthcke, K. E., Rachlin, and R. G. Williamson, 1995: The temporal and spatial characterustics of TOPEX/Poseidon radial orbit error. J. Geophys. Res. **100(C2):25331-25352.**

[70] Martini A., 2003: Envisat RA-2 Range instrumental correction : USO clock period variation and associated auxiliary file, Technical Note ENVI-GSEG-EOPG-TN-03-0009 Available at http://earth.esa.int/pcs/envisat/ra2/articles/USO_clock_corr_aux_file.pdfhttp://earth.esa.int/pcs/envisat/ra2/auxdata/

[71] Ménard, Y., 2003: Minutes of the Joint TOPEX/Poseidon and Jason-1 Science Working Team Meeting. CNES-SALP-CR-MA-EA-15190-CN.

*[72] Obligis, E, N. Tran, and L. Eymard, 2004: An assessment of Jason-1 microwave radiometer measurements and products. Mar. Geod.***27(1-2) 255-277.**

[73] Obligis, E., L. Eymard, M. Ablain, B. Picard, J.F. Legeais, Y. Faugere and N. Picot, 2010: The wet tropospheric correction for altimetry missions: A mean sea level issue.Oral presentation at OSTST meeting, Lisbon, Portugal. Available at http://www.aviso.oceanobs.com/fileadmin/documents/OSTST/2010/oral/19_Tuesday/OBLIGIS.pdf .

[74] Ollivier, A., Y.Faugere and N.Granier, 2008: Envisat validation activities. 2008 yearly report, Available at: http://www.aviso.oceanobs.com/fileadmin/documents/calval/validation_report/EN/annual_report_en_2008.pdf

[75] Ollivier, A., Y.Faugere and J.Legeais, 2010: Envisat validation activities. 2010 yearly report, Available at: http://www.aviso.oceanobs.com/fileadmin/documents/calval/validation_report/EN/annual_report_en_2010.pdf

[76] Ollivier, A., M. Guibbaud, 2012: Envisat RA2/MWR ocean data validation and cross-calibration activities. Yearly report 2011. Available at: http://www.aviso.oceanobs.com/fileadmin/documents/calval/validation_report/EN/annual_report_en_2011.pdf

[77] Ollivier,A., Y. Faugère, N. Picot, and P. Femenias (submitted). Envisat ocean altimeter becoming relevant for Mean Sea Level long term studies? Marine Geodesy.

[78] Peltier, 2004: Global Glacial Isostasy And The Surface of The Ice-Age Earth: The ICE-5G (VM2) Model and GRACE. Annual Review of Earth and Planetary Sciences, May 2004, **Vol. 32, Pages 111-149***, doi: 10.1146/annurev.earth.32.082503.144359*

[79] Picard, B., E. Obligis and S. Philipps, 2008: Monitoring of JMR secondary geophysical products, SALP-NT-MA-EA-21562-CLS.

*[80] Phaden Mc.J., 2003: Evolution of the 2002-03 El Nino, UCLA Tropical Meteorology and Climate Newsletter,***No57***. April.*

[81] Philipps, S. and M. Ablain,2007 : SALP - BC 60453-6-04: Retraitement des GDRs Jason-1 en version 'B' pour les cycles 022 à 127, SALP/BC60453-6-04. September.

[82] S. Philipps, and M. Ablain, 2010: Jason-2 validation and cross calibration activities 2009. SALP-RP-MA-EA-21794-CLS.

[83] S. Philipps, and M. Ablain, 2011: Jason-2 validation and cross calibration activities 2010. SALP-RP-MA-EA-21895-CLS.

[84] S. Philipps, G. Valladeau, J.F. Legeais and M. Ablain, 2012: Jason-2 validation and cross calibration activities 2011. SALP-RP-MA-EA-22042-CLS.

[85] AVISO and PODAAC User Handbook. IGDR and GDR Jason-1 Products, 2008: Edition 4.1, October. SMM-MU-M5-OP-13184-CN (AVISO), JPL D-21352 (PODAAC). Available at http://www.aviso.oceanobs.com/fileadmin/documents/data/tools/hdbk_j1_gdr.pdf.

*[86] Provost., C. Arnault, N. Chouaib, A. Kartavtseff, L. Bunge, and E. Sultan, 2004: TOPEX/Poseidon and Jason Equatorial Sea Surface Slope Anomaly in the Atlantic in 2002: Comparison with Wind and Current Measurements at 23W. Mar. Geod.***27(1-2) 31-45.**

[87] Quartly, G. D., 2004: Sea State and Rain: A Second Take on Dual-Frequency Altimetry. Mar. Geod. 27(1-2) 133-152

*[88] Queffeulou, P., 2004: Long Term Validation of Wave Height Measurements from Altimeters. Mar. Geod.***27:295-510.**

[89] Ray, R., 1999: A Global Ocean Tide Model From TOPEX/Poseidon Altimetry/ GOT99.2 - NASA/TM-1999-209478. Greenbelt, MD, Goddard Space Flight Center/NASA: 58

*[90] Ray, R. D., and B. D. Beckley, 2003. Simultaneaous Ocean Wave Measurements by the Jason and Topex Satellites, with Buoy and Model Comparisons Mar. Geod.***26(3-4): 367-382.**

[91] Ray, R. D., 2003: Benefits of the joint T/P−Jason mission for improving knowledge of coastal tides. Paper presented at the Jason-1 and TOPEX/Poseidon Science Working Team Meeting, Arles (France), November.

[92] Ray, R.D. and R.M. Ponte, 1994: Barometric tides from ECMWF operational analyses. Annales G, **99, 24995-25008**.

*[93] Ruf C., S. Brown, S. Keihm and A. Kitiyakara, 2002a: JASON Microwave Radiometer: On Orbit Calibration, Validation and Performance, Paper presented at the Jason-1 and TOPEX/Poseidon Science Working Team Meeting, New-Orleans (USA),***21-23 October.**

[94] Ruf. C. S., 2002b: TMR Drift - Correction to 18 GHz Brightness Temperatures, Revisited. Report to TOPEX Project, June.

[95] Scharroo R., J. L. Lillibridge, and W. H. F. Smith, 2004: Cross-Calibration and Long-term Monitoring of the Microwave Radiometers of ERS, TOPEX, GFO, Jason-1, and Envisat, **Marine Geodesy, 27:279-297**.

[96] Schaeffer, P., A. Ollivier, Y. Faugere, E. Bronner, and N. Picot, 2010: The new CNES CLS 2010 Mean Sea Surface. Oral presentation at OSTST meeting, Lisbon, Portugal, 18-20 october. Available at http://www.aviso.oceanobs.com/fileadmin/documents/OSTST/2010/oral/19_Tuesday/Schaeffer.pdf.

[97] Schaeffer, P., Y. Faugere, J.-F. Legeais, A. Ollivier, 2012: The CNES_CLS 2011 Global Mean Sea Surface computed from 16 years of satellite altimeter data. submitted to Marine Geodesy.

*[98] Tapley, B.D., M.M. Watkins, J.C. Ries, G.W. Davis, R.J. Eanes, S.R. Poole, H.J. Rim, B.E. Schultz, C.K. Shum, R.S. Nerem, F.J. Lerch, J.A. Marshall, S.M. Klosko, N.K. Pavlis, and R.G. Williamson, 1996: The Joint Gravity Model 3. J. Geophys. Res.***101(B12): 28029-28049.**

.

[99] Tierney, C., J. Wahr, et al., 2000: Short-period oceanic circulation: implications for satellite altimetry. Geophysical Research Letters 27(9): 1255-1258

[100] Thibaut, P. O.Z. Zanifé, J.P. Dumont, J. Dorandeu, N. Picot, and P. Vincent, 2002: Data editing: The MQE criterion. Paper presented at the Jason-1 and TOPEX/Poseidon Science Working Team Meeting, New-Orleans (USA), 21-23 October.

*[101] Thibaut, P. L. Amarouche, O.Z. Zanife, N. Steunou, P. Vincent, and P. Raizonville, 2004: Jason-1 altimeter ground processing look-up tables. Mar. Geod.***27 (3-4), 409-432.**

[102] Tournadre, J., 2002: Validation of the rain flag. Paper presented at the Jason-1 and TOPEX/Poseidon Science Working Team Meeting, Biarritz (France), 10-12 June.

*[103] Tran, N., D. W. Hancock III, G.S. Hayne, 2002: "Assessment of the cycle-per-cycle noise level of the GEOSAT Follow-On, TOPEX and POSEIDON." J. Atmos. Oceanic Technol.,***19(12): 2095-2117.**

*[104] Tran, N. , Labroue, S. , Philipps, S. , Bronner, E. and Picot, N., 2010: Overview and Update of the Sea State Bias Corrections for the Jason-2, Jason-1 and TOPEX Missions, Marine Geodesy,***33:1, 348 - 362***. Avialable at** http://pdfserve.informaworld.com/804727__925502357.pdf

[105] World Meteorological Organization, 2008: El Nino/ La Nina Update (24 June 2008). Available at http://www.wmo.ch/pages/prog/wcp/wcasp/documents/El_Nino_Jun08_Eng.pdf *.*

[106] World Meteorological Organization, 2010: El Nino/ La Nina Update (30 March 2010). Available at http://www.wmo.ch/pages/prog/wcp/wcasp/documents/El_Nino_Mar10_Eng.pdf *.*

[107] World Meteorological Organization, 2010: El Nino/ La Nina Update (30 October 2010). Available at http://www.wmo.ch/pages/prog/wcp/wcasp/documents/El_Nino_Oct10_Eng.pdf *.*

[108] World Meteorological Organization, 2011: El Nino/ La Nina Update (25 January 2011). Available at http://www.wmo.ch/pages/prog/wcp/wcasp/documents/El-Nino_Jan11_Eng.pdf *.*

[109] Valladeau, G., S. Philipps and M. Ablain, 2010: Jason-1 Validation and cross-calibration activities (Annual report 2009). SALP-RP-MA-EA-21795-CLS, CLS.DOS/NT/10-005.

[110] Valladeau, G., S. Philipps and M. Ablain, 2011: Jason-1 validation and cross calibration activities (Annual report 2010). SALP-RP-MA-EA-21903-CLS, CLS.DOS/NT/10-332.

[111] Valladeau, G. and M. Ablain, 2011: Validation of altimetric data by comparison with tide gauge measurements for TOPEX/Poseidon, Jason-1, Jason-2 and Envisat (Annual report 2010). SALP-NT-MA-EA-21691-CLS, CLS.DOS/NT/10-289.

[112] Valladeau, G., 2011: Investigations on C-band SWH behaviour for Jason-1 & Jason-2 space missions. CLS-DOS-NT-11-049.

[113] Valladeau, G., 2012: Validation of altimeter data by comparison with tide gauge measurements for TOPEX/Poseidon, Jason-1, Jason-2 and Envisat (Annual report 2011). SALP-NT-MA-EA-22046-CLS, CLS.DOS/NT/12-016.

[114] Vincent, P., S. D. Desai, J. Dorandeu, M. Ablain, B. Soussi, P. S. Callahan, and B. J. Haines, 2003a: Jason-1 Geophysical Performance Evaluation. Mar. Geod. **26(3-4): 167-186.**

[115] Vincent, P., S. Desai, J. Dorandeu, M. Ablain, B. Soussi, Y. Faugère, B. Haines, N. Picot, K. Case, A. Badea, 2003b: Summary about Data Production and Quality. Paper presented at the Jason-1 and TOPEX/Poseidon Science Working Team Meeting, Arles (France), November

[116] Vincent, P., J.P. Dumont, N. Steunou, O.Z. Zanife, P. Thibaut, and J. Dorandeu, 2003c: Jason-1 I/GDR science processing: ground retracking improvements. Paper presented at the European Geophysical Society meeting, Nice, April.

[117] Zanife, O. Z., P. Vincent, L. Amarouche, J. P. Dumont, P. Thibaut, and S. Labroue, 2003: Comparison of the Ku-band range noise level and the relative sea-state bias of the Jason-1, TOPEX and Poseidon-1 radar altimeters. Mar. Geod. **26(3-4): 201-238.**

[118] Zelensky, N.P., B.D. Beckley, F.G. Lemoine, S.M. Klosko, R.D. Ray, S. Holmes, D.D. Rowlands, S.B. Luthcke, D.S. Chinn, O. Bordyugov, 2010: The pussling 59-day altimeter data signal and possible causes. Oral presentation at OSTST meeting, Lisbon, Portugal, 18-20 october 2010. Available at http://www.aviso.oceanobs.com/fileadmin/documents/OSTST/2010/oral/20_Wednesday/morning/20_1150_zelensky_aud3.pdf .